Instituto Tecnológico y de Estudios Superiores de Monterrey

Campus Monterrey

School of Engineering and Sciences

The mechanics of additively manufactured reentrant honeycombs: apparent elastic modulus and energy absorption ability under cyclic loadings.

A thesis presented by

Amador Chapa Cárdenas

Submitted to the
School of Engineering and Sciences
in partial fulfillment of the requirements for the degree of

Master of Science

In

Manufacturing Systems

Monterrey Nuevo León, June 14th, 2021.

Dedication

To my beloved parents, whose unconditional love always inspire me to pursue my dreams. I cannot find the words to express my gratitude to you. Thank you for always giving me more than what I needed. This and all the achievements of my life are for you.

Special thanks to my best friends whose words of encouragement kept me working hard while I was away from my hometown. Miguel, Lina, Pedro, and Rubi, thanks a lot for believing in me, even when I did not do it. You are the family I chose. I love you, guys.

To my grandparents, for their love and support at the distance. Seeing you proud of me gave me the strength to keep working while I was away.

To my three thesis advisors Dr. Pedro, Dr. Armando, and Dr. Enrique, thanks a lot for your guidance and support on these two years of hard work. I feel very grateful to you for your patience and empathy during these hard days were the pandemic changed things as we never imagine.

My sincere gratitude to Abraham and Ruben for their guidance during my postgraduate experience.

To the people I met while I was away in a new city, thanks for making this journey less scary than what it could have been. The friends I made, and the amazing professors whom I had the opportunity to meet and learn from them. I do not know how I could survive the loneliness without my volleyball teammates Juan, Alex, and Johan. Thank you, guys.

Acknowledgements

Firstly, I want to acknowledge the excellent work of three professors who accompanied me during the last two years:

Dr. Armando Román Flores, I feel very grateful to you for having believed in me without knowing me and the opportunity you gave me to enter this small group of extraordinary people.

To my thesis advisor, Dr. Pedro Daniel Urbina Coronado, all my gratitude for your guidance through every step of the research process. Thanks for all the recommendations, your words encourage me to keep working hard and propose new ideas for this project.

Special thanks to Dr. Enrique Cuan Urquizo whose words of support kept me motivated and proud of my work even in the saddest days of this adventure. Thanks a lot for introducing me to this magical world of metamaterials. I admire your work and dedication to the science. You are a role model to many of us.

I would like to thank Tecnológico de Monterrey support on tuition and CONACyT for the opportunity to be part of the graduate program with tuition and living support.

The mechanics of additively manufactured reentrant honeycombs: apparent elastic modulus and energy absorption ability under cyclic loadings.

By

Amador Chapa Cárdenas

Abstract

Advances in additive manufacturing (AM) technologies have made possible the design and fabrication of more complex parts such as the cellular solids. Auxetic honeycombs are a type of cellular solid with already demonstrated enhanced mechanical properties and great potential as energy absorber. This work consists in the fabrication and characterization of reentrant honeycombs structures to study the feasibility of AM technology fused deposition modeling (fdm) as the manufacturing process and its effect on the mechanical properties of the printed parts. Numerical and experimental analysis were carried out to obtain the apparent elastic modulus of reentrant honeycombs and its relationship with the relative density of the specimens. Disadvantages of selecting fdm include low accuracy in the shapes printed and inability to print cell-wall thicknesses lower than 1 mm in cellular solids. A non-linear relationship between relative density of auxetic honeycombs and their apparent elastic modulus was found.

Abbreviations

ABS	Acrylonitrile Butadiene Styrene
AM	Additive Manufacturing
CAD	Computer-aided Design
FDM	Fused Deposition Modeling
FEA	Finite Element Analysis
FFF	Fused Filament Fabrication
NPR	Negative Poisson’s Ratio
PLA	Polylactic Acid
RH	Reentrant Honeycomb
SEA	Specific Energy Absorbed
STL	Stereolithography
TPU	Thermoplastic Polyurethane

List of figures

List of tables

Contents

Chapter 1: Introduction

The importance of advanced materials has increased drastically in the last decades. Recently, metamaterials (a type of material engineered to have a property that is not found in naturally occurring materials) have received much attention due to their extraordinary mechanical properties including outstanding specific stiffness and strength. The uncommon mechanical properties of metamaterials derived from the architecture and distribution of material rather than the bulk behavior of its components. These unusual properties generate high expectations for their use in different fields of science as energy storage, soft robotics, acoustics, etc.

The cellular structures are a type of metamaterial which present perfect combination of lightweight and energy absorption capacity. These man-made materials are created from a constant repetition of unit cells to achieve unique mechanical properties for a specific application. They can be formed by periodic and stochastic arrangements of open or closed cell types using two-dimensional configurations like the honeycombs, or three-dimensional polyhedral layouts such as the lattice structures.

Cellular structures that exhibit negative Poisson's ratio (NPR) are commonly known as "auxetic"; these materials tend to shrink under compression forces and expand laterally under stretching. Auxetic materials can be found in nature. Bones, animal skin, teeth, wood, horns, α-cristobalite, and face centered cubic (FCC) crystals are some good examples.

Auxetics are great energy absorber structures. The NPR effect in materials leads to achieve higher stiffness and shear modulus, improves indentation resistance, and enhances energy absorption ability. The addition of this feature in the materials helps in the creation of new structures that can serve as energy absorbers because of its nontraditional deformation mechanism which results in reduced specimen volume and increased plateau stress during an impact process. Nowadays, this type of metamaterials is being used as crash mitigation devices in

vehicles and airplanes, protective packaging, and personal/sportive protection equipment.

In recent years, there has been experimental and simulation research efforts to understand the deformation mechanism of auxetics. The main goal is to uncover the energy absorption behavior and most influential factors on this phenomenon. Many researchers have discovered relevant results which may be helpful for engineering applications.

Re-entrant honeycombs (RHs) are auxetic cellular structures with a lot of scientific attention due to their high stiffness and energy absorption ability. This is a clear metamaterial example whose auxetic behavior has proved NPR materials may offer upgraded mechanical properties when compared to traditional geometries like the regular honeycombs. Several researchers have proposed improvements in the design (such as ribs) achieving good results by obtaining a better mechanical performance. The abilities of RHs are still waiting to be uncovered, tested, and verified.

1.1 Motivation

A review in literature related in the design and characterization of cellular structures was carried out as presented in Chapter 2. From the analysis it was identified a new trend in the design and study of auxetic materials to prove the benefits of structures showing a negative Poisson's ratio against traditional materials.

Studies have demonstrated that auxetic designs enhance the mechanical performance of materials. They are attracting interest due to their unusual mechanical response, and because they offer a route to attaining extreme (high or low) values of other material properties not easily achievable in conventional materials. The idea of propose new auxetic materials benefits to present potential applications of these nontraditional structures as structural protection in the automotive industry or as sporting protective equipment [1]. They are now being used in different applications like car crash absorbers, shoes, and helmets; in all

these examples, auxetics are used to reduce the consequences of an impact event.

It is expected that this type of metamaterials can be used in applications where they are constantly subjected compressive loadings or to impacts. Auxetic structures are becoming popular for their good ability to absorb energy and there are already studies showing their ability to withstand 1.75 times more impact cycles compared to traditional non-auxetic geometries [2].

There is an area of opportunity to continue characterizing this type of metamaterials. It is also interesting the lack of actual applications of auxetic cellular structures, so it is established the goal to propose a use of these materials in impact applications thanks to its already proven energy absorption abilities.

1.2 Problem Statement and Context

The concept of metamaterials has gained a lot of popularity over the past decades. This modification of materials enhances its mechanical properties so they can be used in more specific applications showing excellent results. Auxetic materials are now being studied because of its high energy absorption ability. They present low stiffness when compared to traditional materials but show high resilience (the ability to absorb energy when it is deformed elastically, and release that energy uploading) during impact events.

There exists an area of opportunity to fully explore its crushing behavior, impact response, and the effect of the design parameters on the structure's mechanical properties. The auxetic materials present anisotropy and nonlinear properties which is of interest to this research also.

Due to its complex geometry, auxetic structures had been impossible to fabricate some decades ago. Thanks to the development of the additive manufacturing technologies, this limitation has been mitigated. Techniques like fused deposition modeling (also referred to as fused filament fabrication) has made possible to start building more complex designs, but it generates anisotropic parts because of its

process parameters like building orientation. It is important to understand the effect of FDM technique as manufacturing process and optimize the printing parameters to obtain the best mechanical response from the structures.

1.3 Research Question

Does 3D printed auxetic cellular structures fabricated by additive manufacturing techniques such as fused deposition modeling and using polymers like thermoplastic polyurethane offer enough strength and energy-absorbing ability to be used in the manufacture of energy absorbers?

1.4 Solution overview

In recent years, several investigations have been made on the mechanical behaviors of the auxetic cellular structures. It has been demonstrated that materials with negative Poisson's ratio exhibit superior mechanical properties when compared to traditional geometries. This whole work consists in understanding the mechanical behavior of the re-entrant honeycombs and identifying the effect of design and printing parameters on its absorbing energy ability. It is expected to present a proposal with an innovative design on the RHs to enhance the deformation mechanism to achieve higher specific energy absorptions. The design will be tested on laboratory and compared with software simulations. Samples will be 3D printed using the Fused Deposition Modeling technique and tested their compressive strength and damping ability to assess their energy absorption capabilities.

1.5 Research Objectives

The objective of this research is to characterize the mechanical response of thermoplastic polyurethane reentrant honeycomb structures, and their ability to withstand multiple compressions up to densification, in order to estimate the potential of these cellular solids as energy absorbers in engineering applications.

Other of the main goals of this project is explore the use of fdm as the manufacturing process and its accuracy in the fabrication of thin-walled honeycombs.

The specific objectives of the work are:

- Understand different ways on enhancing the energy absorption ability of metamaterials.
- Establish and analyze the relationship between design parameters of metamaterials and their mechanical performance.
- Propose a design of experiments to study the effect of relative density on the mechanical response of the structures.
- Fabricate the specimens using a fused deposition modeling 3D printer.
- Apply cyclic compressive testing on specimens to measure the ability of reentrant honeycombs to withstand multiple compressions up to full densification.
- Obtain the stress-strain profiles of samples with different relative density.
- Recognize the potential of additive manufactured parts as impact absorbers.
- Identify the mechanical properties of the auxetic specimens and propose potential applications as impact absorbers in the automotive industry.

1.6 Thesis overview

The structure of this research project is divided in five different chapters where it is presented an introduction to the topic, the methodology followed, results obtained, and the conclusions.

In Chapter 2, it is shown a literature review on very relevant concepts related to this research work. It follows an order from general to particular topics where it is presented the significance of metamaterials and cellular solids. Some of the information presented helps to understand the process of design, manufacturing, and analysis on the mechanical response of cellular structures. Previous works are mentioned to illustrate the selection of materials and manufacturing process to fabricate cellular structures with the best quality and mechanical properties.

A study of mechanical response in scaled up reentrant honeycombs is presented in Chapter 3. This set of experiments tries to demonstrate a hypothesis that cellular

solids with same topology and same relative density must exhibit the same apparent Young's modulus. Numerical and experimental approaches were carried out to estimate the structure's apparent elastic modulus and the effect of the selected manufacturing process may have on that.

Chapter 4 explores the effect of relative density on the mechanical response of reentrant honeycombs when subjected to compression in both different directions. A set of experiments is presented to estimate the apparent Young's modulus and establish experimentally a relationship with the cell-wall thickness of the unit cells. Cyclic compressive tests were carried out to obtain the strength and energy absorption capabilities of reentrant honeycombs structures. Conclusions were made on whether or not the selection of flexible polymers like thermoplastic polyurethane is a good option to create resilient cellular solids in order to be used in impact applications as energy absorbers.

In Chapter 5 are presented the conclusions based on the results obtained. A set of recommendations for further works is also included to give some continuity to this research project.

Chapter 2: Literature review on the mechanics and fabrication of reentrant honeycombs

The literature analysis aims to illustrate the relationship among primary topics relevant to this work. Understanding its concept and evolution is vital to establish the foundations of this project, and to be able to generate new knowledge from the information provided by other researchers over time. In this section, the information will be presented as follows:

- Metamaterials
- Cellular solids
- Auxetic structures
- Two-dimensional auxetic honeycombs
- Energy absorption of cellular solids
- Additive Manufacturing: Fused Deposition Modeling
- Additively manufactured auxetic structures
- Mechanical testing in cellular structures

2.1 Metamaterials

A metamaterial is not a material properly speaking. It is an artificial material designed by humans to obtain special properties not easily found in nature. This concept is derived from two different terms: the Greek word *meta* meaning *beyond,* and the Latin word *materia* meaning *matter.* The idea of metamaterials was created once the engineering applications started to demand materials with certain enhanced properties. Due to the lack of such specific materials in nature or their difficulty to be obtained, scientists began to design new structures in laboratories to satisfy the need of materials with enhanced chemical, electromagnetic, acoustic, or mechanical properties. The performance of a metamaterial is determined by its microstructure rather than the chemical and physical properties of the material constituting it [3].

Experimental research in metamaterials first emerged in optics but progressed soon after to acoustics and mechanics. Initially, rationally designed mechanical

metamaterials were developed to control wave propagation in acoustic media, thin elastic sheets, curved shells, and harness elastic instabilities to generate auxetic behavior. The idea of manipulating materials to obtain specific properties emerged at the end of the nineteenth century. One of the pioneers in the study of metamaterials is Jagadish Chandra Bose, who in 1898 published his work on the effect of twisted structures subjected to electromagnetic waves. With this in mind, these newly developed mechanical metamaterials have a variety of counterintuitive mechanical properties, and thereby they are not limited just to switching between two pattern states as before [4].

When a metamaterial is designed to optimize its mechanical properties, it is called *mechanical metamaterial.* They possess a precise engineered structure, composed of repeating unit cells that form delicate architectures with an excellent mechanical performance. The properties of metamaterials can be tailored by manipulating the internal structure to obtain materials with desired Young's modulus, shear modulus, or Poisson's ratio.

It can be concluded that metamaterials are a result from human ingenuity. They enable us to design our own atom-like units, and thereby create materials with unprecedented effective properties [4]. An ongoing challenge for modern materials science is to create these artificial structures with an unconventional response, programmed by a suitable geometrical or topological design. The fabrication and testing of rationally designed metamaterial microstructures in three dimensions are just emerging.

2.2 Cellular solids

A cellular solid is a structure composed of interconnected solid struts which form the edges and faces of cells. Several materials present a cellular structure with either a two-dimensional array of cells as in honeycombs, or a three-dimensional array as in foams. Different combinations of internal structures provide a wide range of properties that can be very useful in engineering design. Four major areas of application of cellular materials are thermal insulation, packaging, structural, and

buoyancy [5]. The low thermal conductivity of foams can be exploited in applications such as coffee cups, or in modern buildings to prevent fire hazards. They can also be used in packaging thanks to their low weight so it can be fabricated packages with easy handling. Another application of cellular materials is in the structural field where they can be used as sandwich panels, structures with high stiffness, to substitute the traditional structural materials such as wood. Cellular solids are also being used in marine applications to construct boats with structural rigidity and buoyancy.

In 1987, Ashby and Gibson published their book “Cellular Solids. Structures and Properties” [5] in which they present a rigorous study on the design and analysis of cellular structures. They stated that to understand the mechanical behavior of cellular solids and foams, firstly it was necessary to understand the mechanics of 2D hexagonal honeycombs.

The topology of a cellular solid plays a key role in the performance of the structure. It has been established that the mechanical properties of cellular solids depend more on the cell shape rather than the cell size. By understanding the effect of the cell geometry on the mechanical performance, optimized structures can be designed to obtain desired properties for specific engineering applications.

Relative density is considered the most important feature of cellular solids. It is commonly defined with the Greek letter ρ, and it is calculated according to the following:

$$\overline{\boldsymbol{\rho}} = \frac{\boldsymbol{\rho}^*}{\boldsymbol{\rho_s}}$$

where $\boldsymbol{\rho}^*$ is the density of the cellular solid, and $\boldsymbol{\rho_s}$ is the density of the bulk material. A derived concept from the relative density is the porosity, which can be defined as the fraction of voids, and it is obtained by subtracting the relative density from the unity $(\mathbf{1} - \overline{\boldsymbol{\rho}})$.

The mechanics of cellular solids are also dependent of the Poisson's ratio of the structures. The Poisson's ratio is a dimensionless constant, denoted by the Greek letter v, that defines the negative ratio of the lateral and longitudinal strains in a structure when stretched or compressed. For two-dimensional structures, this value lies in the range -1 to 1; in three-dimensional auxetic isotropic structures, the value of v lies between -1 and 0.5; for anisotropic materials, the Poisson's ratio has no limits and can range from minus infinity to unity.

Even though most of the traditional material possess a positive Poisson's ratio, there are some rare cases where materials exhibit non-traditional deformation mechanisms which can be translated into negative Poisson's ratios. These materials are commonly known as auxetics.

2.3 Auxetic structures

The word "auxetic" refers to materials showing a negative Poisson's ratio; it derives from the Greek word "auxetikos" meaning "what tends to increase". The main characteristic of auxetics is the presence of a lateral expansion when stretched, and a densification when compressed; this deformation mechanism is the opposite to the one exhibited by most of the traditional materials (observe Fig. 1). This concept was first established in 1987 by Lakes [6] when he discovered a re-entrant structure on a polyurethane (PU) foam; he referred to these materials with nontraditional mechanical deformation as "anti-rubbers". In 1993, Lakes [7] published a review on auxetic materials where he identified different materials with NPR and their potential applications in sandwich panels due to its good resilience and energy absorbing capacity.

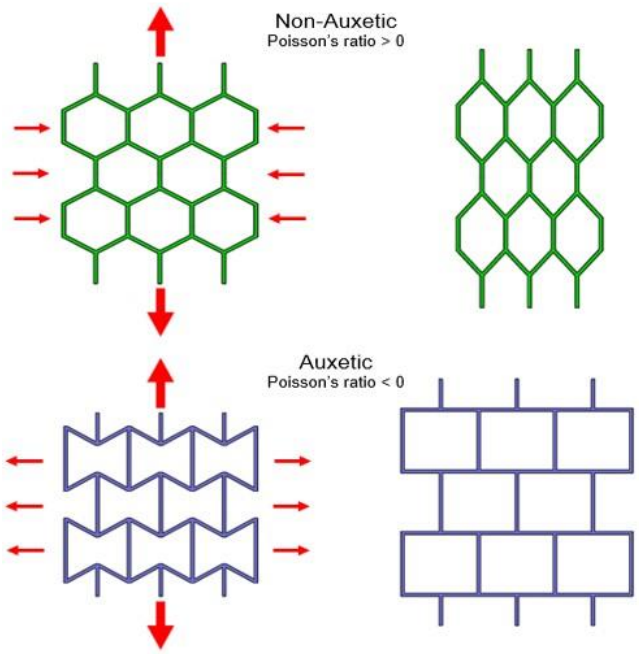

Figure 1. Deformation mechanism of non-auxetic and auxetic cellular solids.

In the last decades, a wide variety of metamaterials showing the auxetic effect have been studied [8]. The most common classes are two-dimensional and three-dimensional frames, chiral structures, rotating rigid or semi-rigid structures, and carbon fiber laminate materials. Several researchers have theoretically predicted the auxetic effect but, in some cases, traditional manufacturing methods make it difficult to fabricate these materials with complex geometries. The amount of unit cells [9] and cell size [10] are two of the most important decisions to make while designing these cellular arrays, since the experimental results fully depend on these decisions [11]. The class of auxetics derived from a honeycomb cell has acquired high popularity thanks to its simple design and fabrication.

2.4 Two-dimensional auxetic honeycombs

The word “honeycomb” is commonly used to describe all the two-dimensional arrays of cellular solids independently of the topology each design could have. The most popular and most studied topology is the regular hexagonal honeycomb [12], named and inspired by the structures fabricated by the bees. A regular honeycomb is characterized by having six equal sides and six internal angles of 120 degrees.

This topology exhibits three rotational degrees of symmetry which has as a result in-plane isotropy. It provides stiffness and lightness to structures due to the optimization of the amount of material used only where it is necessary.

When two internal and opposite angles of a honeycomb are higher than 90°, the unit cell is commonly referred as “re-entrant honeycomb” (see Fig. 2). Re-entrant means “directed inward”, and directly applies to the ribs of the traditional “bow tie”. This auxetic honeycombs have attracted much attention due to their fascinating properties compared with conventional topologies such as increased shear modulus, increased indentation resistance, enhanced fracture toughness, better energy absorption, and so on. These unit cells have been used to model the deformation of auxetic foams and, were found to be highly anisotropic [13].

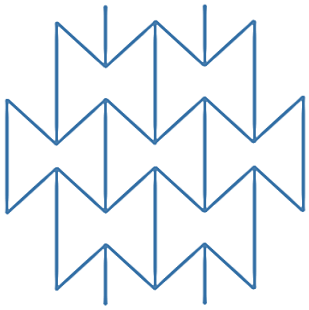

Figure 2. Reentrant honeycomb array.

The re-entrant honeycomb design is primarily described by four parameters: length of vertical ribs and diagonal ribs, angle between ribs, and the rib thickness. It has been theoretically and experimentally demonstrated that a variation in these parameters affect notoriously the mechanical properties of the structure. The re-entrant honeycomb structure has a negative Poisson’s ratio, and its value depends on the inverted angle of the cell edge. Lee et al. [14] found that the Young’s modulus of re-entrant structures decreases with an increase in the inverted angle . Whitty et al. [15] applied finite element (FE) modeling to show that a reduction in vertical rib thickness produce a reduction in the structure’s stiffness and Poisson’s ratio (becoming more negative). Yang et al. [16] applied the Eringen’s elastic theory to derive a FE model of the re-entrant hexagonal honeycomb; it was proved

that the degree of auxeticity was dependent on the re-entrant angle and cell rib length ratio h/l.

Several works have tried to predict the mechanical properties of these auxetic structures and find relationships with the design parameters [17][18]. Most of the studies on 2D re-entrant honeycombs are focused on the deformation and properties in the elastic range. However, when used in load bearing applications, large deformations may occur. A theoretical approach was therefore formulated to predict NPR of re-entrant hexagonal honeycombs, based on the large deformation model [19]. The mechanical properties of the auxetics may differ when studying large deformation mechanisms. In 2004, Wan et al. demonstrated that Poisson's ratios are non-linearly dependent on strain at large deformations [19]. Fu et al. analyze the nonlinear behavior of these auxetic structures under large deformation; the nonlinear shear modulus was found to increase with the re-entrant angle and decrease with the increase of cell rib length ratio [20]. Vyavahare et al. [21] published their work in 2020 where they study the effect of different design parameters on the stiffness and SEA of reentrant honeycombs fabricates using ABS and PLA; they conclude ABS specimens are better energy absorbers and PLA ones presents a higher stiffness in the mechanical testing. This is a clear example that even to these days, simple topologies like regular and reentrant honeycombs are very popular still capturing the attention.

2.5 Energy absorption in cellular solids

When a cellular solid like honeycombs are subjected to compressive loadings, it is created a particular stress-strain curve with three main different stages: the elastic zone, the plateau region, and the densification stage. To explain better these three stages, an example of a stress-strain curve for cellular solids is presented in Fig. 3. The linear elastic region is defined by the bulk material, and during this first step the elements start to buckle. Once the cellular solid yields, the second stage starts where the stresses produced in the structure are kept constant while it continues compressing. For the third and final zone, called the densification region, all the

elements touched, the curve tends to go vertical, and the cellular solid starts to behave as a solid structure with the bulk material's properties.

The energy per unit volume absorbed by the structure due to the compression phenomenon is simply the area under the stress-strain curve. Since cellular solids commonly exhibit small linear regions, the amount of absorbed energy in this first stage is very small. Therefore, it is the plateau region the main goal of the designers in order to create cellular solids that can possess long, and flat plateau stages so higher amounts of energy can be absorbed during the crushing process.

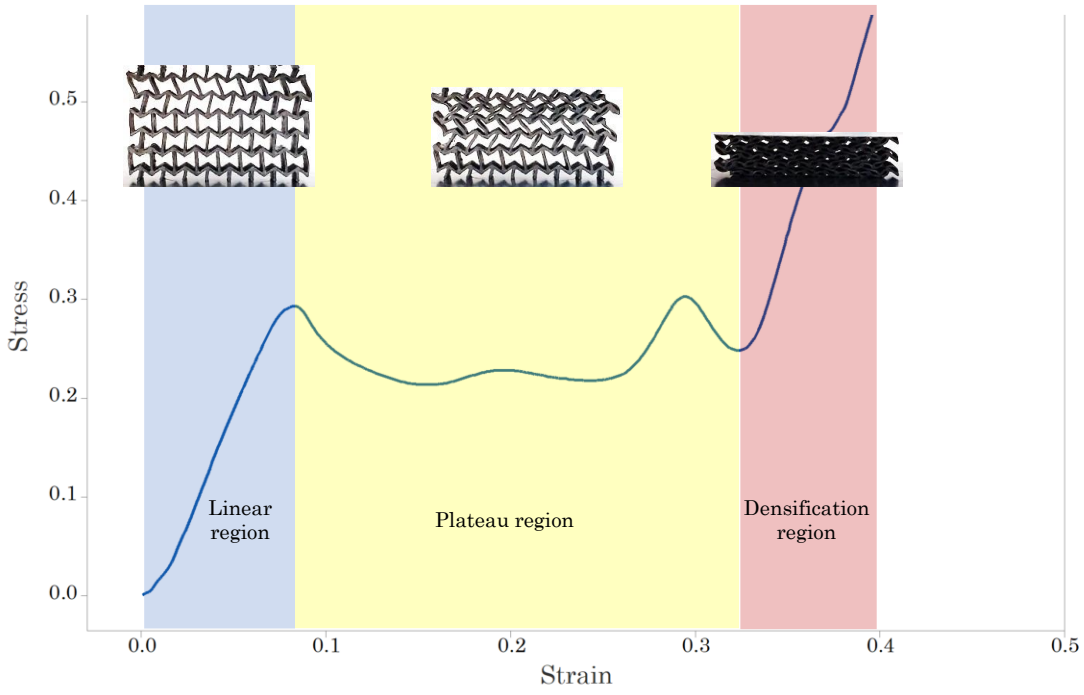

Figure 3. Main stages in the stress-strain curve of cellular solids subjected to compression.

The cellular solids can be compressed up until full densification. This is defined as the moment where the opposing walls of the cells crush together. As previously presented in Fig. 3, during full densification the stress-strain curve rises steeply. One may think that the densification strain, ϵ, is equal to the porosity ($\mathbf{1} - \bar{\boldsymbol{\rho}}$) of the cellular solid since at that strain all voids would be occupied. Results have demonstrated that the densification strain is normally smaller than the porosity. In

their work, Ashby and Gibson proposed a formula to estimate the densification strain for open-cell foams, which is presented next:

$$\boldsymbol{\varepsilon = 1 - 1.4\,\bar{\rho}}$$

To analyze the effectiveness of cellular solids as energy absorbers, it is necessary to compressed them up until full densification and integrate the stress-strain curve to obtain the amount of energy absorbed per volume unit, known as “specific energy absorbed” or SEA.

2.6 Additive manufacturing: fused deposition modeling

Also known as “3D printing”, additive manufacturing (AM) is a set of technologies that build objects by joining materials layer-by-layer as opposed to traditional fabrication methods. One of the most popular AM techniques is the fused deposition modeling (FDM). FDM 3D printers work by extruding thermoplastic filaments such as ABS and PLA, through a heated nozzle, melting the material and applying the plastic one layer at a time until the part is complete. A simplified fdm technology is shown in Fig. 4.

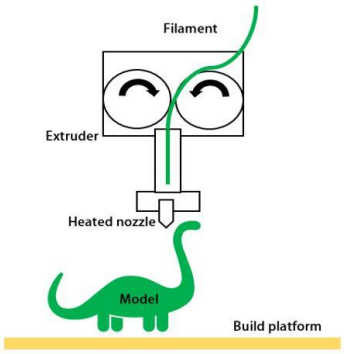

Figure 4. Fused deposition modeling technique.

The FDM technique is the extensively employed methodology. Advantages of this technology include low manufacturing costs, and high printing speed. One of the limitations in FDM is the effect of process parameters which has been demonstrated affect directly the mechanical performance of the 3D printed parts [22]. Now researchers are working on this major area of concern to get an optimized parameter for the generalized process [23]. Studies have been made to

investigate the effect of building orientation, layer height, printing speed, and infill density on the printed part's mechanical performance.

One of the biggest limitations which prevent the FDM process from being employed in industries is the constrained availability of materials that can be used as a filament. PLA and ABS are the most employed filament materials in the current scenario each having their distinct property [24]. More flexible materials such as polyamides [25] and thermoplastic polyurethane [26] have been gaining popularity in the fabrication of 3D printed cellular solids but their mechanical properties are still being uncovered. Elmrabet et al. [27] analyzed the compressive strength of 3D printed TPU and PLA parts concluding that dimensional variation may cause inhomogeneity and anisotropy in the specimens. Nevertheless, it has been demonstrated great potential of these materials to fabricate highly compliant lattice structures, a good option for energy absorption devices.

2.7 Additively manufactured auxetic structures

Despite their attractive mechanical properties, auxetic materials possess complex geometries that are difficult to manufacture by the traditional methods. The prevailing manufacturing method for auxetic structures was first developed by Lakes in 1987 [6]. His manufacturing method is summarized in three primary steps: heat a regular foam, pressed it into a mold, and cool down the structure to release it from the mold. The disadvantage of this manufacturing method is that only works for simple shapes.

The aforementioned limitations have been reduced thanks to the development of new technologies and the rise of additive manufacturing techniques. In 2012, Yang et al. [28] manufactured for the first time a three-dimensional auxetic structure, using electron beam melting (EBM). At that time, available metal additive machines restrict the size of the samples and the specimens fabricated present a bad surface roughness which affects negatively in the mechanical properties of the structure.

In 2017, Yang et al. [18] tested fdm parts fabricated using PLA and TPU showing the effectiveness of auxetic structures in shock forces reduction. Bates et al. [29]

published their work on repeated tailored energy absorption of regular honeycombs fabricated using thermoplastic polyurethane. They established a methodology to create and characterize the mechanical response of very resilient auxetic structures subjected to cyclic compressive loadings. In 2020, Chen et al. [25] fabricated 3D re-entrant honeycomb specimens made of polyamide using the AM technology. This open new ways to fabricate auxetics using polymers such as acrylonitrile butadiene styrene, polylactic acid, or thermoplastic polyurethane [2], which are materials that can provide the lightness and flexibility the structures require. Some of the AM techniques that are gaining popularity for the auxetics manufacture are the fused deposition modeling and multi-jet fusion technologies [30].

2.8 Feasibility of FDM technique

in additive manufacturing technologies have made possible to design and fabricate parts with more complex geometries. Cellular solids were a manufacturing challenge due to its high porosity in two or three dimensions. 3D printing techniques have become the best option to fabricate cellular structures thanks to its low costs of fabrication and materials. Fused deposition modeling has gained a lot of popularity among researchers who are starting to characterize cellular solids. This technique is a good option, especially for honeycomb structures where the topology is only extruded along the out-of-plane direction.

It has been previously demonstrated that printing parameters significantly affect the mechanical properties of fdm parts, so it is necessary to study and optimize each parameter to obtain the desired mechanical response in each design. Popescu et al. [31] studied the influence of process parameters in polymer specimens and identified that key parameters influencing fdm parts were the build orientation, infill percentage, layer thickness, and raster angle. Vyavahare et al. [32] also study the effect of process parameters namely layer thickness, raster angle and line contours on fdm parts, and it were identified the first two as the most influential on the mechanical response of 3D printed auxetic structures. The effect of feed rate [33] and printing speed [34] on the strength of fdm parts has also been studied.

Remarkable limitations of the fdm technique are its low accuracy and the need to add supports when creating overhangs. Guerra Silva et al. [35] made a feasibility study on fdm to fabricate miniature lattice structures demonstrating its inability to manufacture struts with cell-wall thickness lower than 1 millimeter. Other manufacturing issue with fdm is the presence of uneven thickness along the struts of cellular structures [36]. The presence of these defects on the printed samples is usually added to the numerical approaches since the CAD models present full solid infill with perfectly shaped elements [37]. Some attributes commonly added to the FE models include variable strut diameters, centroid deviations, and varying cross-section shape [38].

2.9 Mechanical testing on cellular structures

To fully characterize a structure, it is necessary to obtain experimentally all its mechanical properties like Young's modulus, yield strength, and Poisson's ratio. These properties can be obtained by testing the materials in the laboratory using different mechanical testing machines (see Fig.5). There is a lack of standards in the testing of cellular solids. The most debatable factor is the amount of unit cells it is necessary to properly characterize the mechanical properties of these cellular arrays. Authors proposed different configuration in the number of unit cells repeated along the two or three axes. It has been previously stated that the higher the number of unit cells, the more accurate the mechanical testing will describe the response of these structures. As the number of unit cells increase, the cell size effect is reduced and more reasonable conclusions may be obtained [10]. Next, there are presented the most common mechanical testing found in the literature review that researchers use in order to characterize the mechanical response of metamaterials:

- *Tensile and compressive test*

Tension and compression responses are very important characteristics in any material. When evaluating these mechanical properties, you can understand the behavior of the material to utilize it in a new design for a specific application. The universal testing machine is one of the most used techniques by researchers to

calculate the tension and compression response of different metals or polymers like ABS.

- *Split-Hopkinson pressure bar*

SHPB or Kolsky apparatus is a popular technique which measures the dynamic stress-strain response of materials. The test consists in the positioning of a specimen between the ends of two straight bars; a stress wave is created which propagates through the bar toward the specimen. Most modern setups use strain gauges on the bars to measure strains caused by the waves.

- *Charpy impact test*

Also known as the Charpy V-notch test is a standardized high strain-rate test which determines the amount of energy absorbed by a material during fracture. It differs from the Izod impact test because Charpy's sample is held in a cantilevered beam configuration as opposed to a three-point bending configuration.

- *Drop-weight impact test.*

The drop-weight impact test method consists in the drop of a macroscopic particle in vertical direction guided by a tube or rails that strikes a sample of the testing material. Knowing the height and weight, the energy absorption during impact can be calculated. Amer Beharic et al. [39] applied this technique to investigate the performance of sandwich structures (with different cellular core designs) under low energy impact and demonstrated that the geometry of the cellular cores affects directly the performance in the energy absorption process. Shepherd et al. [40] tested 3D printed TPU auxetic lattices using flat and hemispherical hammers to characterize their energy absorption ability in order to be used as impact absorbers in sports applications.

- *Izod impact test.*

The Izod impact test measures a material's toughness (capacity to absorb energy). It consists of a pivoting arm is raised to a specific height and then released against a notched sample, breaking the specimen. It is a very common technique used by many authors like X.Y. Xu et al. [41] who studied the mechanical properties and deformation behavior of Acrylonitrile Butadiene Styrene (ABS) blends at different strain rates.

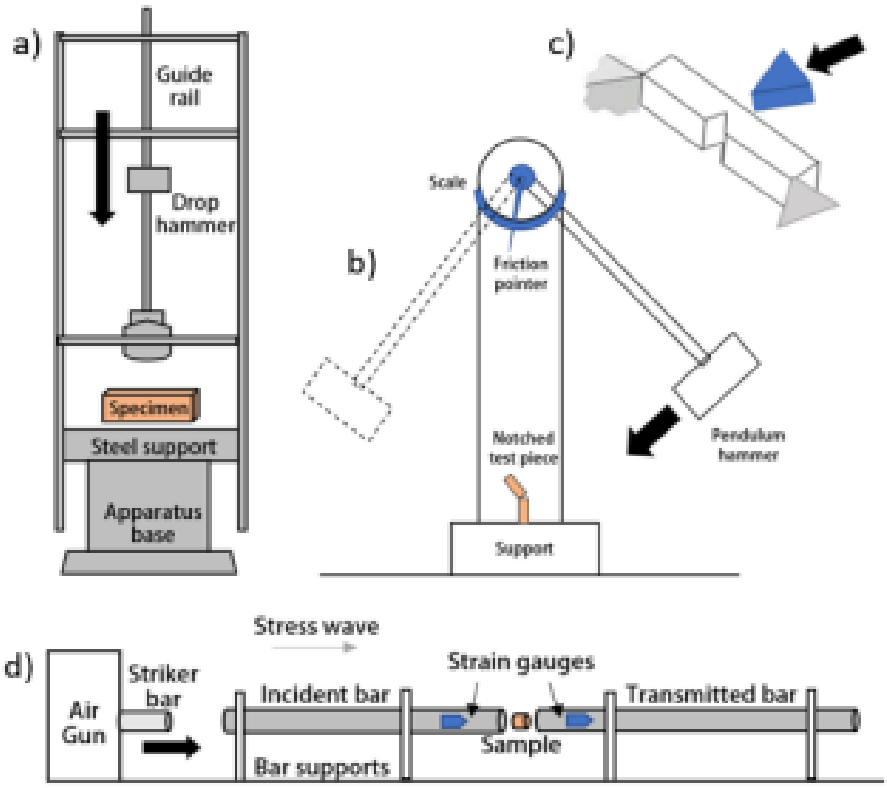

Figure 5. Impact resistance tests: (a) drop-weight test, (b) Izod impact test, (c) Charpy V-notch test, (d) Split-Hopkinson bar test

.

Chapter 3: Apparent elastic modulus of scaled up reentrant honeycombs.

As the first step in this research project, the selection of the manufacturing process is analyzed. This chapter presents a study of the effect of the manufacturing process on the mechanical response of three scaled up reentrant honeycomb cellular solids. It is known that by keeping the same topology, same relative density, and same material, structures with different sizes must exhibit the same apparent elastic modulus under compressive loadings. To demonstrate how the fabrication technique may vary the apparent elastic modulus of scaled up structures, three samples were proposed and fabricated. Compressive testing was carried out on three replicates for each design and results were obtained. Differences appear in the apparent elastic modulus, which can be attributed to the accuracy of the fdm 3D printing process. Simulations of the mechanical testing were also carried out to make comparisons.

3.1 Geometric modeling

The topology studied in this work is called “reentrant honeycomb”, which is a variation of a regular hexagon but with the difference that the oblique elements are inclined inwards. The unit cell is fully described by four main parameters:

1. Cell-wall thickness, t
2. Length of vertical elements, h
3. Length of inclined elements, l
4. Angle between vertical and inclined elements (commonly known as “reentrant angle”), Θ.

The vertical side elements of the unit cell are designed with half the thickness of the others to avoid elements with double cell-wall thickness when the cell is repeated along the X axis. This will allow that once the cells have been repeated, all the elements possess the same thickness, except for those found at both ends of the cellular solid structure. The unit cell for the reentrant honeycomb topology is presented in Fig.6.

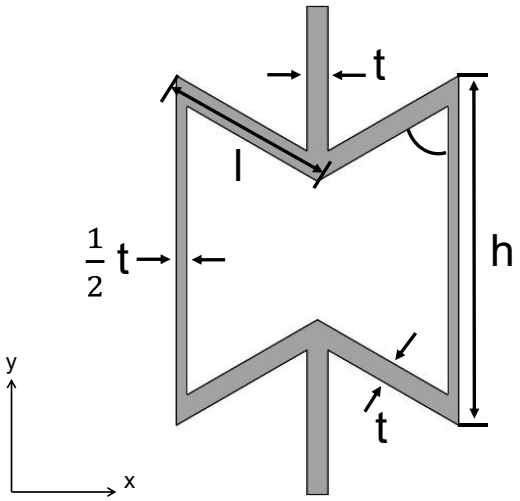

Figure 6. Reentrant honeycomb unit cell.

For this section, it was designed a unit cell with h, l, Θ, and t of 10 mm, 5 mm, 60°, and 1 mm, respectively. The unit cell was replicated five times along the X axis, and three times along the Y axis to form an array. To create other two models, this array was scaled up 1.5 and 2 times bigger than the original. The CAD samples are presented in Fig. 7. Samples were assigned with letters a, b, and c, for the original, 1.5X scaled up, and 2X scaled up samples, respectively. The dimensions and relative density of the three models is presented in Table 1. It can be demonstrated that by scaling up the original topology, the relative density is kept constant.

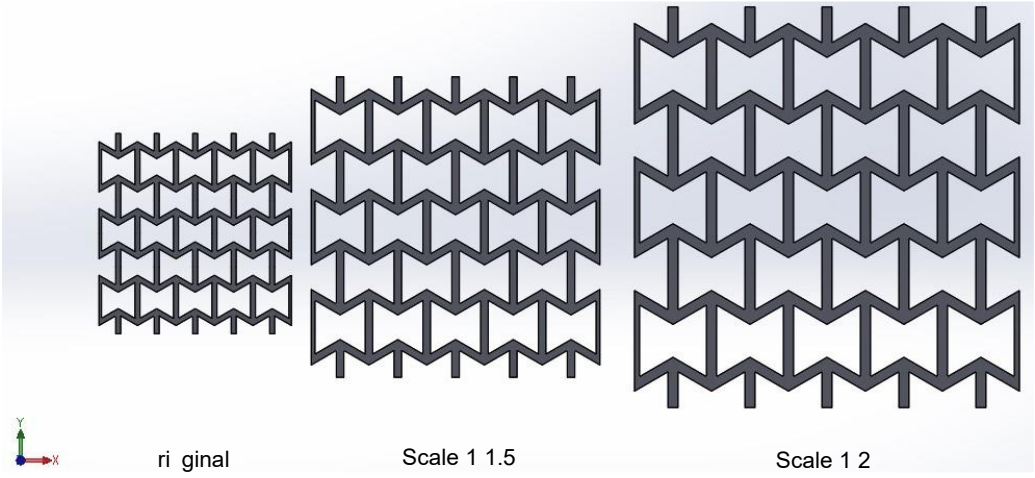

Figure 7. Scaled up reentrant honeycomb structures.

Table 1. Data of the scaled up models.

Sample	Length [mm]	Height [mm]	Depth [mm]	Relative density
a	38.30	39.80	13.33	0.319
b	57.45	59.70	20	0.319
c	76.60	79.60	26.66	0.319

3.2 Simulation stage

To simulate a compressive mechanical testing, each sample was studied using finite element analysis in SolidWorks. For the testing, the boundary conditions (see Fig. X) were configured as follows:

- A force of 10 Newtons was applied in the top faces equally distributed,
- The bottom faces were fixed,
- The constituting material was PLA,
- A probe on the top face was added to calculate the longitudinal deformation.

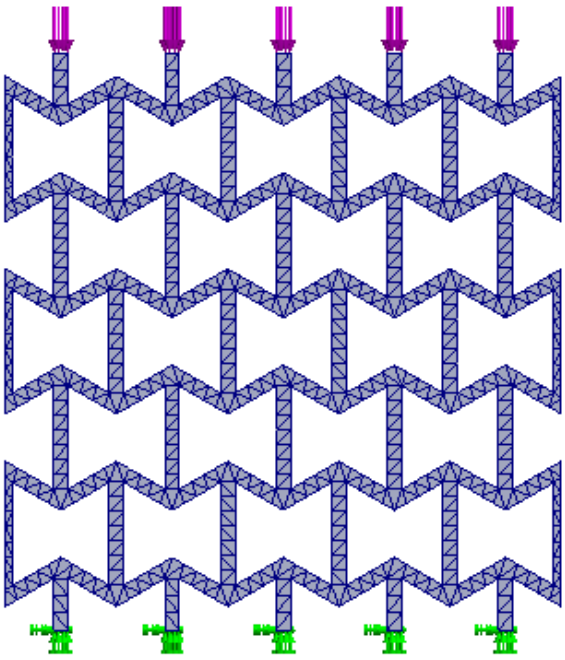

Figure 8. Boundary conditions for the FEA of scaled up reentrant honeycombs.

3.3 Experimental stage

- CURA slicing

The CAD models were converted to STL files and exported to the CURA 4.9.1. software. The infill density and layer thickness were 100% and 0.2 mm, respectively. Captures of the sliced models are presented in Fig. 9.

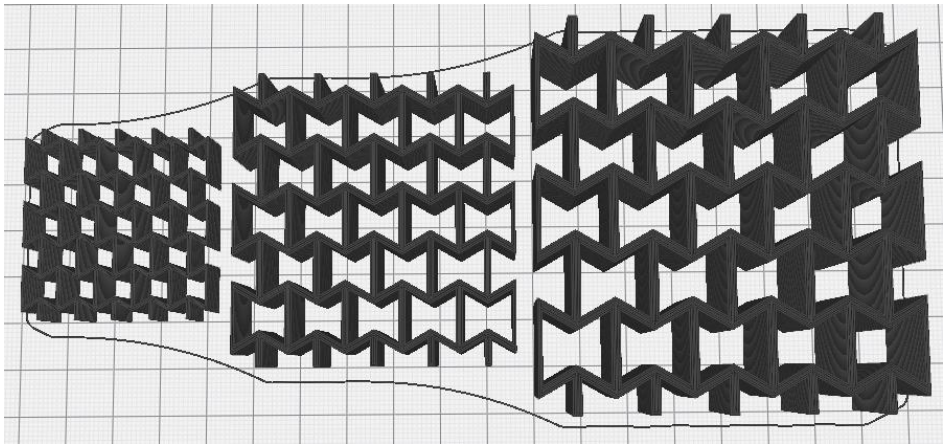

Figure 9. CURA sliced models of the three different scaled up reentrant honeycombs.

By analyzing a single unit cell of the three different structures, it can be identified the creation of empty spaces between line contours (see Fig. 10). This is due to the different sizes of the cell-wall thickness which must be divided by the nozzle diameter. If a comparative inspection is made, it is clearly noted that the smallest sample presents the higher number of voids inside the structure; this is going to affect the results since it is expected that specimens would be fully solid on the inside.

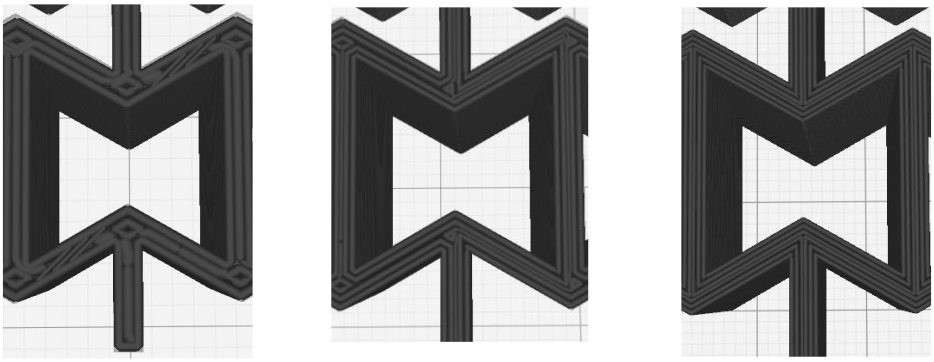

Figure 10. Images taken from CURA slicer of a unit cell for sample: a (right), b (medium), and c (left).

- Fabrication of samples

Three replicates were fabricated for each different CAD model in the 3D printer Ultimaker S3 which uses the fused deposition modeling technique. The samples were manufactured with filament rolls of black PLA. The fabricated specimens are presented in Fig. 11.

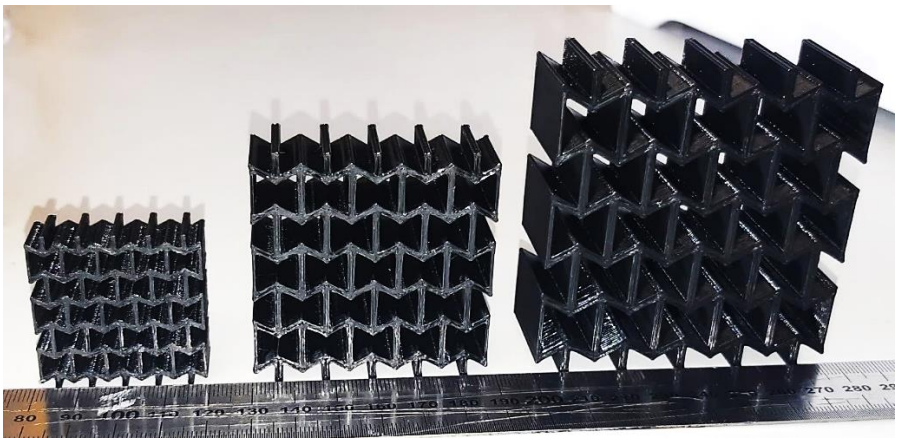

Figure 11. Printed specimens of scaled up reentrant honeycombs made of PLA.

- Mechanical testing

The samples were compressed at a strain rate of 4 mm/min up until 50% of their original heights. Before each test, the specimen was placed between two solid plates, as presented in Fig. 12. The top plate was positioned so it slightly touches the top faces of the specimen and the zero was configured at that position. Nine tests were carried out (3 samples, 3 replicates). Load and displacement data was obtained.

Figure 12. Set up for compressive test on PLA reentrant honeycomb samples.

3.4 Results

3.4.1 Simulation results

The longitudinal displacements for each model are presented next. To estimate the apparent elastic modulus, the apparent stress and strain must be calculated. The apparent stress results from dividing the force by the cross-sectional area. For the strain, the displacement obtained in the simulation is divided by the original height of the model. The apparent elastic modulus for all three scaled up reentrant honeycombs are presented in Table 2.

Table 2. Apparent elastic modulus of scaled up reentrant honeycombs.

Sample	Displacement [mm]	Stress [MPa]	Strain	Apparent elastic modulus [MPa]
a	0.0102	0.0195	0.000256	76.3
b	0.0067	0.0087	0.000113	76.4
c	0.0051	0.0048	0.000064	76.3

After analyzing the FEA results of three reentrant honeycomb structures with same topology and same relative density, it is demonstrated that all exhibit an apparent Young's modulus of 76 MPa. Perhaps bigger samples require higher compressive forces and suffering higher longitudinal displacements, this is compensated with the higher cross-sectional and heights that they present.

3.4.2 Experimental results

Load-displacement curves of samples a1, b1, and c2 are presented in Fig. 13 to observe the mechanical performance. They were specifically selected since they best described each group.

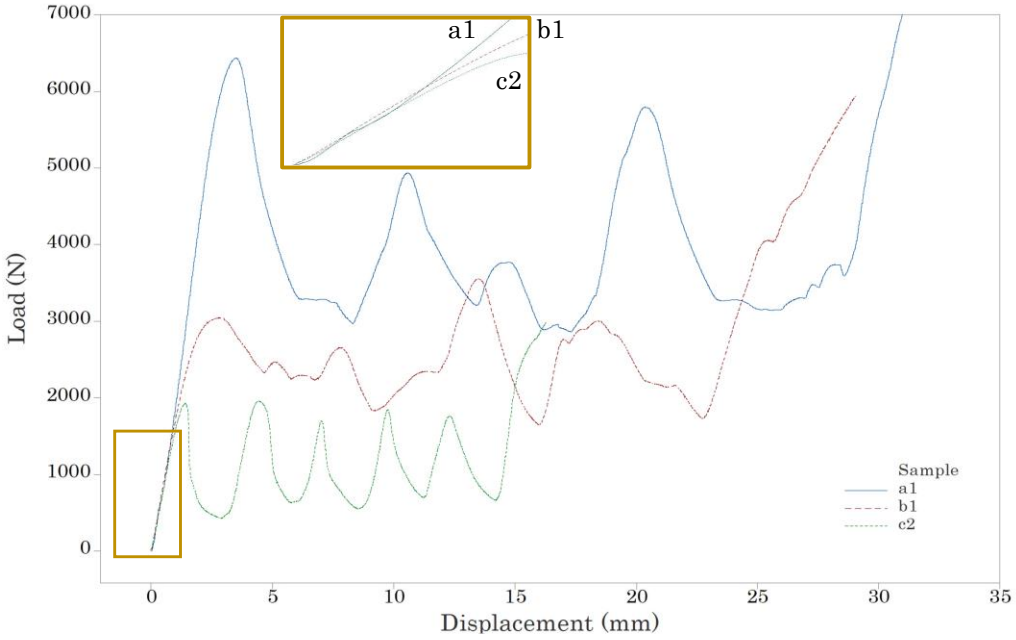

Figure 13. Load vs. displacement experimental results of samples a1, b1, and c2.

Figures 14-16 present the stress-strain curves for scaled up reentrant honeycomb structures fabricated with PLA filaments. Results of the three replicates are presented in each graph.

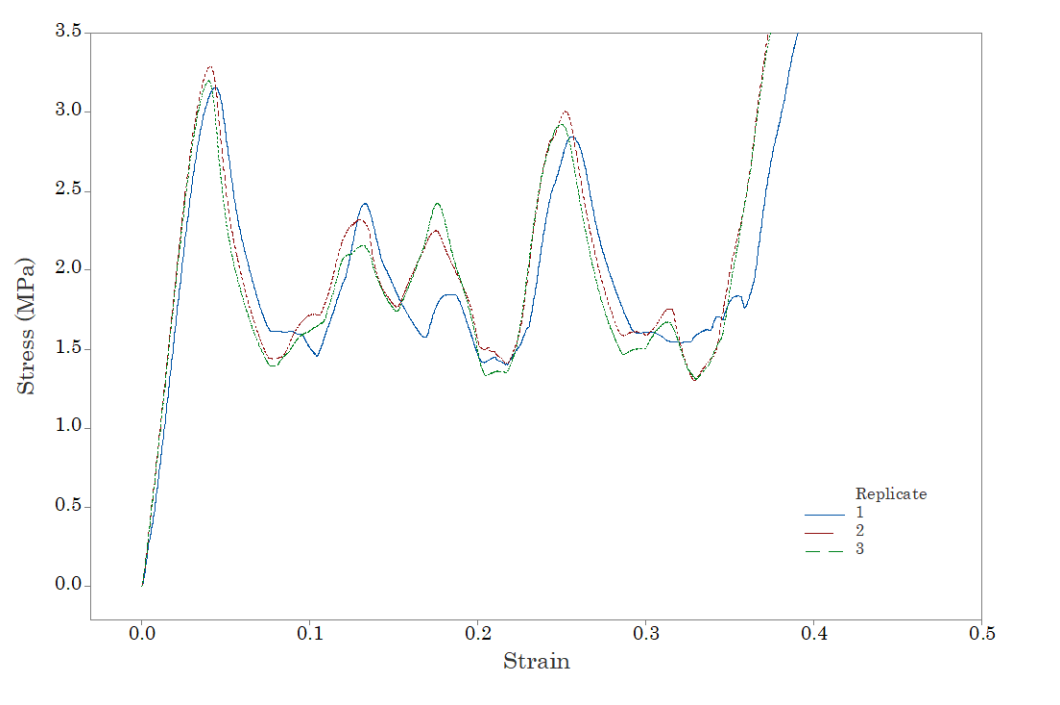

Figure 14. Stress vs. strain curve of PLA reentrant honeycomb sample "a" with three replicates.

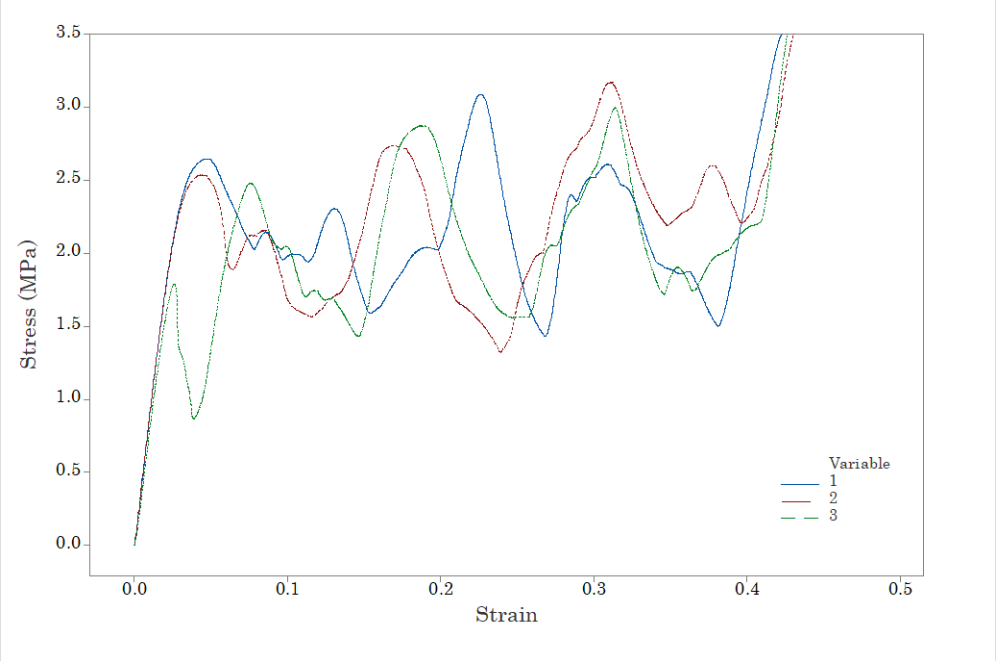

Figure 15. Stress vs. strain curve of PLA reentrant honeycomb sample "b" with three replicates.

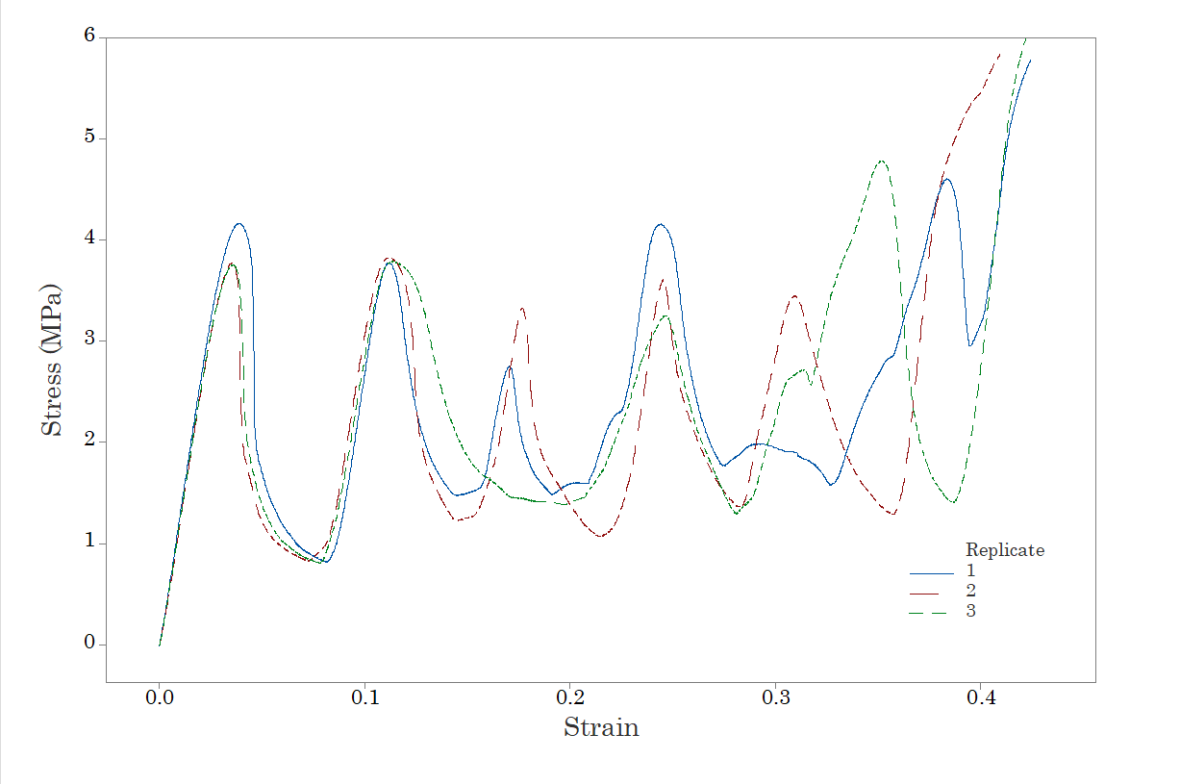

Figure 16. Stress vs. strain curve of PLA reentrant honeycomb sample "c" with three replicates.

To obtain the apparent elastic modulus of each 3D printed specimen, the data included in the linear stage was analyzed. Applying a linear regression model, the slope of the curve formed by that set of data was found. Results are presented in Table 3.

.

Table 3. Apparent elastic modulus of scaled up reentrant honeycombs with average and standard deviation of the three replicates.

Sample	Replicates			Mean	Standard deviation
	1	2	3		
a	87.82	97.10	95.09	93.33	4.88
b	86.60	85.18	81.43	84.40	2.67
c	132.8	127.3	127.5	129.2	3.11

*All values are in MPa

3.4.3 Conclusions

This set of experiments help to demonstrate the feasibility of fabricate cellular solids using the fused deposition modeling technique. Simulation results proved the hypothesis that samples with the same topology and relative density exhibit the same apparent elastic modulus. Truth is this only happens in perfectly shaped models simulated computationally. The fabrication and testing of reentrant honeycombs scaled up specimens did not show the same results. Even though, all samples should exhibit the same apparent elastic modulus, results demonstrated that samples “c” presented the highest Young’s modulus with an average of 129.2 MPa. This can be interpreted as that these structures suffer higher internal stresses to exhibit the same strain when compared to the other groups (“a” and “b”).

These differences may be attributed to the defects due to the manufacturing process. The smaller the cell-wall thickness of the cellular solids, the more difficult it gets for the fdm 3D printer to achieve good accuracy. Having as limitation the diameter of the nozzle, sometimes the printed parts include internal voids between the line contours or between the deposited layers. Samples which belong to the group “c” presented significant accumulation of material in different regions which may have made the structures more rigid than what they should be. This extra amount of filament in the specimens could have made the structures stronger since higher forces would be required to compress the cellular solids.

It is recommended to design and carry out a new set of experiments to continue exploring the apparent elastic modulus of scaled up reentrant honeycombs. For the next try, specimens should be analyzed before the testing. Length and thickness of the elements can be measured using a vernier caliper or digital scanning to assess the accuracy of the printing process. A scanning electronic microscope could also be used to observe the microstructure inside the cellular solids. By analyzing the printed layers and material distribution at a microscopic level, it is easier to establish some conclusions based on the experimental results.

Chapter 4: Mechanical response and energy absorption ability of 3D printed thermoplastic polyurethane reentrant honeycombs.

The mechanics of additively manufactured cellular solids are experimentally investigated in this research work via mechanical tests. Once the fdm process was better comprehended, now it is time to analyze the mechanical response of the reentrant honeycomb topology fabricated using the aforementioned manufacturing process. To study the effect of relative density on compressive behavior of reentrant honeycomb metamaterials, different samples are designed using a CAD software and then 3D printed using the fused deposition modeling technique. For this second set of experiments, the material proposed is thermoplastic polyurethane since it is a more flexible material, and it may be helpful to fabricate more resilient samples. The design and fabrication of compliant cellular solids may be helpful to propose new applications where they can be subjected to constant compressions or impact forces. To test their ability to withstand multiple compressions, it is proposed to apply cyclic compressive tests on the fabricated samples. Load-displacement data for each test is captured and plotted to observe the mechanical response of the auxetic structure and its deformation mechanism. The apparent elastic modulus and energy absorption ability for each structure is obtained and analyzed. The approach adopted in this project is presented in the flow chart in Fig. 17.

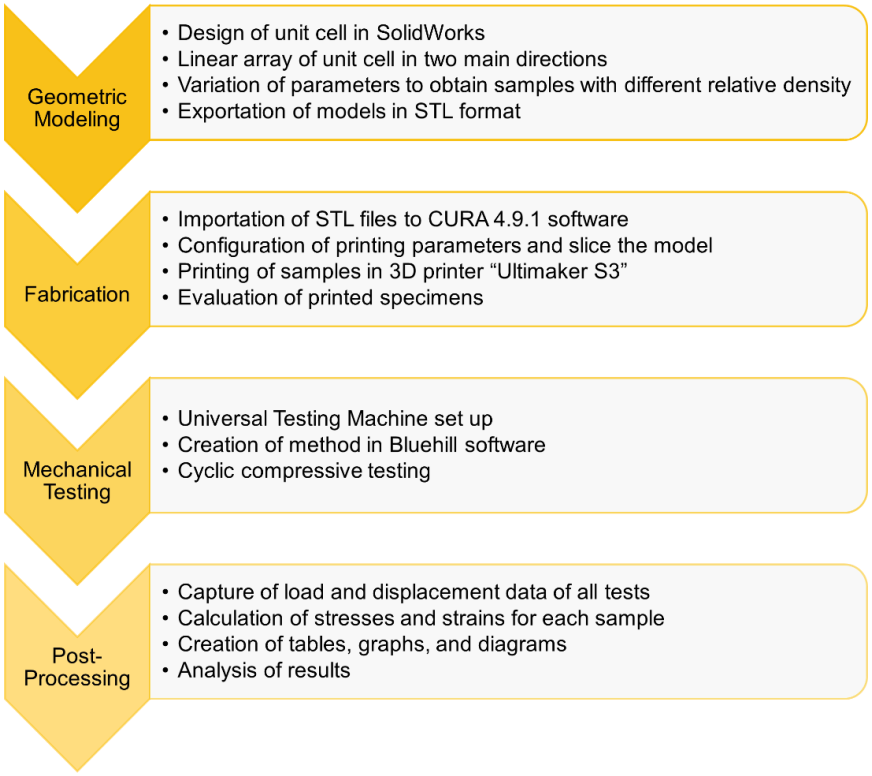

Figure 17. Methodology flow chart.

4.1 Geometric Modeling

- Unit cell design

To obtain unit cells with different relative density it is necessary to change any of these previously mentioned geometric parameters. In this case, it is selected to vary the cell-wall thickness. Five different values of thickness were selected among the range of 0.6 and 1.4 mm. The five different unit cells are presented in Fig 18.

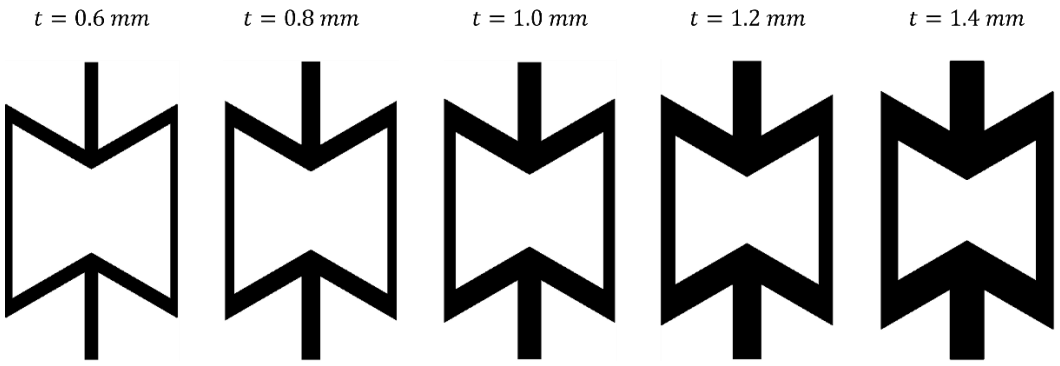

Figure 18. Unit cells with varying cell-wall thickness.

- Cellular array

Once the five different unit cells are modeled, it is necessary to replicate them in linear arrays to form the structures. The number of repeated unit cells in both directions depends on the author, but it has been stated that higher number of unit cells describe better the behavior of cellular solids. Since the samples will be subjected to compressive loads, it is important to design structures with higher length (L) when compared to their heights (H); this, to avoid or reduce the effect of global buckling of samples during compressions and diminish the effects of vertical free boundaries on the global compressive behavior.

Since the topology's mechanical response will be studied in both main directions, two different arrays of unit cells are proposed. To study the first direction, structures with 8 x 3 unit cells array were created using the linear pattern tool in SolidWorks. For the second direction, structures with 5 x 5 arrays were created. The ten different samples are presented in Figure 19. To identify them in an easier way, they were named using a code with a letter for the two different directions, and a number for the five different cell-wall thicknesses. For example, the model V0.6, represents the vertical array (8 x 3 unit cells) with the cell-wall thickness of 0.6 millimeters.

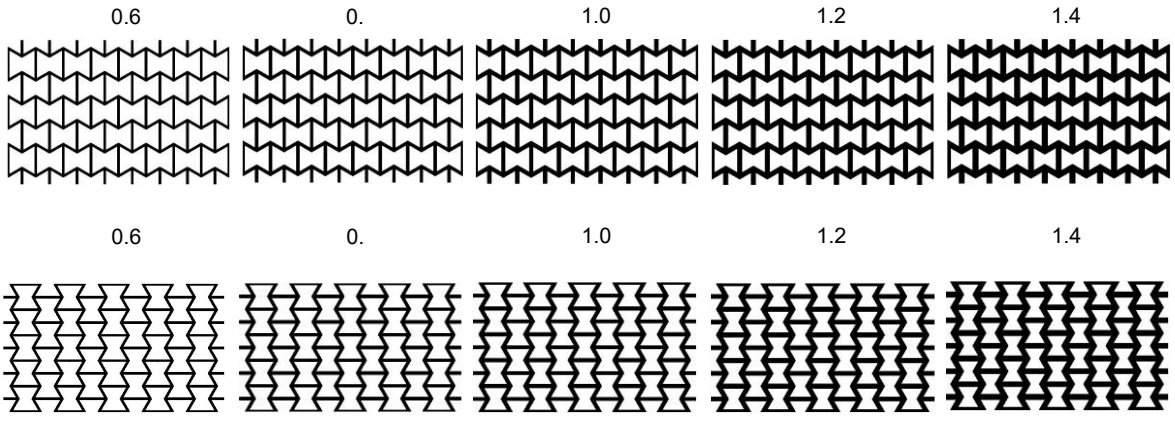

Figure 19. CAD models with different cell-wall thickness and number of unit cells.

- Relative density

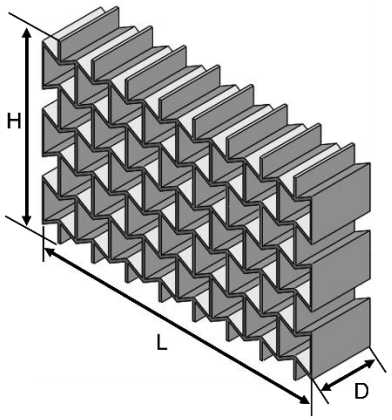

Figure 20. Isometric view of samples.

The relative density, or volume fraction, is described by the ratio between the solid volume ($\boldsymbol{V_s}$) and the external volume ($\boldsymbol{V_e}$) it occupies each sample. The solid volume is obtained by evaluating the sample in SolidWorks software; it gives you the amount of material in cubic millimeters used in the model. The external volume refers to the cuboidal space occupied by the sample, and it is calculated by multiplying the length, height, and depth of the sample (see Fig. 20), according to the following equation:

$$\boldsymbol{V_e = L \times H \times D}$$

Calculation of the relative density follows the next formula:

$$\boldsymbol{\bar{\rho} = \frac{V_s}{V_e}}$$

Here it is presented, as an example, the procedure to calculate the relative density for sample V0.6:

1. The solid volume is obtained from the SolidWorks evaluate tool. It has a total of 7156.13 mm^3.
2. The three dimensions of the sample are measured to obtain the external volume. The model size is 64.48 x 41.88 x 14 millimeters (see Fig. 21).

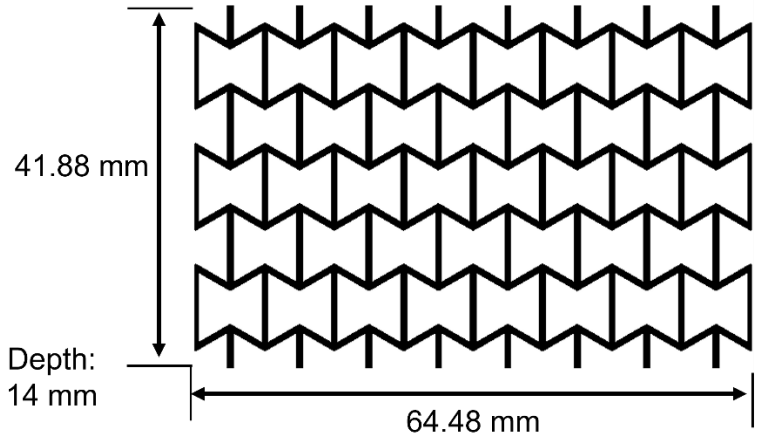

Figure 21. Dimensional measurement of sample V0.6

3. The external volume is calculated:

$$\boldsymbol{V_e = L \times H \times D = 64.48\ mm \times 41.88\ mm \times 14\ mm = 37,805.91\ mm^3}$$

4. The relative density is calculated:

$$\boldsymbol{\bar{\rho} = \frac{V_s}{V_e} = \frac{7156.13\ mm^3}{37805.91\ mm^3} = 0.189}$$

The same procedure is applied to all different samples. Results on relative density are presented in Table 4.

Table 4. Relative density of samples with different cell-wall thickness.

Sample	L (mm)	H (mm)	D (mm)	V_s (mm^3)	V_e (mm^3)	$\bar{\rho}$
V0.6	64.48	41.88	14	7156.13	37805.91	0.189
V0.8	62.88	40.84	14	9138.01	35952.27	0.254
V1.0	61.28	39.8	14	10918.13	34145.22	0.320
V1.2	59.68	38.76	14	12496.51	32384.76	0.386
V1.4	58.08	37.64	14	13859.39	30605.84	0.453
H0.6	69.80	40.3	14	7454.30	39381.16	0.189
H0.8	68.07	39.3	14	9518.76	37452.11	0.254
H1.0	66.34	38.3	14	11373.06	35571.51	0.320
H1.2	64.61	37.3	14	13017.20	33739.34	0.386
H1.4	62.73	36.3	14	14436.86	31879.39	0.453

It can be observed in Table 4 that samples with same cell-wall thickness exhibit the same relative density. This is because independently of the unit cell array, the topology is kept constant for both types of samples (V and H).

Lastly, all models are exported from SolidWorks as STL files.

4.2 Fabrication of samples

The reentrant honeycomb structures in this work were manufactured via 3D printing using the Ultimaker S3 Original desktop 3D printer shown in Fig.22. This 3D printer uses the fused deposition modeling technique. The samples were made of thermoplastic polyurethane. Filament used was Ultimaker Black TPU 95A which has a density of 1.22 g/cm^3.

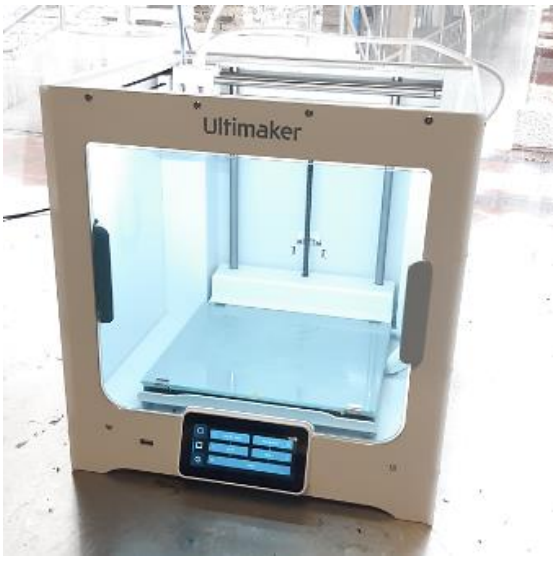

Figure 22. 3D printer "Ultimaker S3".

- 3D printer set up

The STL files for all ten different structures were imported in software CURA 4.9.1. to make the printing parameter configuration and slicing. Printing parameters were either proposed by the software or selected by the author to optimize the material and time of fabrication. In Table 5 are presented all the printing parameters used to manufacture the structures.

Table 5. Printing parameters.

Printing Parameter	Value
Layer height	0.2 mm
Line width	0.4 mm
Nozzle diameter	0.4 mm
Infill density	100 %
Extruding temperature	225 °C
Bed temperature	85 °C
Print speed	25 mm/s

After setting all the printing parameters in CURA, each model is sliced to observe how the material will be deposited in the heating bed (see Fig. 23). The final accommodation of the ten different samples in the CURA software is demonstrated in Fig. 24 with a manufacturing time of approximately 17 hours, according to the software.

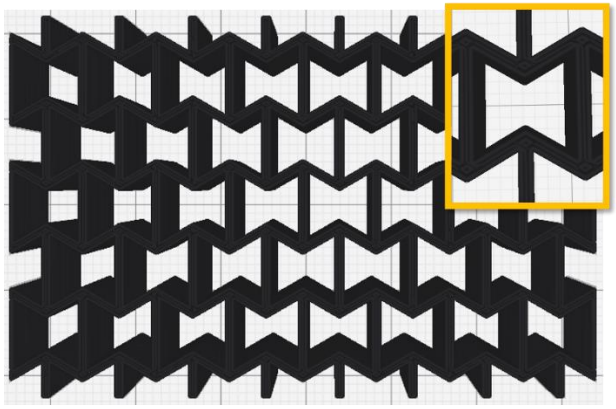

Figure 23. CURA sliced model. Image includes a zoom on a unit cell to observe the line contours required to achieve the cell-wall thickness.

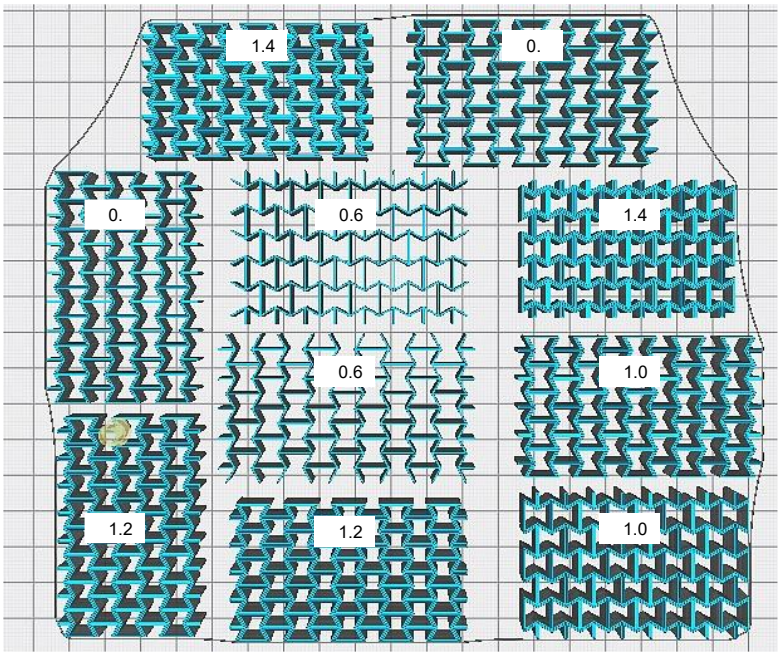

Figure 24. Accommodation of the structures on the printing bed of the Ultimaker S3.

- 3D printing

The ten different samples were accommodated on the printing area of the machine so they can be fabricated at the same time, as seen in Fig. 25. Three replicates of the samples were produced to study the repeatability of the experiments. An overview of the 3D printed models is presented in Fig. 26.

Figure 25. Printing process of reentrant honeycomb structures.

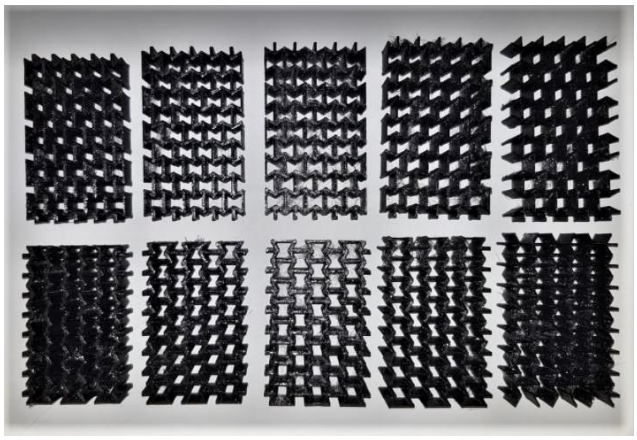

Figure 26. Additively manufactured reentrant honeycomb structures.

- Accuracy of manufacturing process

One of the main disadvantages in additive manufacturing, specifically in the fused deposition modeling technique, is its poor print quality to replicate relatively small geometries. In the case of printing cellular solids or lattice structures, it is difficult to manufacture elements with perfect geometries and sharp ends. Next, some common errors that occurred during the printing process of reentrant honeycomb structures are shown. In Fig. 27, it can be observed the shape accuracy presented in the printed specimens where the most common problem was the creation of round ends instead of sharp ends in the connection of two or more elements.

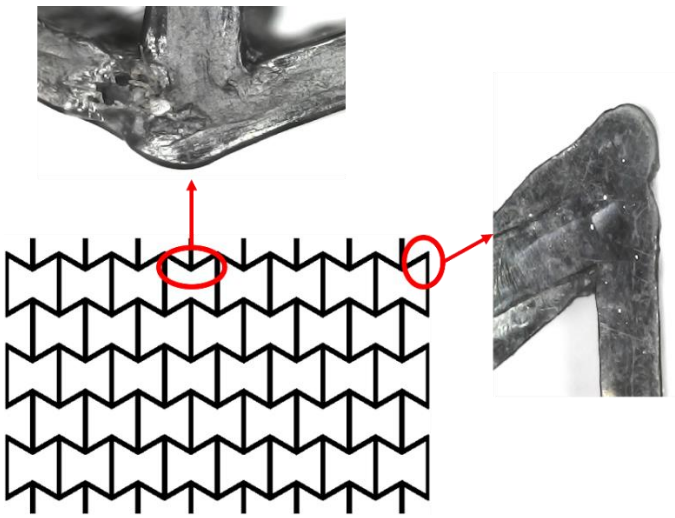

Figure 27. Shape accuracy of manufacturing process.

Another important problem during the fabrication of samples was the lack of some printed struts as shown in Fig. 28. This issue occurred in the samples with the lowest relative density (V0.6 and H0.6) due to their low cell-wall thickness. Since these samples have a cell-wall thickness of 0.6 millimeters, some of their elements would be half of it (0.3 mm) which make it impossible to print since the diameter of the nozzle used in the Ultimaker S3 is 0.4 millimeters. This restriction has a consequence that two of the ten printed specimens will be slightly different when compared to their respective CAD model.

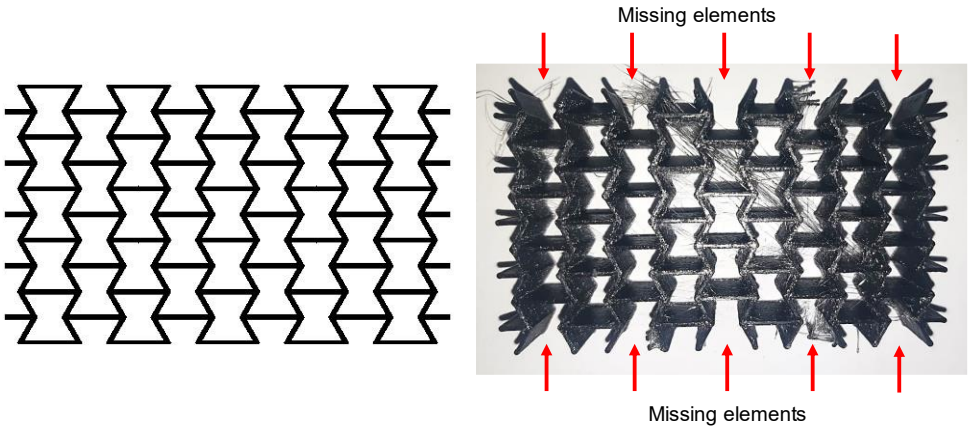

Figure 28. Missing elements on printed specimen.

As it can be observed in Fig. 29, some samples required a post-processing to try to remove extruded material residues that were deposited by the nozzle during its continuous path. The presence of these thin strands of material can be reduced or eliminated by optimizing the nozzle path or extrusion temperature.

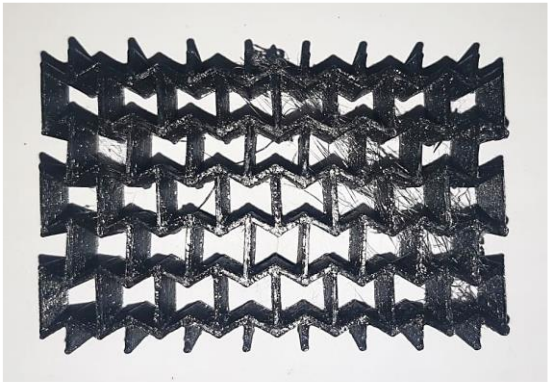

Figure 29. Extruded material residuals in printed samples.

- Variation of relative density

The precision of the 3D printing process to fabricate polymeric parts may vary due to different factors such as printing speed, printing temperature, humidity, equipment calibration, etc. As consequence, the printed parts commonly exhibit differences from its original model perfectly designed (as presented in the previous section). A way to evaluate the quality of the produced specimen is by comparing its relative density against the one calculated previously with the CAD models.

To assess the quality of printed specimens, it was obtained the real relative density by measuring the weight and external volume (as presented in Fig. 30). A digital weight was used to measure the amount of TPU milligrams each structure possessed. The size of all specimens was also evaluated with a Vernier caliper.

Figure 30. Measurement of relative density in printed specimens. The image shows the way of measuring a) mass, b) length, c) height, and d) depth of each sample.

The real relative density ($\overline{\boldsymbol{\rho}}_{\boldsymbol{r}}$) is estimated as the ratio between the amount in cubic millimeters of TPU present in the specimen and the external volume it occupies. To obtain the amount of material, the mass -obtained in the digital weight- is divided by the density of the TPU (1.22 g/cm^3).

Here it is presented, as an example, the procedure to calculate the relative density for sample V0.6:

1. The mass of the sample is obtained (8.9067 grams).

2. The amount of TPU is calculated:

$$V_{TPU} = \frac{m_{TPU}}{\rho_{TPU}} = \frac{8.9067\ g}{1.22\ g/cm^3} = 7.3005\ cm^3 = 7300.5\ mm^3$$

3. The three dimensions of the specimen are measured using the vernier caliper, obtaining a length, height, and depth of 64.80 mm, 41.96 mm, and 13.70 mm, respectively.
4. The external volume is calculated:

$$V_e = L \times H \times D = 64.80\ mm \times 41.96\ mm \times 13.70\ mm = 37250.40\ mm^3$$

5. The relative density of the specimen is obtained:

$$\bar{\rho} = \frac{V_s}{V_e} = \frac{7300.5\ mm^3}{37250.40\ mm^3} = 0.195$$

By comparing this measured relative density of 0.195 with the one obtained by the CAD model (0.189), a manufacturing error of +4% is found. This same procedure is applied to all samples. Measured relative densities for all samples are presented in Table 6.

Table 6. Measured relative density.

Sample	L (mm)	H (mm)	D (mm)	Mass (g)	V_s (mm^3)	V_e (mm^3)	$\bar{\rho}$
V0.6	64.80	41.96	13.70	8.9067	7300.5	37250	0.196
V0.8	63.63	41.10	13.62	9.9791	8179.6	35619	0.230
V1.0	61.54	40.03	13.70	12.4401	10196.8	33749	0.302
V1.2	60.33	38.92	13.99	14.3229	11740.1	32849	0.357
V1.4	58.57	37.70	13.86	16.3519	13403.2	30604	0.438
H0.6	69.95	40.29	13.86	9.5216	7804.6	39061	0.200
H0.8	68.33	39.33	13.75	11.8070	9677.9	36952	0.262
H1.0	66.34	38.46	13.55	12.9100	10582.0	34572	0.306
H1.2	64.55	37.31	14.10	15.0560	12341.0	33958	0.363
H1.4	62.85	36.22	13.77	16.8610	13820.5	31346	0.441

To evaluate the quality of the 3D printing process, a comparative analysis is presented in Table 7 to see differences between CAD models and printed parts. The results obtained by measuring the samples were compared against the relative density of the perfectly modeled CAD designs and it was observed relatively low differences between each pair of samples. The manufacturing error is

placed in a range between -6% and +5% of difference between the relative densities. This can be attributed to the accuracy of the manufacturing process which fabricates samples with empty spaces between layers or leaves extra strands of extruded filaments in places where it is supposed to be a void because of the nozzle temperature that melts the filaments during the whole trajectory. This issues in the manufacturing process were presented in previous sections.

Table 7. Assessment of manufacturing quality.

Replicate	Sample	CAD Model	Measured	Error
	V0.6	0.189	0.187	-1%
	V0.8	0.254	0.258	1%
1	V1.0	0.320	0.316	-1%
	V1.2	0.386	0.385	0%
	V1.4	0.453	0.438	-3%
	V0.6	0.189	0.187	-1%
	V0.8	0.254	0.258	1%
2	V1.0	0.320	0.319	0%
	V1.2	0.386	0.384	-1%
	V1.4	0.453	0.439	-3%
	V0.6	0.189	0.189	0%
	V0.8	0.254	0.260	2%
3	V1.0	0.320	0.310	-3%
	V1.2	0.386	0.382	-1%
	V1.4	0.453	0.443	-2%
	H0.6	0.189	0.195	3%
	H0.8	0.254	0.259	2%
1	H1.0	0.320	0.309	-3%
	H1.2	0.386	0.363	-6%
	H1.4	0.453	0.440	-3%
	H0.6	0.189	0.185	-2%
	H0.8	0.254	0.265	4%
2	H1.0	0.320	0.311	-3%
	H1.2	0.386	0.401	4%
	H1.4	0.453	0.442	-2%
	H0.6	0.189	0.197	4%
	H0.8	0.254	0.267	5%
3	H1.0	0.320	0.306	-4%
	H1.2	0.386	0.391	1%
	H1.4	0.453	0.437	-3%

4.3 Mechanical Testing

- Universal testing machine set up

Cyclic compressive testing was proposed for the reentrant honeycomb specimens to estimate the strength of the structures; their ability to withstand multiple compressions up to densification; and obtain the stress-strain profiles of each sample in two different directions to establish a comparative analysis of their ability to absorb energy due to deformation.

Cyclic compressive tests were carried out using the universal testing machine Instron 3365 (shown in Fig. 31) with a 5 kN load cell and maximum speed of 1000 mm/s. The equipment is in Monterrey, Nuevo León, at the “Parque de Investigación e Innovación Tecnológica”.

Figure 31. Universal testing machine Instron 3365.

For the Instron 3365 setup, two steel plates were mounted on both ends of the machine. The inferior plate has a maximum load capacity of 10 kN and has a serial number T489-74. The superior plate has the same load capacity but with a serial number T1223-1022. The final configuration can be observed in Fig. 32.

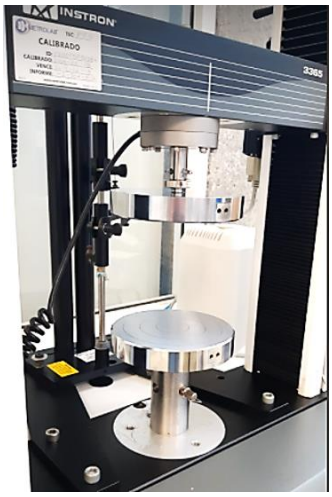

Figure 32. Set up of Instron 3365 with two solid plates mounted.

- Design of method

The creation of the methodology for the cyclic compressive test was carried out using the Instron machine's software Bluehill 3. Five cycles of loading and unloading were configured at a strain rate of 24 mm/min up until full densification. The densification strain was previously calculated for each sample and the method was constantly changing to adapt the displacements with the different samples. It was programmed to export the results for load and displacement in terms of Newtons and millimeters, respectively. The raw data would be saved in Excel worksheets for the post processing of the results obtained.

- Cyclic compressive testing

Before the test, the sample must be placed between the two solid plates, as shown in Fig. 33. The upper plate was positioned so it slightly touches the sample, and the zero for load and displacement was defined. The crushing process was filmed with a 16 megapixels camera to analyze the deformation mechanism.

- Effect of strain rate

A set of experiments was proposed to study the effect of strain rate on the energy absorption capabilities of TPU reentrant honeycombs. These structures are usually tested in quasi-static conditions with relatively low rates up to 10 mm/min. Since it is important to study the mechanical response under impact conditions, higher

strain rates of 50 and 100 mm/min were proposed. For this study, samples V0.8 and V1.4 were selected to analyze the effect of strain rate in compressive tests of cellular solids with low and high relative density.

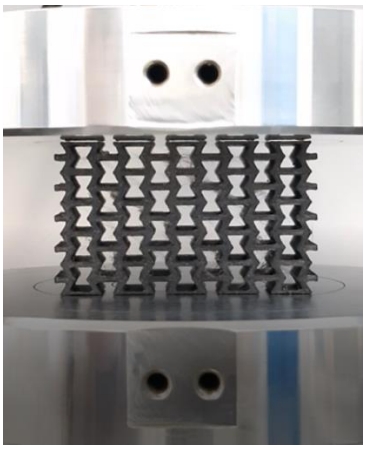

Figure 33. Set up for compression test.

4.4 Results and Discussion

This section presents the results of the mechanical testing on 3D printed reentrant honeycombs fabricated by fused deposition modeling using thermoplastic polyurethane filaments. It shows the load and displacement data obtained and the deformation mechanism exhibited. The stress and strain curves were estimated using the apparent cross sectional area (including the voids), and the height of each specimen. Apparent Young's moduli were calculated and a relationship with the increase of relative density is presented. The absorption of energy in the cellular solids is simply the area under the stress-strain curve up to the densification strain. The amount of energy absorbed in each cycle is calculated and presented for all samples with different relative densities. To explain this, the chapter is divided in five main topics:

- Load and displacement results
- Estimation of apparent Young's modulus
- Relationship between apparent Young's modulus and relative density
- Cyclic compressive behavior
- Energy absorption ability and softening phenomenon.
- Effect of strain rate

- Load vs. displacement results

Results for the first loading cycle of each sample are presented from Figs. 34-43 for both unit cell orientations. These graphs represent the mechanical response of the first replicate for each relative density and include images of the crushing process in different displacement stages to show the deformation process up to the full densification of the cellular solids.

From the results obtained it can be observed that all samples exhibit an initial linear response corresponding to the elastic region of the curve. This stage is defined by the elastic modulus of the material the structure is made of, and by the buckling of the vertical elements. When the elements stop the resistance, the linear stage ends, the force required to continue the compression is reduced, and the plateau stage begins. This plateau region is characterized by a slow variation of the force applied while rows of the cellular material are being crushed one at a time. A more constant and horizontal plateau is observed in the V-type samples, while the H-samples exhibit an irregular plateau stage with lower values of forces when compared to the peak crush force at the end of the linear region.

The strength of the samples increases as the cell-wall thickness increases. When comparing specimens with the same unit cell orientation, it can be observed that the maximum force supported is higher for samples with higher relative density since they possess more amount of material that need to be compressed by the testing machine.

By comparing the strength between structures with same relative density but different unit cell orientation, it is concluded that structures with horizontal elements withstand higher forces. This can be attributed to the fact that horizontal elements create a cross-sectional area with more material which make them more resistant than the other samples were the cross-sectional area is composed by thin vertical elements easy to be buckled.

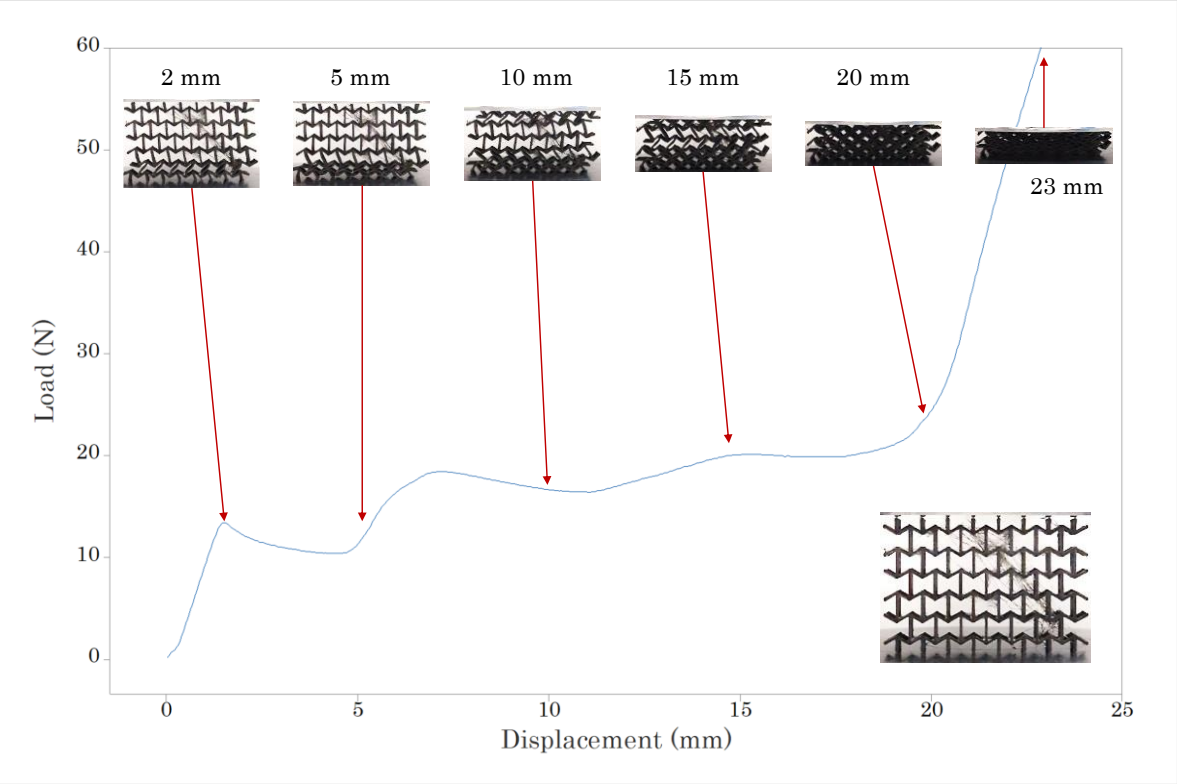

Figure 34. Load vs. displacement curve for replicate 1 of sample V0.6.

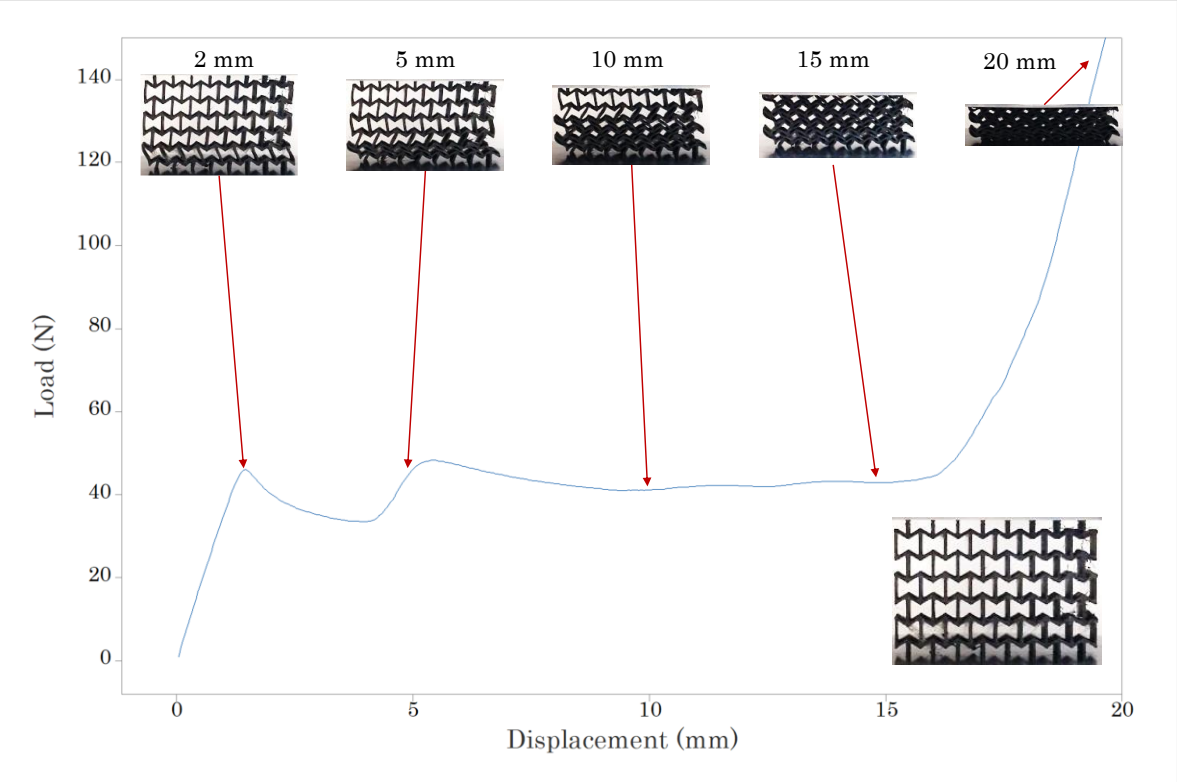

Figure 35. Load vs. displacement curve for replicate 1 of sample V0.8.

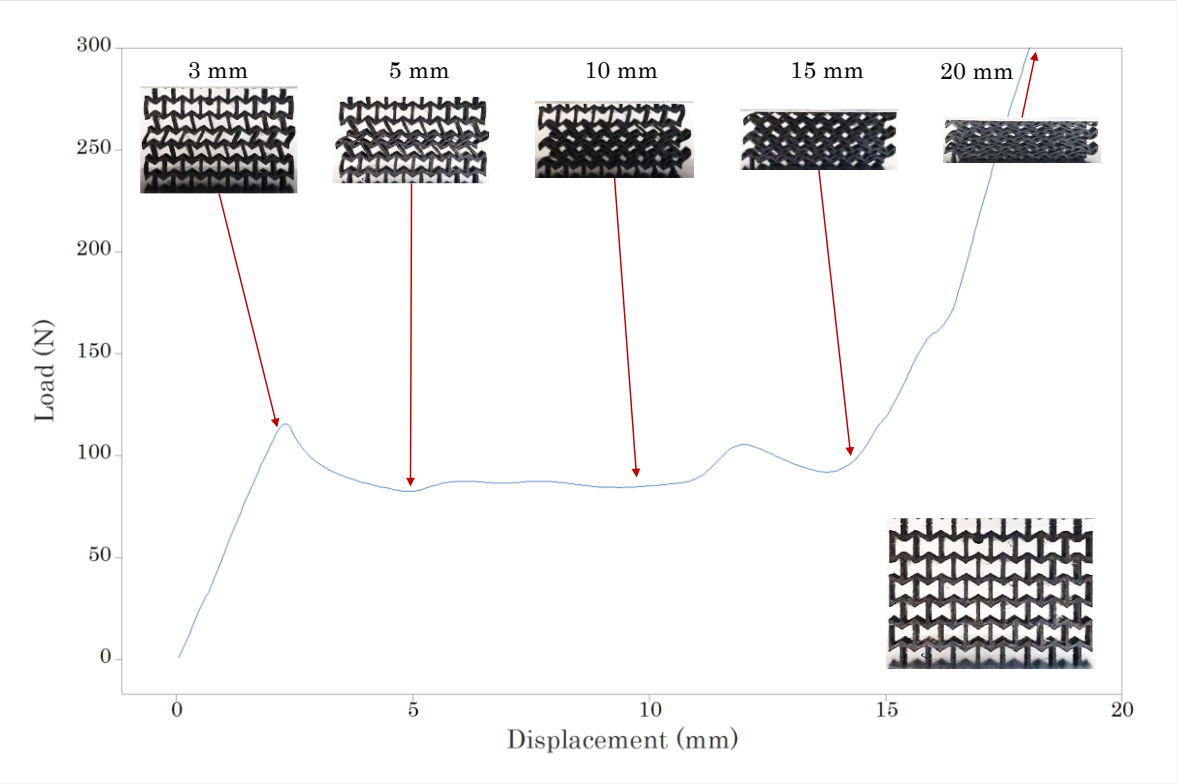

Figure 36. Load vs. displacement curve for replicate 1 of sample V1.0.

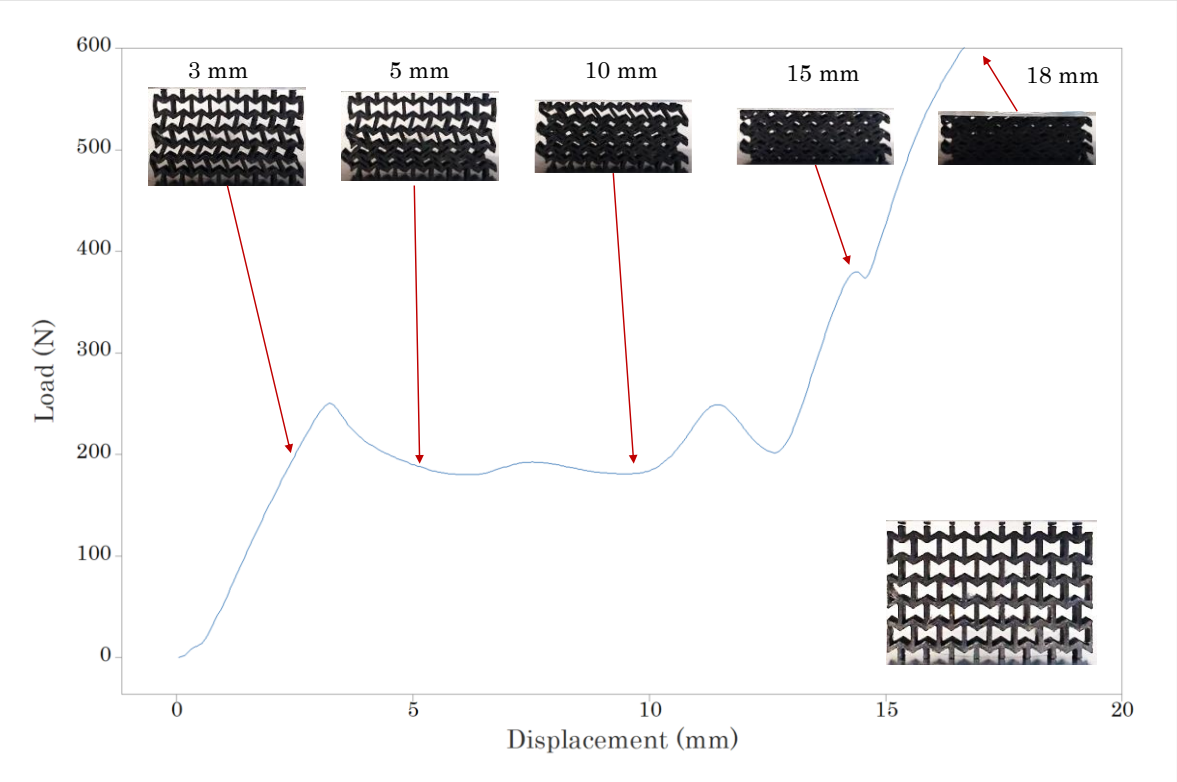

Figure 37. Load vs. displacement curve for replicate 1 of sample V1.2.

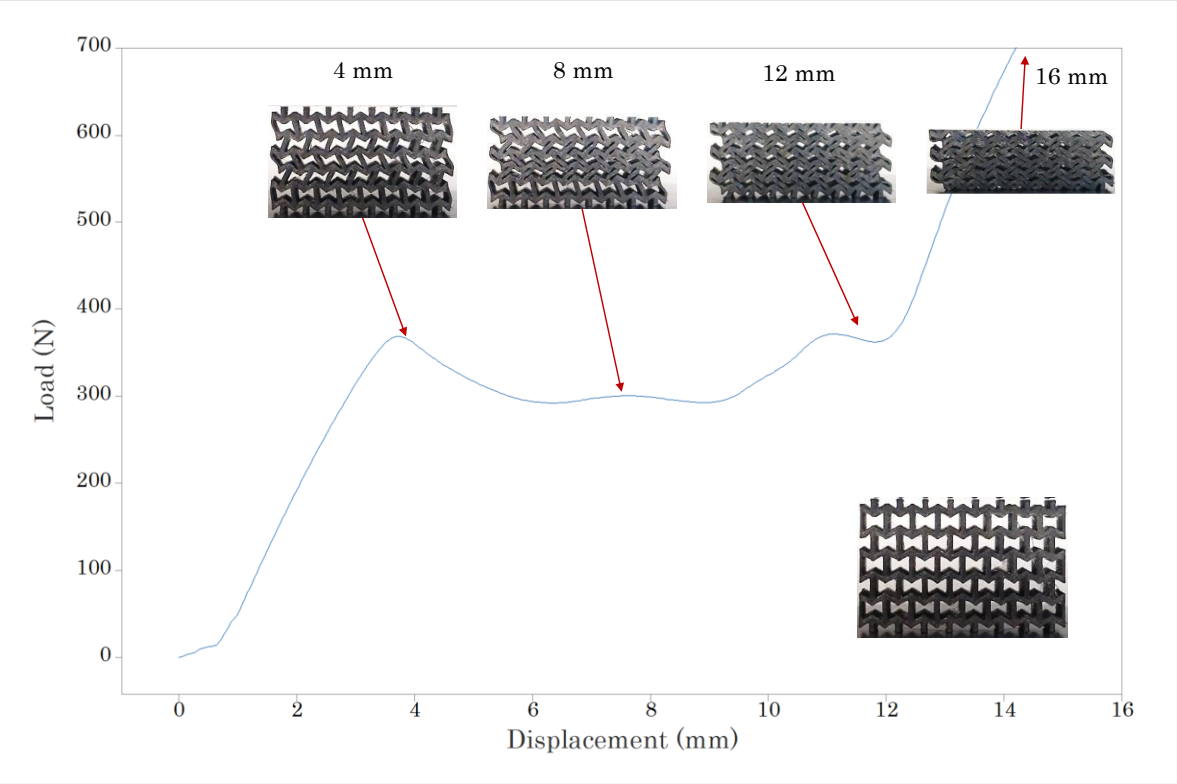

Figure 38. Load vs. displacement curve for replicate 1 of sample V1.4.

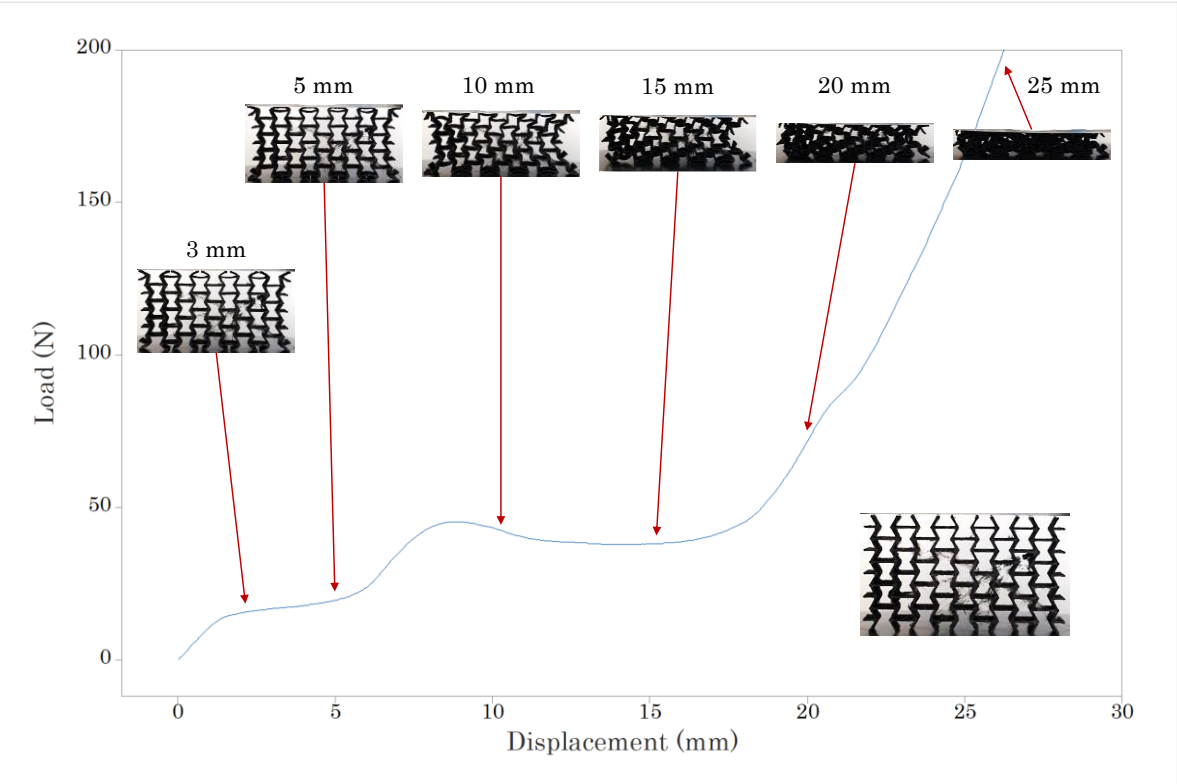

Figure 39. Load vs. displacement curve for replicate 1 of sample H0.6.

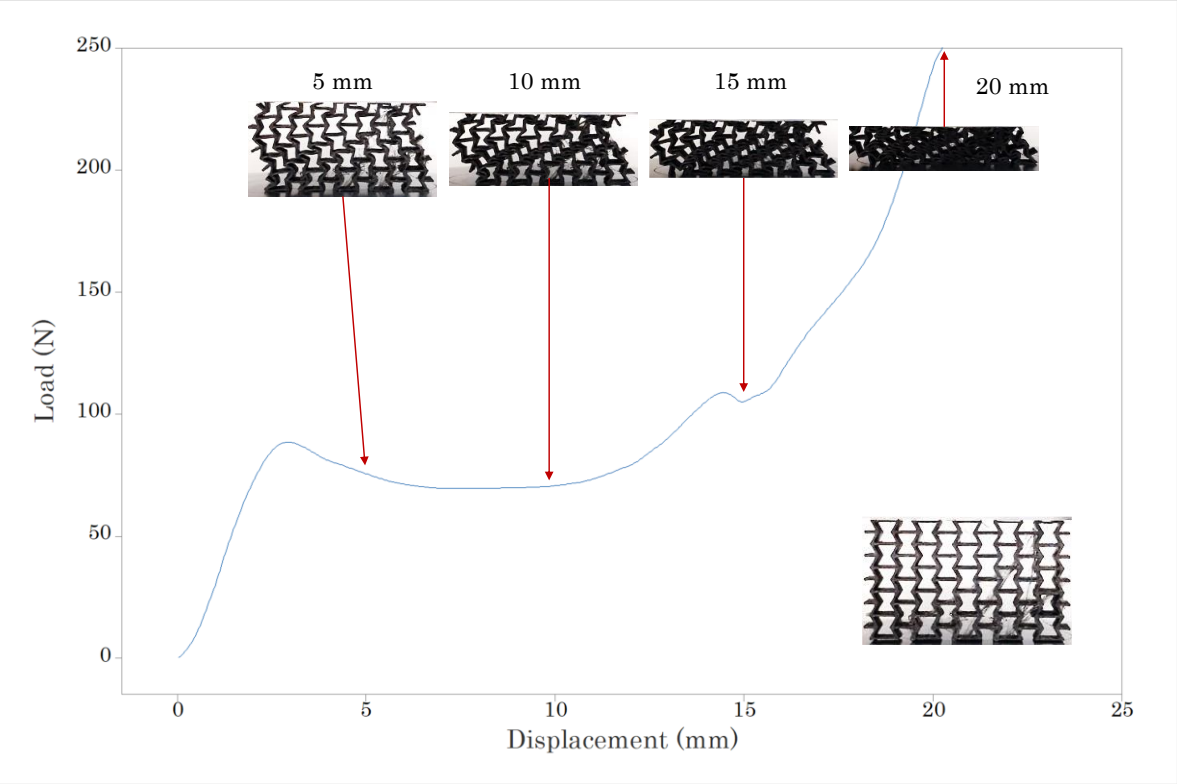

Figure 40. Load vs. displacement curve for replicate 1 of sample H0.8.

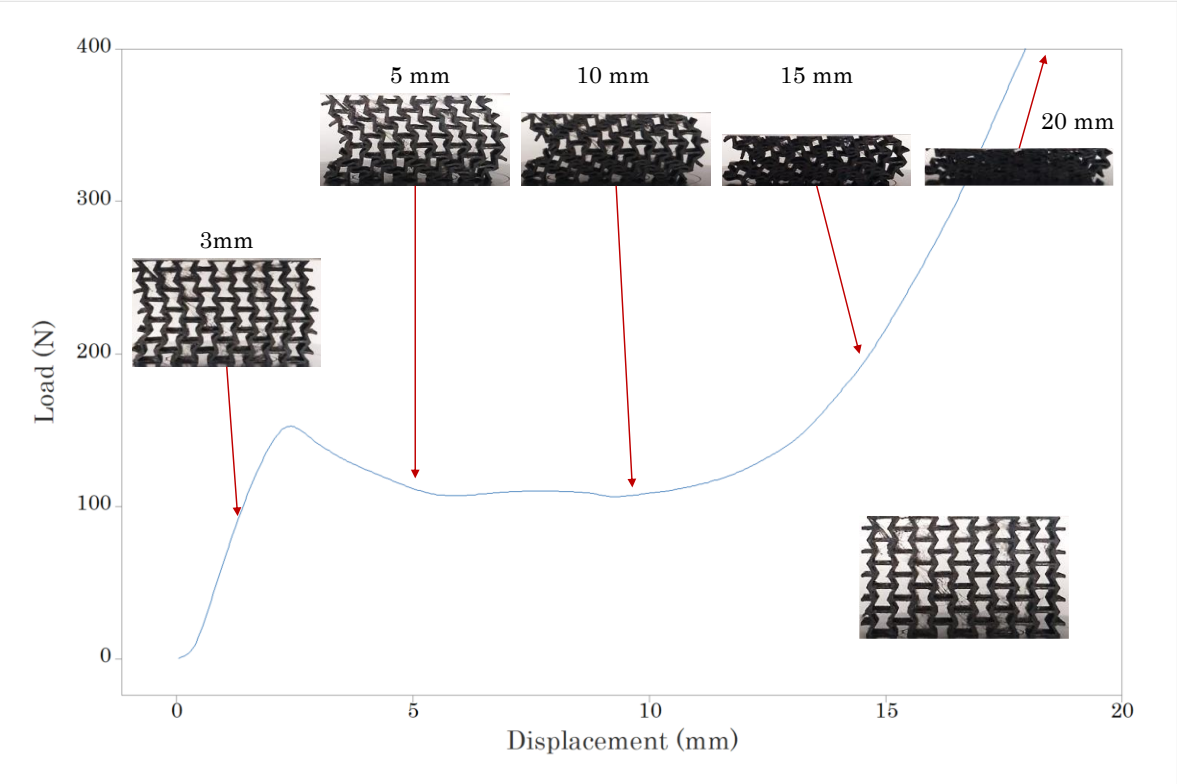

Figure 41. Load vs. displacement curve for replicate 1 of sample H1.0.

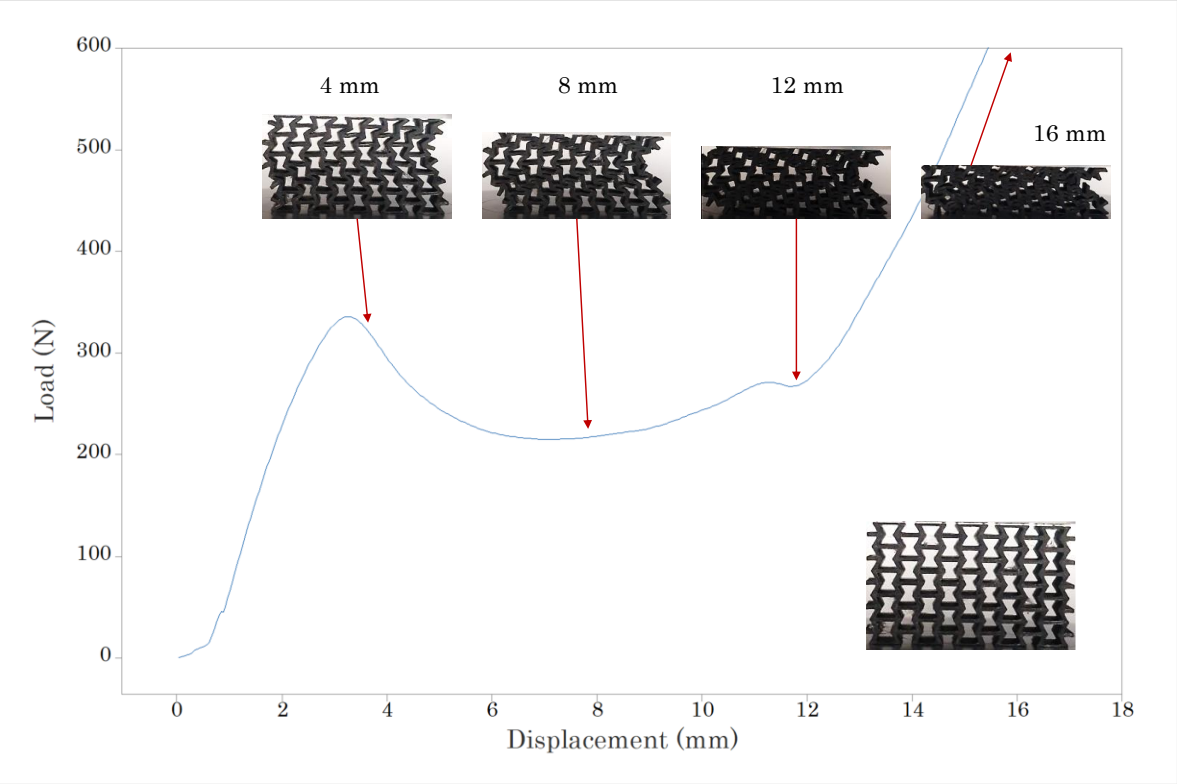

Figure 42. Load vs. displacement curve for replicate 1 of sample H1.2.

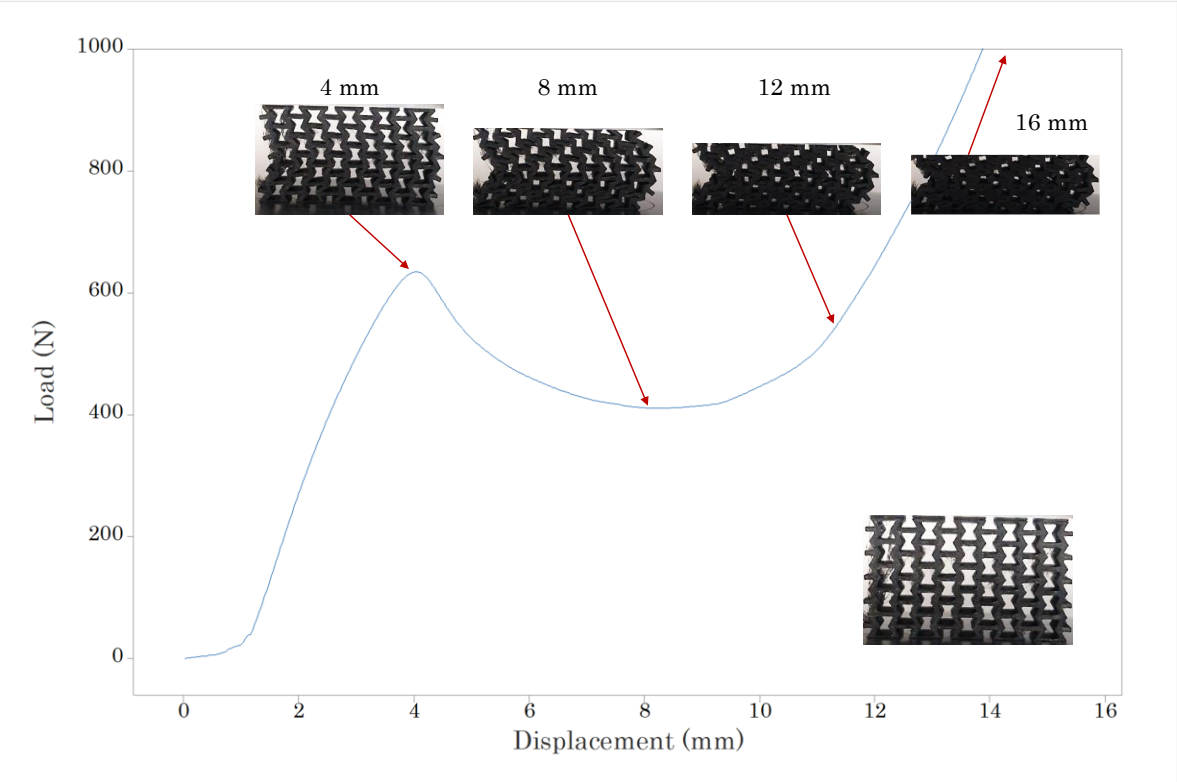

Figure 43. Load vs. displacement curve for replicate 1 of sample H1.4.

- Apparent elastic modulus

To obtain and analyze the elastic modulus of the samples, the load-displacement data must be treated and converted to stresses and strains suffered by the specimens. To calculate the stress, the force applied must be divided by the cross-sectional area of the structure. Since the samples present a non-regular cross-sectional area, this is simply considered as the multiplication of the length and depth of the samples and called “apparent area”. The strain is defined as the ratio between the longitudinal displacement and the original height of the specimen.

The stress-strain curves for all the ten different samples are presented in Figs. 44-53. All graphs include the three replicates for each configuration.

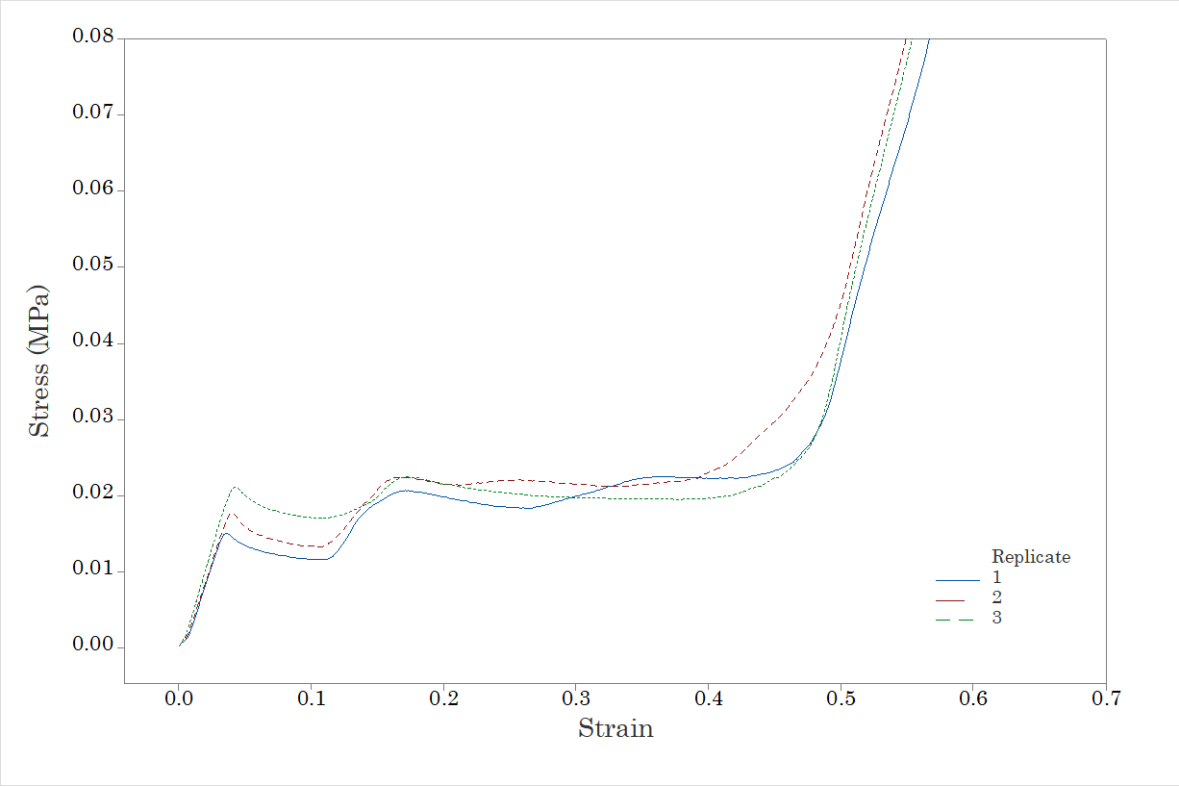

Figure 44. Stress vs. strain curve for compression test results of sample V0.6 with three different replicates.

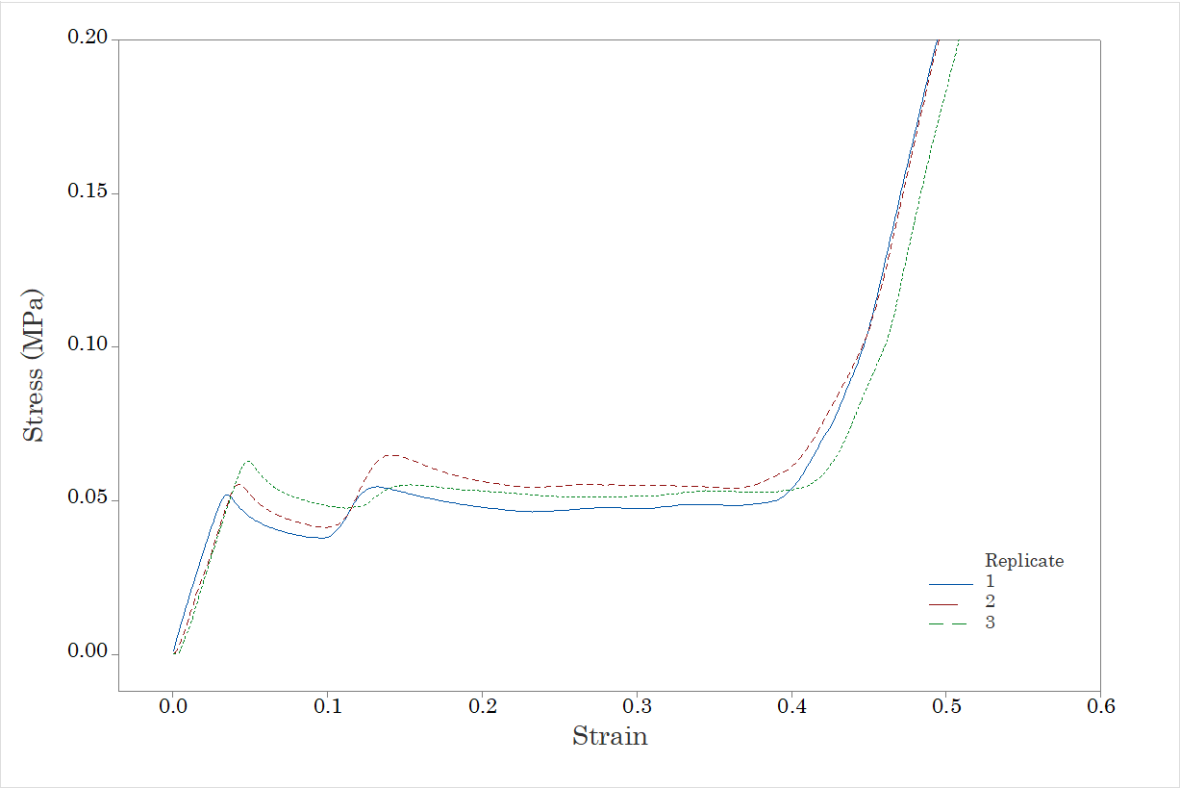

Figure 45. Stress vs. strain curve for compression test results of sample V0.8 with three different replicates.

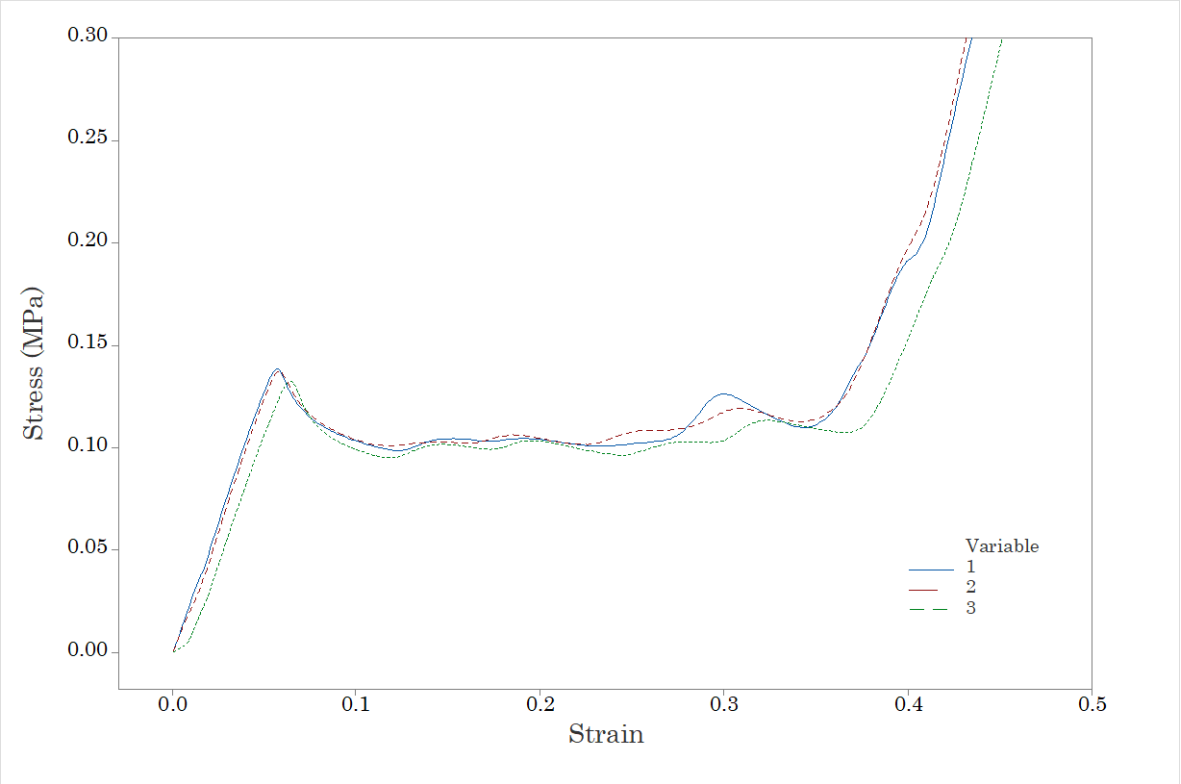

Figure 46. Stress vs. strain curve for compression test results of sample V1.0 with three different replicates.

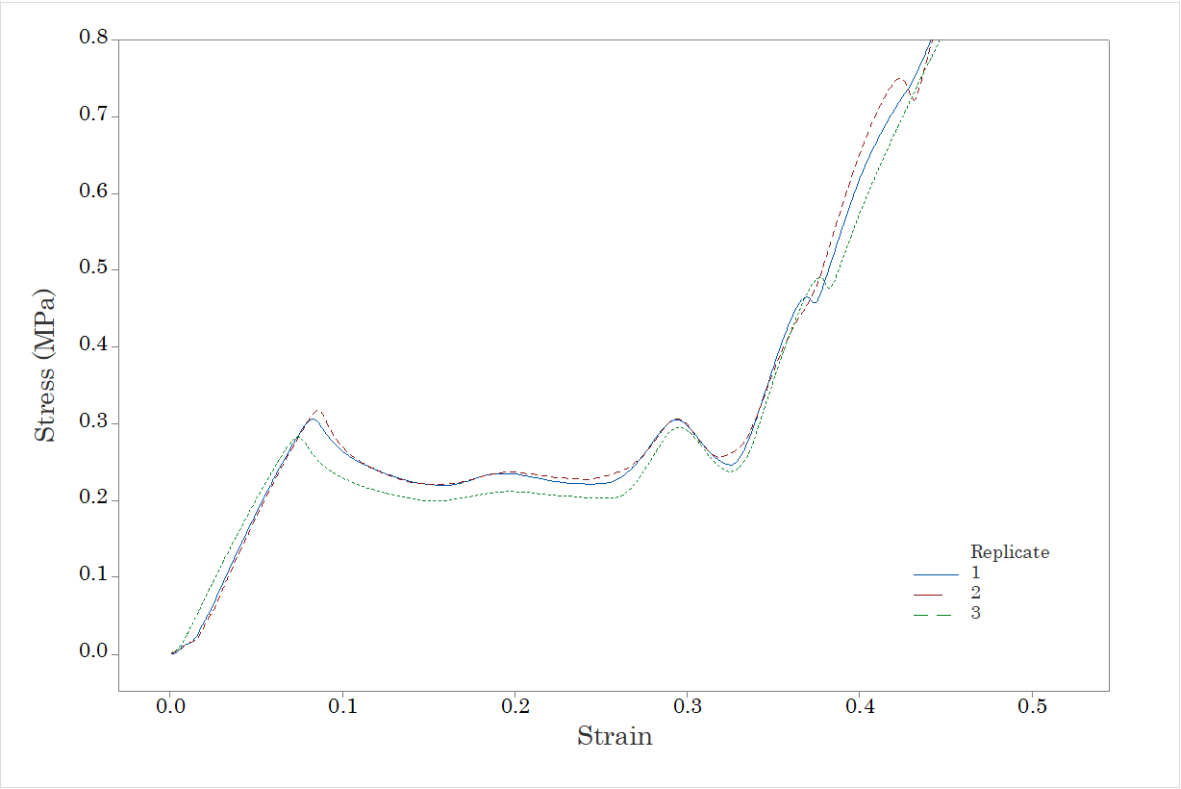

Figure 47. Stress vs. strain curve for compression test results of sample V1.2 with three different replicates.

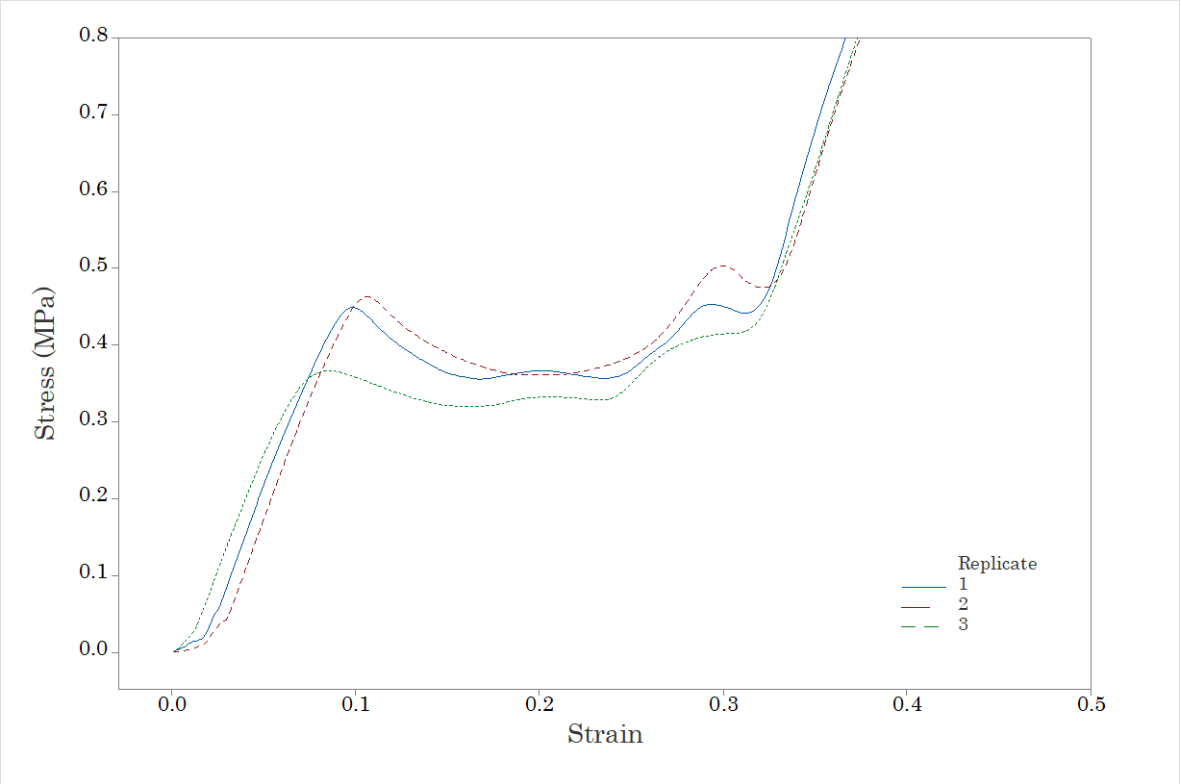

Figure 48. Stress vs. strain curve for compression test results of sample V1.4 with three different replicates.

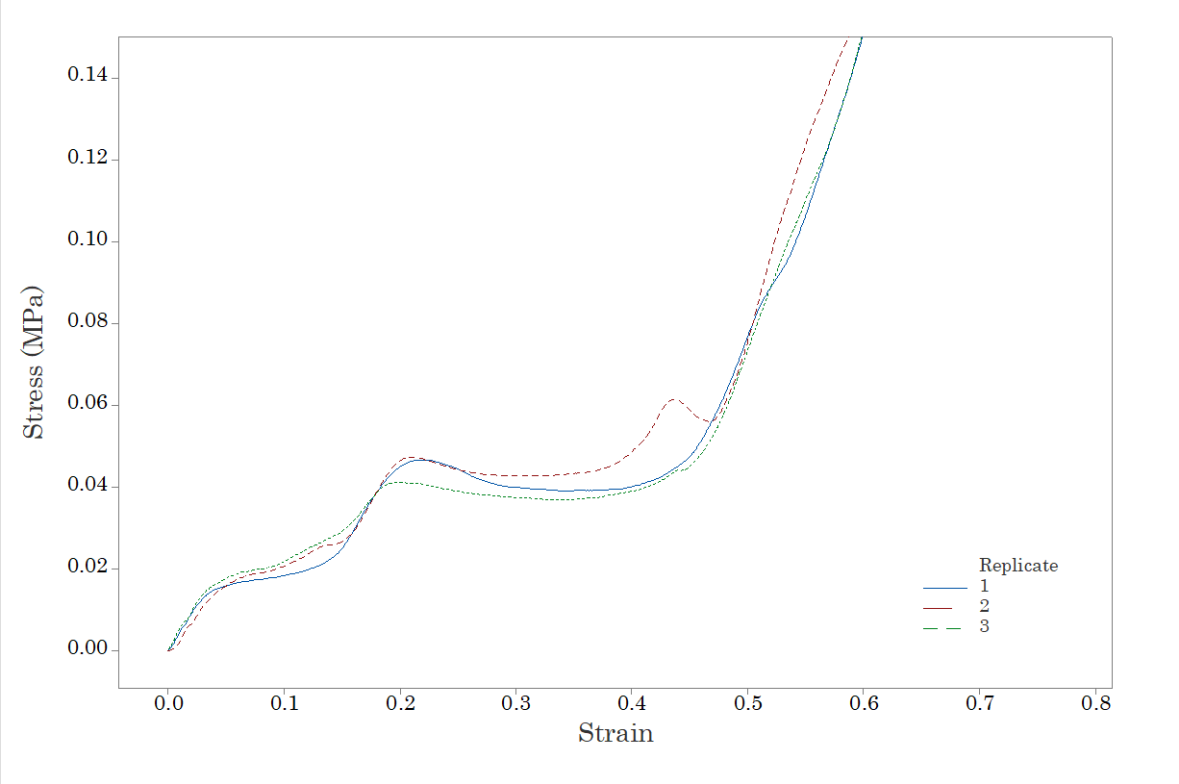

Figure 49. Stress vs. strain curve for compression test results of sample H0.6 with three different replicates.

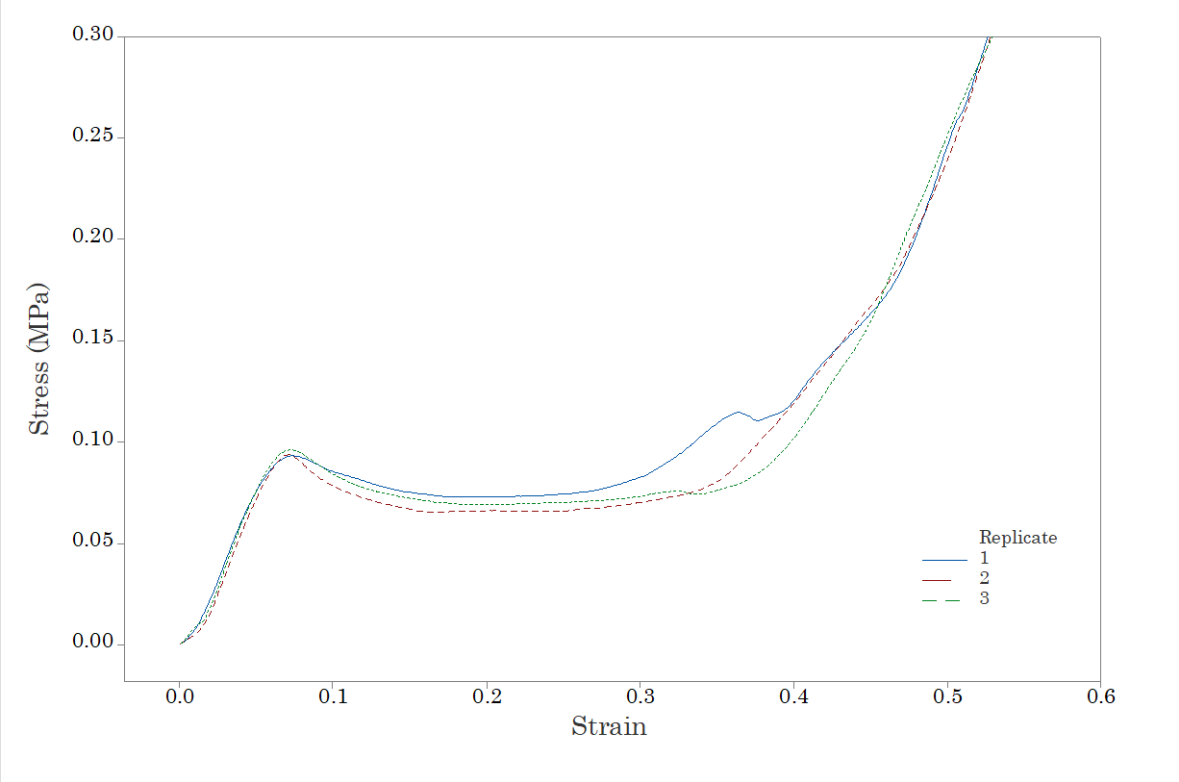

Figure 50. Stress vs. strain curve for compression test results of sample H0.8 with three different replicates.

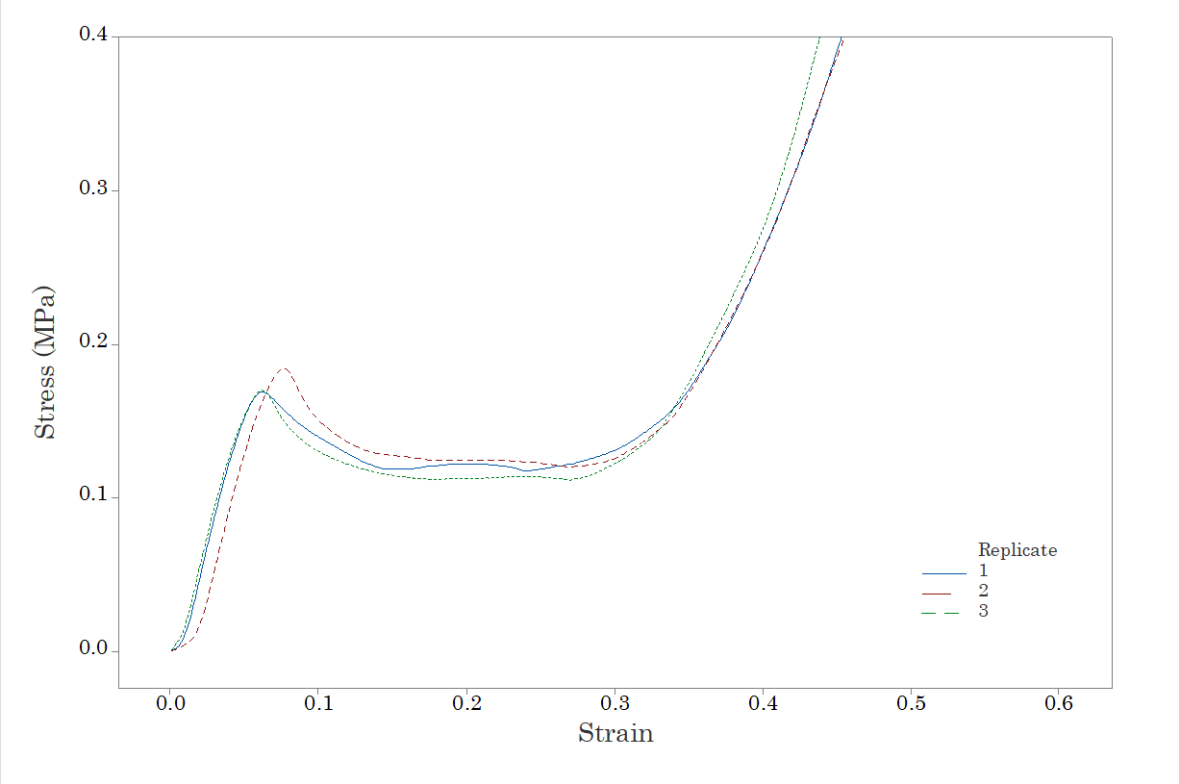

Figure 51.Stress vs. strain curve for compression test results of sample H1.0 with three different replicates.

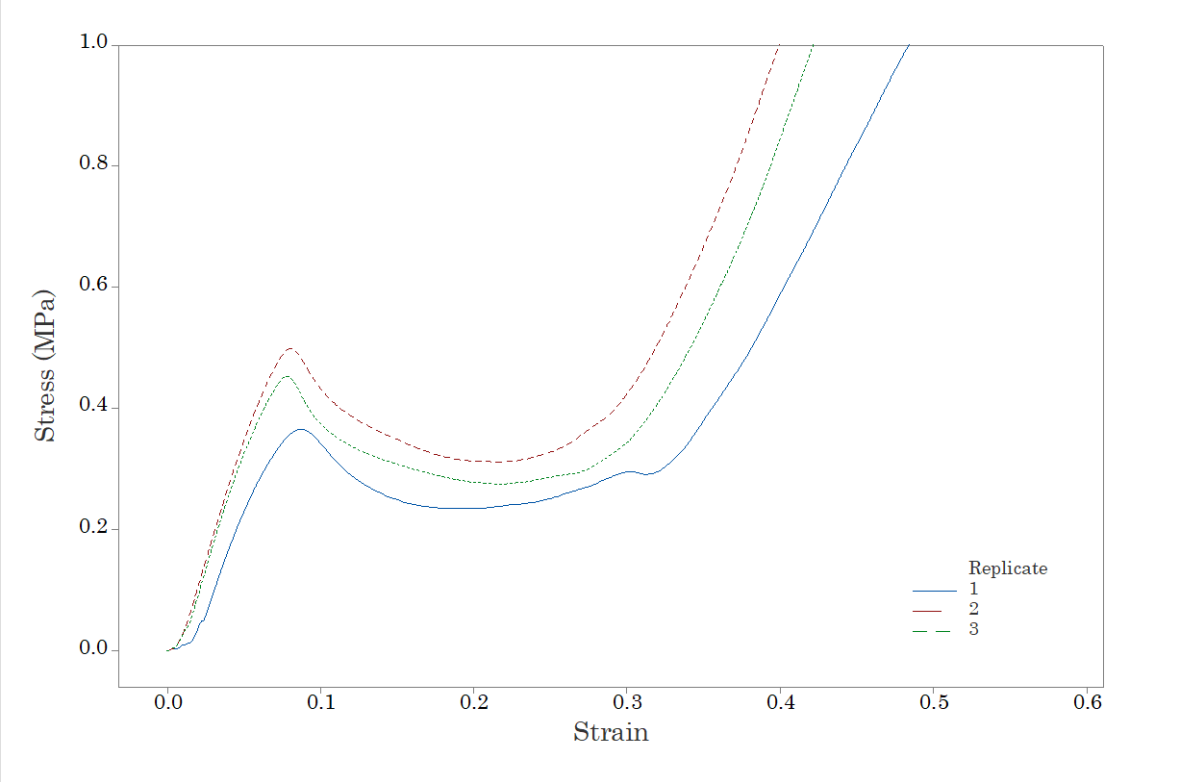

Figure 52. Stress vs. strain curve for compression test results of sample H1.2 with three different replicates.

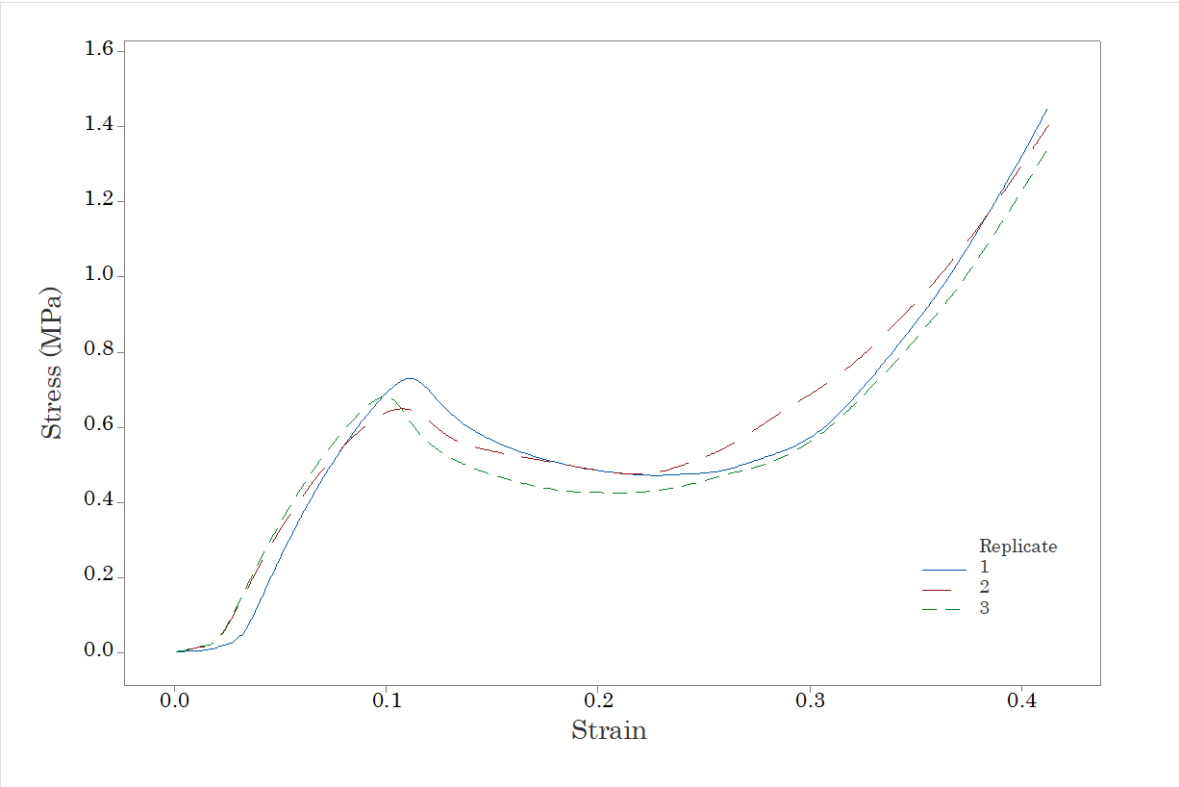

Figure 53. Stress vs. strain curve for compression test results of sample H1.4 with three different replicates.

The apparent elastic modulus of the structure is defined by the slope of the stress-strain curve in the linear elastic region. For each sample, the linear region was identified, and the data was analyzed using a linear regression model. For each sample and replicate, the apparent elastic modulus was obtained. The mean and standard deviation were calculated for each set. Results are presented in Table 8.

Table 8. Apparent elastic modulus.

Sample	Replicates			Mean	Standard Deviation
	1	2	3		
V0.6	0.5317	0.5281	0.5893	0.550	0.034
V0.8	1.572	1.483	1.590	1.548	0.057
V1.0	2.621	2.534	2.338	2.498	0.145
V1.2	4.694	4.437	4.219	4.450	0.238
V1.4	6.048	6.407	5.898	6.118	0.262
H0.6	0.4427	0.3798	0.4491	0.424	0.038
H0.8	1.795	1.806	1.826	1.809	0.016
H1.0	3.674	3.597	3.765	3.679	0.084
H1.2	6.872	7.882	7.829	7.528	0.568
H1.4	9.272	8.496	9.233	9.000	0.437

*All values in MPa

The average stress-strain data for each sample was obtained and plotted in Fig. 54 and Fig. 55 for compression in Y and X directions, respectively. The three distinctive regions in the curve of compressed cellular solids are exhibited: elastic region, plateau region, and densification. It is identified a tendency in both group of samples that an increase in density corresponds to a decrease in the strain densification. The plateau regions of samples compressed in the Y direction are flatter than samples compressed in the X direction. This can be attributed to the fact that specimens of the H-group suffered global buckling and showed less resistance once the rows of unit cells started to deform.

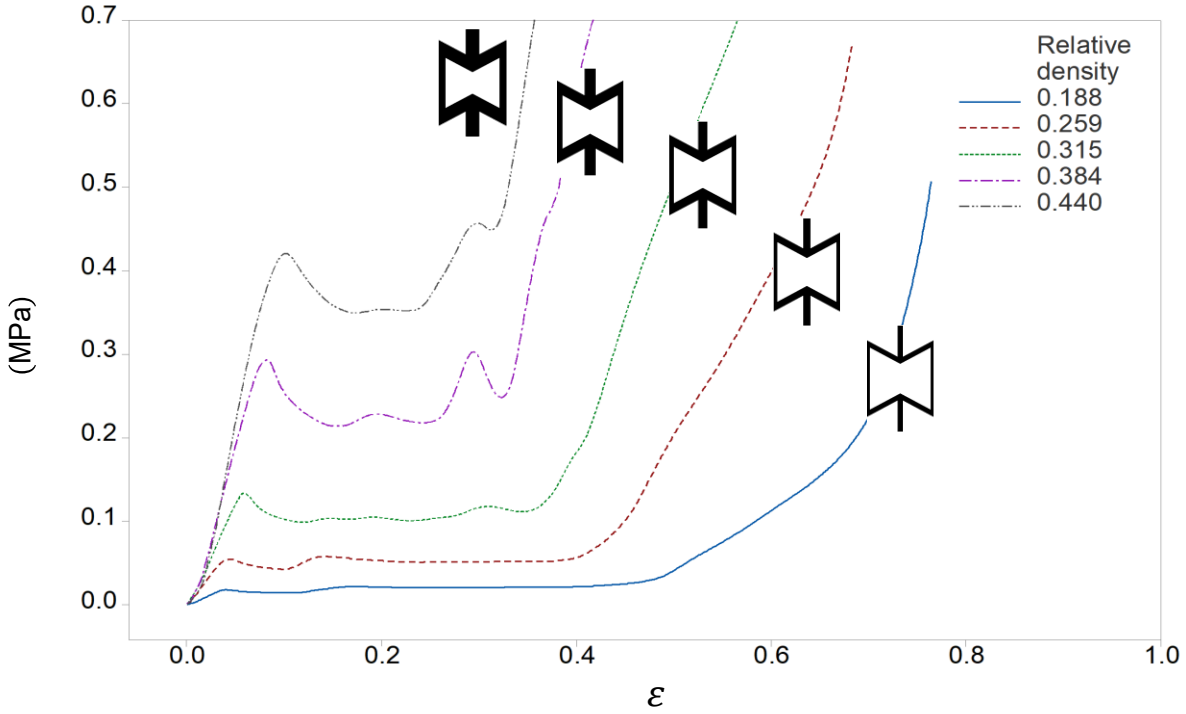

Figure 54. Stress vs. strain behavior of TPU reentrant honeycombs compressed in the Y direction.

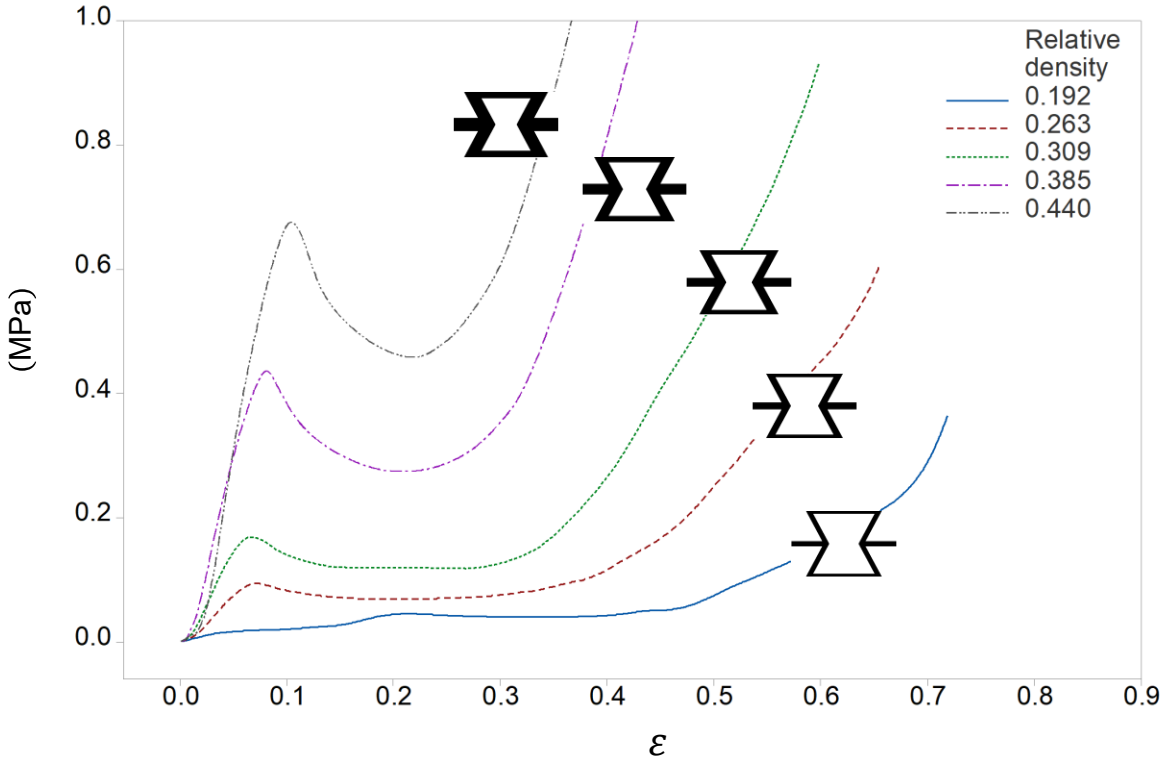

Figure 55. Stress vs. strain behavior of TPU reentrant honeycombs compressed in the X direction.

- Relative density vs. apparent Young's modulus

The apparent elastic modulus and relative density values of all three replicates were averaged and presented in Figs. 36-37, for compressive tests in Y and X direction, respectively. It can be observed a non-linear dependency between two factors. It is concluded that the apparent elastic modulus of the reentrant honeycombs increases as their relative density increases in a cubic relationship.

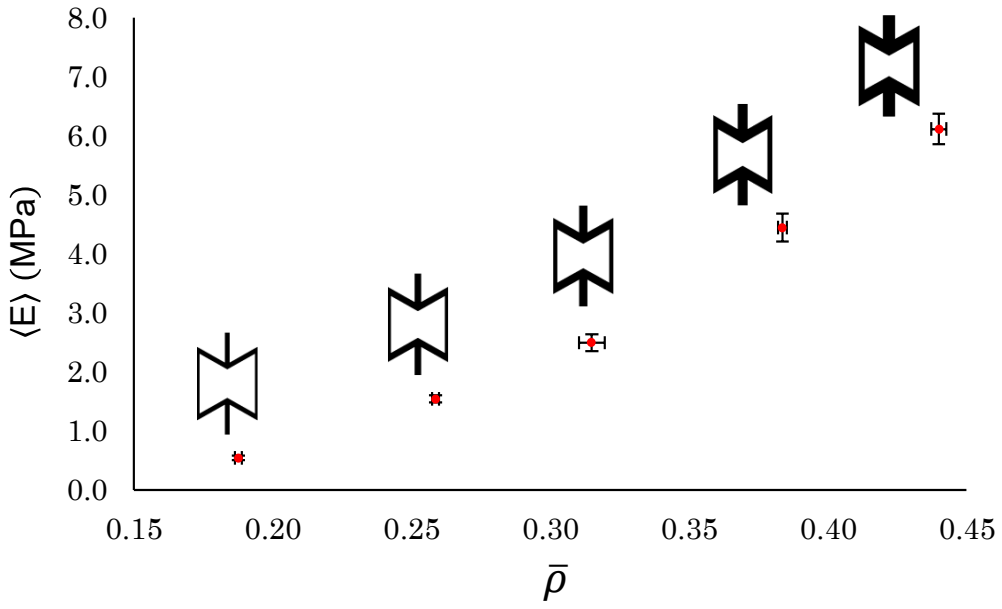

Figure 56. Apparent elastic modulus vs. relative density of reentrant honeycombs compressed in the Y direction.

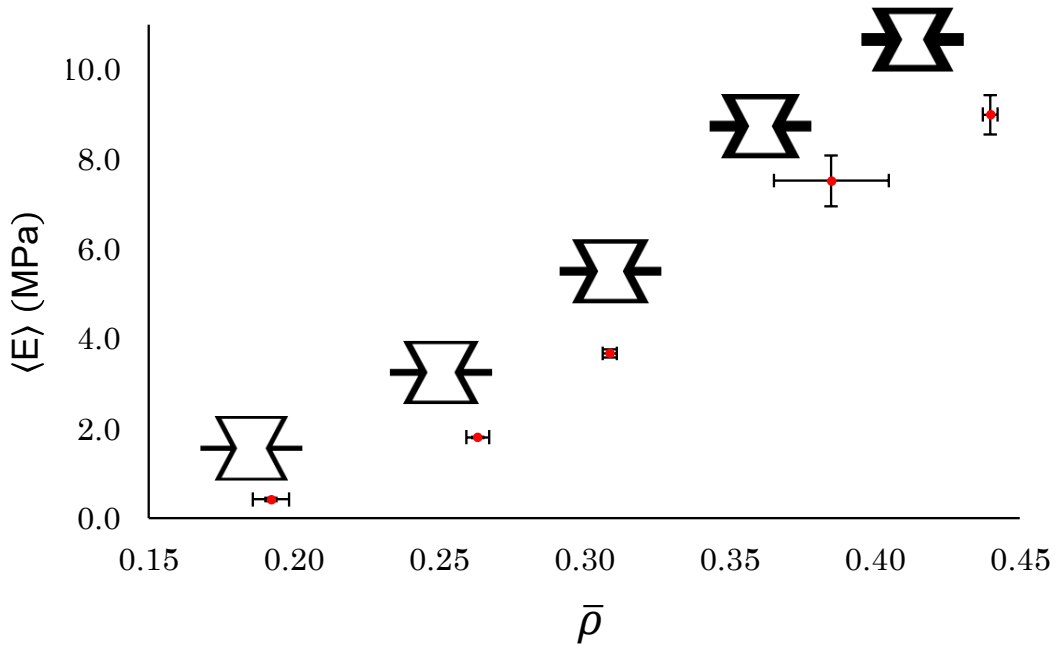

Figure 57. Apparent elastic modulus vs. relative density of reentrant honeycombs compressed in the X direction.

- Cyclic compressive behavior

Results on the five loading and unloading compressive cycles are presented below for the ten different specimens. In Figs. 58-67 it is presented the cyclic compressive behavior of 3D printed reentrant honeycombs made of thermoplastic polyurethane. The curves present the five loading cycles up until densification strain, ϵ, and then an unloading process. From the results, it can be observed that the specimens are more compliant as the number of cycles increases. This behavior starts to converge in cycle #2 and the difference is less noticeable from cycle #5. It is important to state that all samples did not return to its original height after the first compressive cycle. A slight difference of 3-5 millimeters of height was observed in all samples.

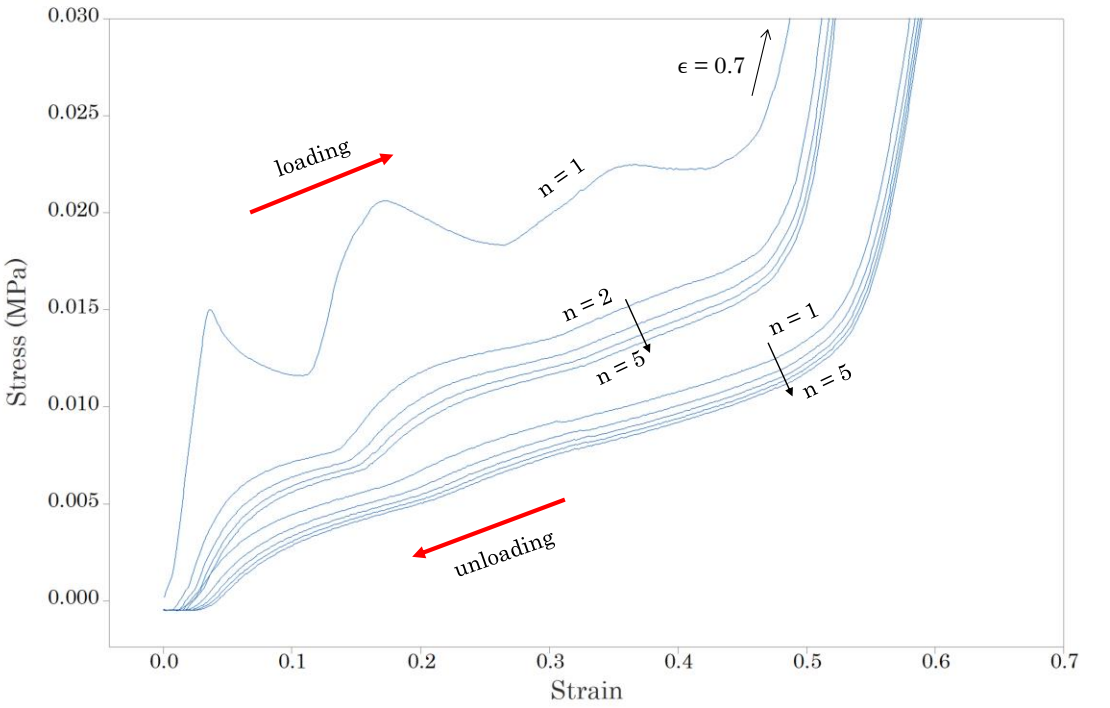

Figure 58. Stress vs. strain curve for the five loading and unloading cycles for TPU sample V0.6 at a strain rate of 24 mm/min.

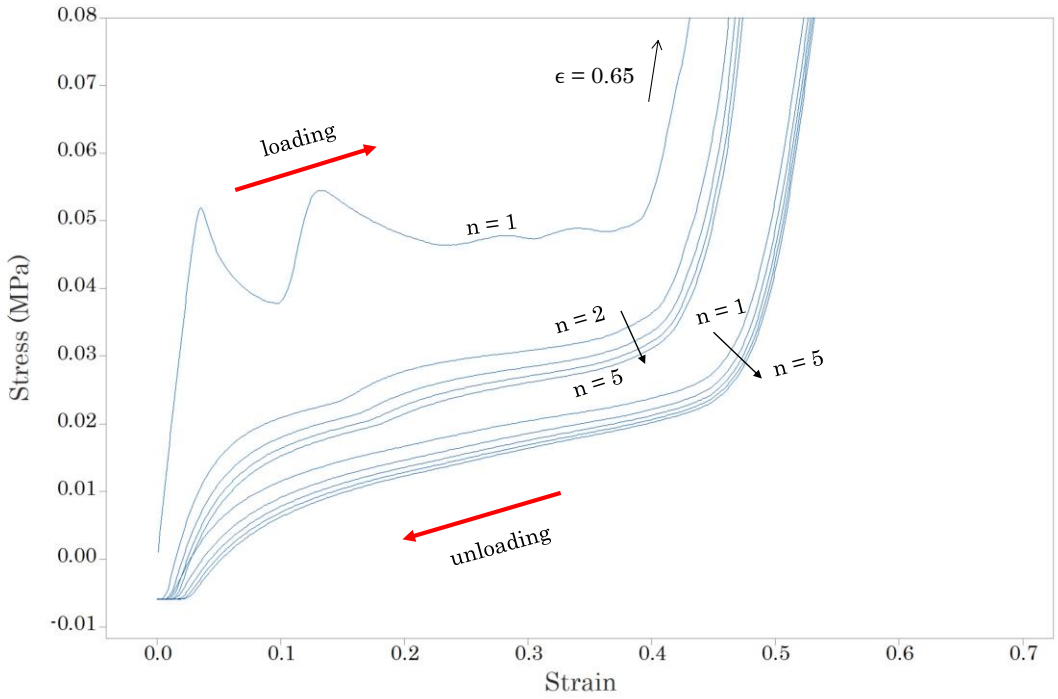

Figure 59. Stress vs. strain curve for the five loading and unloading cycles for TPU sample V0.8 at a strain rate of 24 mm/min.

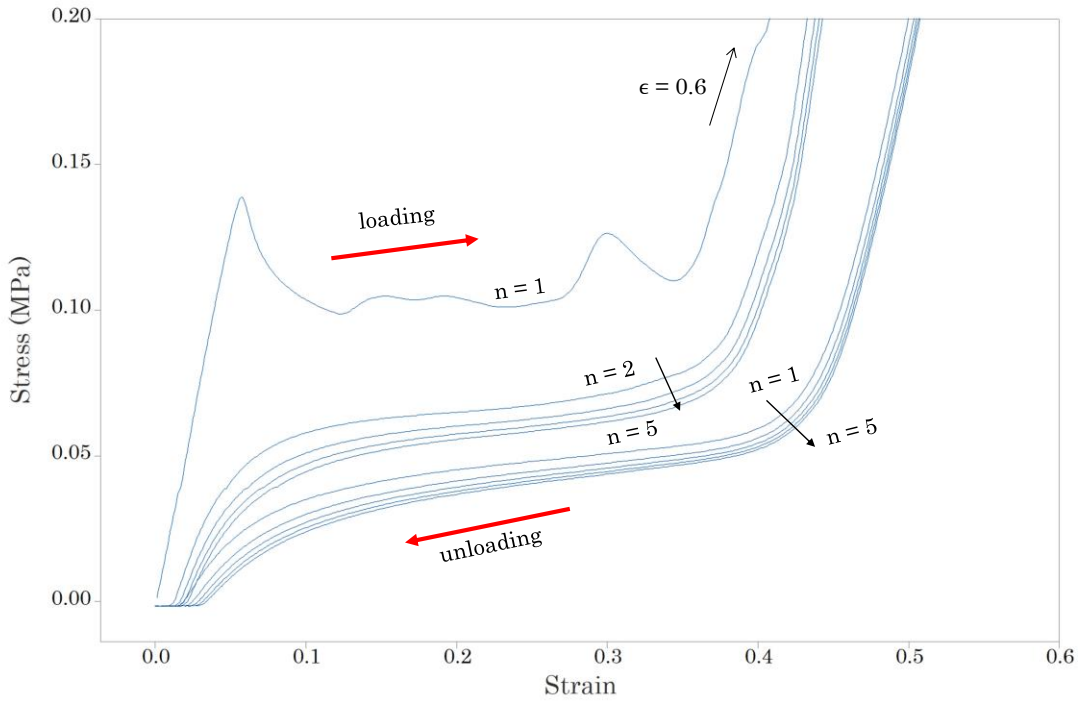

Figure 60. Stress vs. strain curve for the five loading and unloading cycles for TPU sample V1.0 at a strain rate of 24 mm/min.

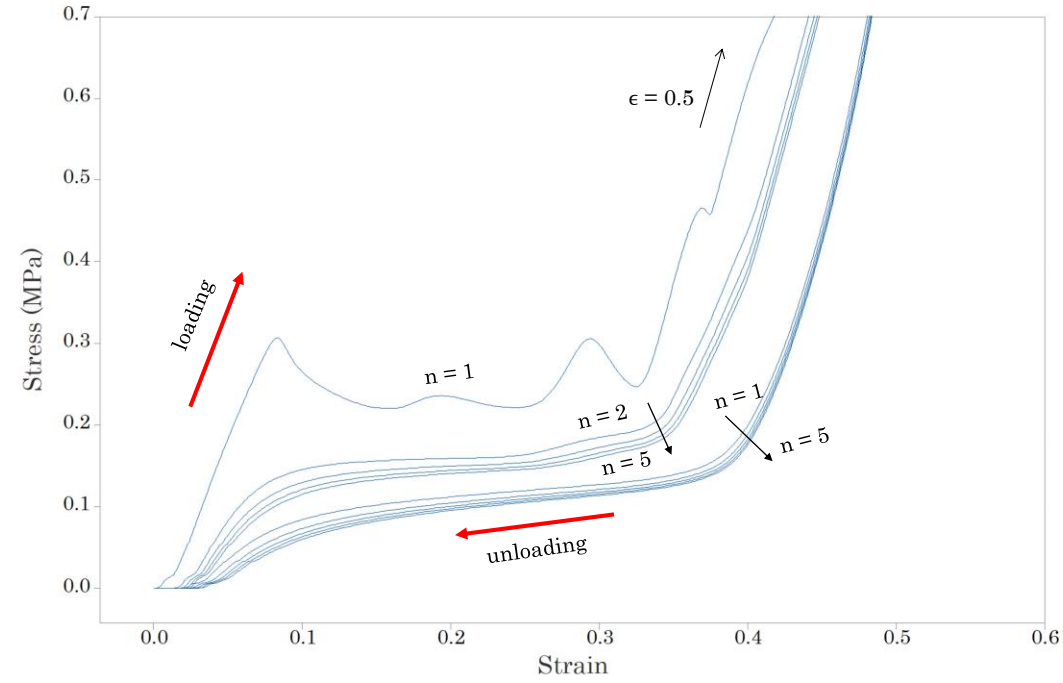

Figure 61. Stress vs. strain curve for the five loading and unloading cycles for TPU sample V1.2 at a strain rate of 24 mm/min.

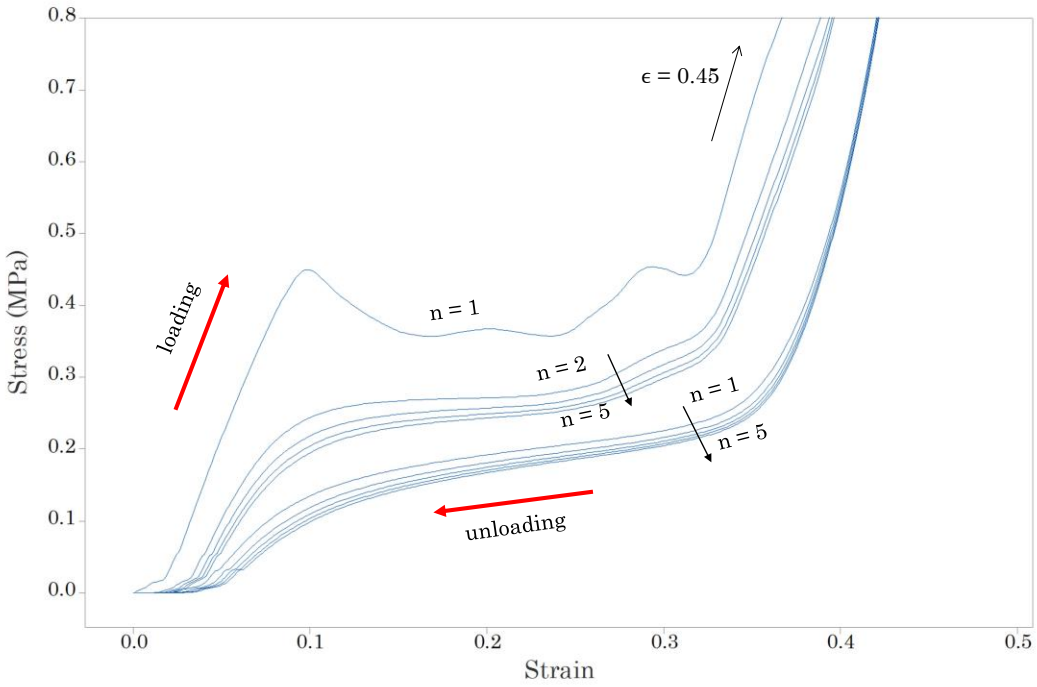

Figure 62. Stress vs. strain curve for the five loading and unloading cycles for TPU sample V1.4 at a strain rate of 24 mm/min.

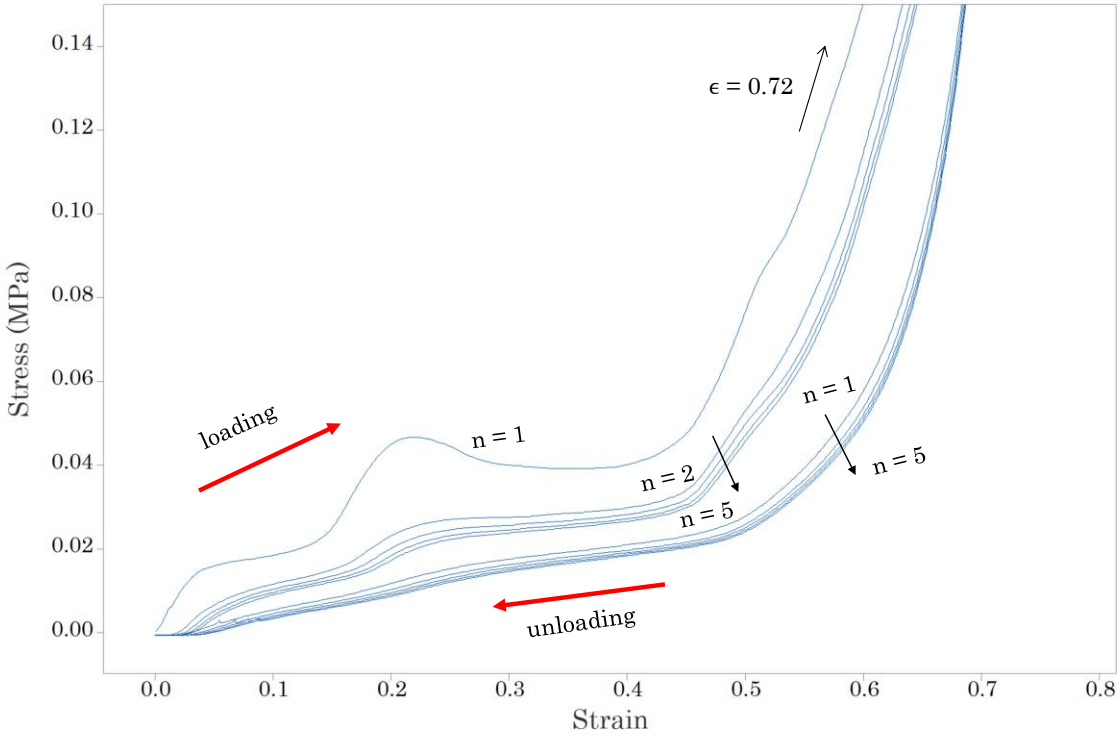

Figure 63. Stress vs. strain curve for the five loading and unloading cycles for TPU sample H0.6 at a strain rate of 24 mm/min.

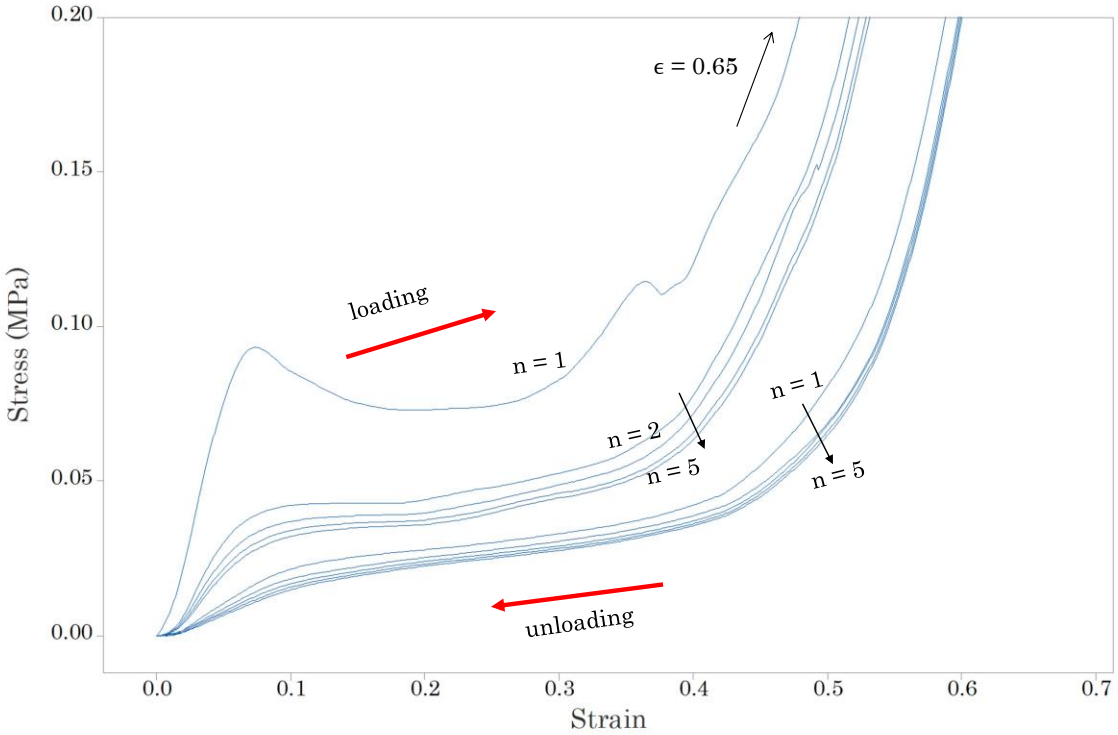

Figure 64. Stress vs. strain curve for the five loading and unloading cycles for TPU sample H0.8 at a strain rate of 24 mm/min.

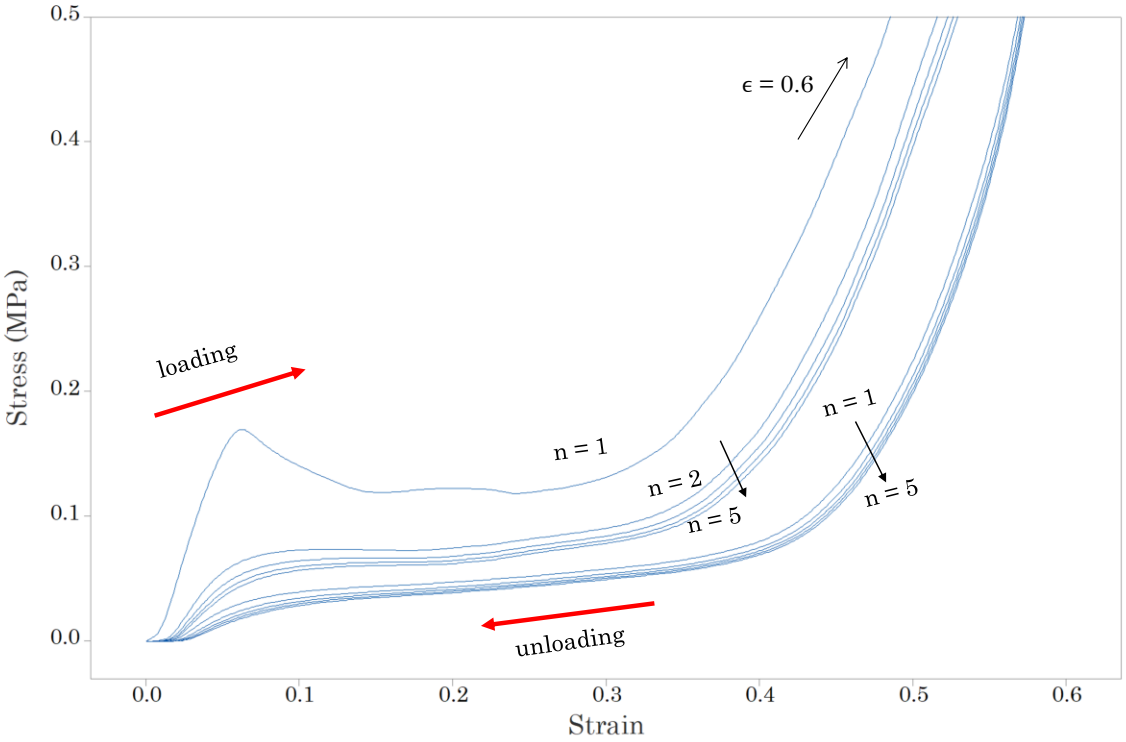

Figure 65. Stress vs. strain curve for the five loading and unloading cycles for TPU sample H1.0 at a strain rate of 24 mm/min.

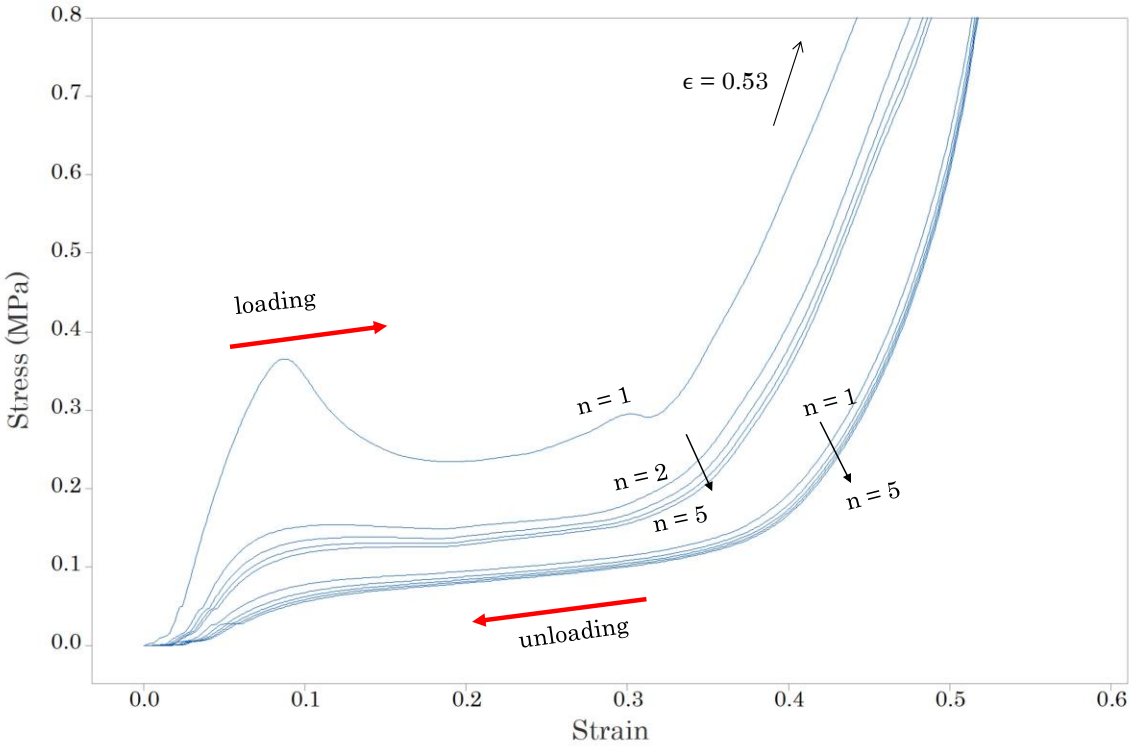

Figure 66. Stress vs. strain curve for the five loading and unloading cycles for TPU sample H1.2 at a strain rate of 24 mm/min.

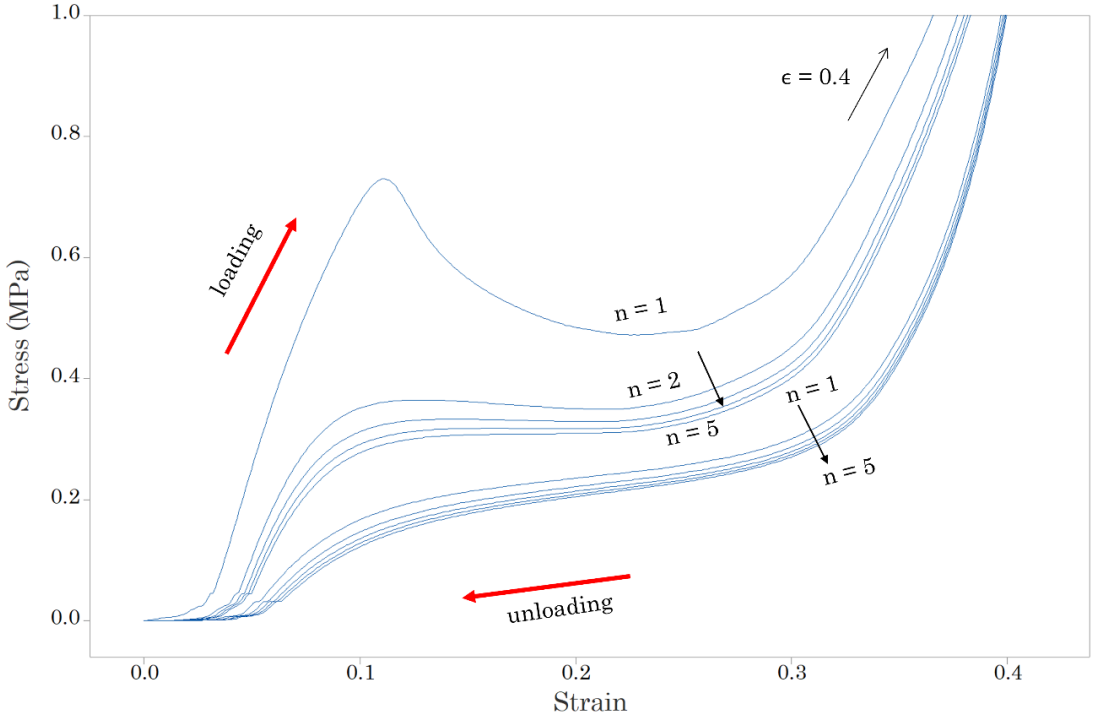

Figure 67. Stress vs. strain curve for the five loading and unloading cycles for TPU sample H1.4 at a strain rate of 24 mm/min.

- Energy absorption capability

To study the total amount of energy absorbed by the structures due to compression, the five loading cycles were analyzed to obtain the area under the curve which indicates the amount of energy stored due to energy. Results are presented in Table 9.

All samples exhibited a noticeable reduction in their ability to absorb energy with the highest difference between the first and second cycle of compression. The V-type samples presented a reduction between 17-23% while the H-type samples showed higher differences among 23-28% of SEA when comparing the two first cycles. It can be observed that the performance of the specimens in terms of absorbing energy per cycle is significantly diminished after the first loading cycle but converges when reaching the fifth cycle.

Table 9. Specific energy absorbed on five loading compressive cycles.

Sample	**Cycle number**				
	1	**2**	**3**	**4**	**5**
V0.6	0.0512	0.0425	0.0408	0.0399	0.0397
V0.8	0.1050	0.0834	0.0792	0.0768	0.0752
V1.0	0.1694	0.1322	0.1256	0.1220	0.1194
V1.2	0.2065	0.1583	0.1501	0.1468	0.1437
V1.4	0.2271	0.1778	0.1685	0.1619	0.1598
H0.6	0.0561	0.0435	0.0415	0.0401	0.0389
H0.8	0.1137	0.0825	0.0772	0.0735	0.0717
H1.0	0.1660	0.1251	0.1178	0.1137	0.1109
H1.2	0.2351	0.1698	0.1592	0.1537	0.1498
H1.4	0.2446	0.1841	0.1734	0.1674	0.1634

*All values in J/cm^3

In Figs. 68-77 is presented the energy absorbed by the specimens up to densification strain (different to each array). The damping capability is also reduced after the first cycle, as it is seen the area between each cycle is smaller each time.

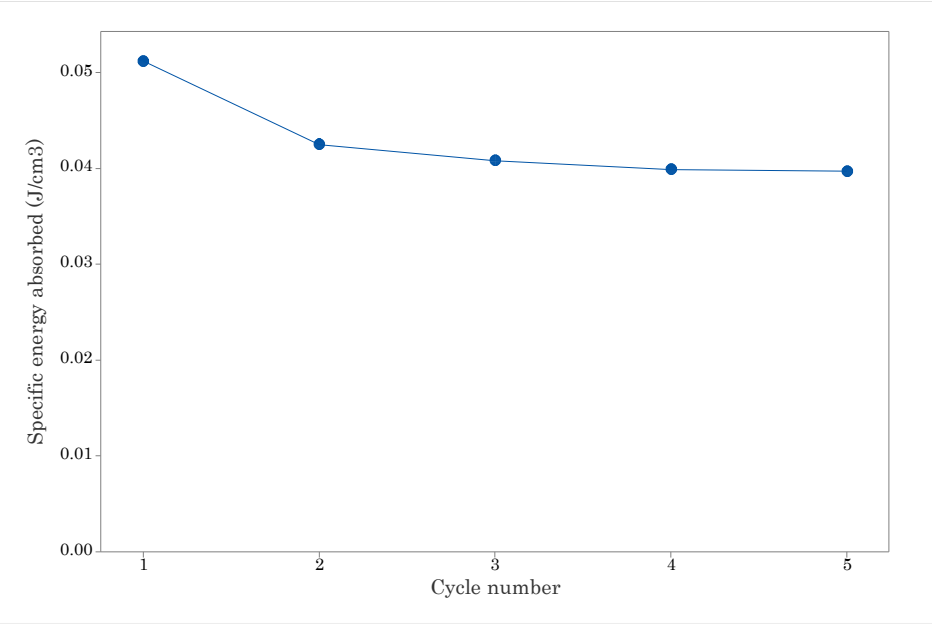

Figure 68. Energy absorbed on each compressive cycle on sample V0.6 with percentage reduction indicated.

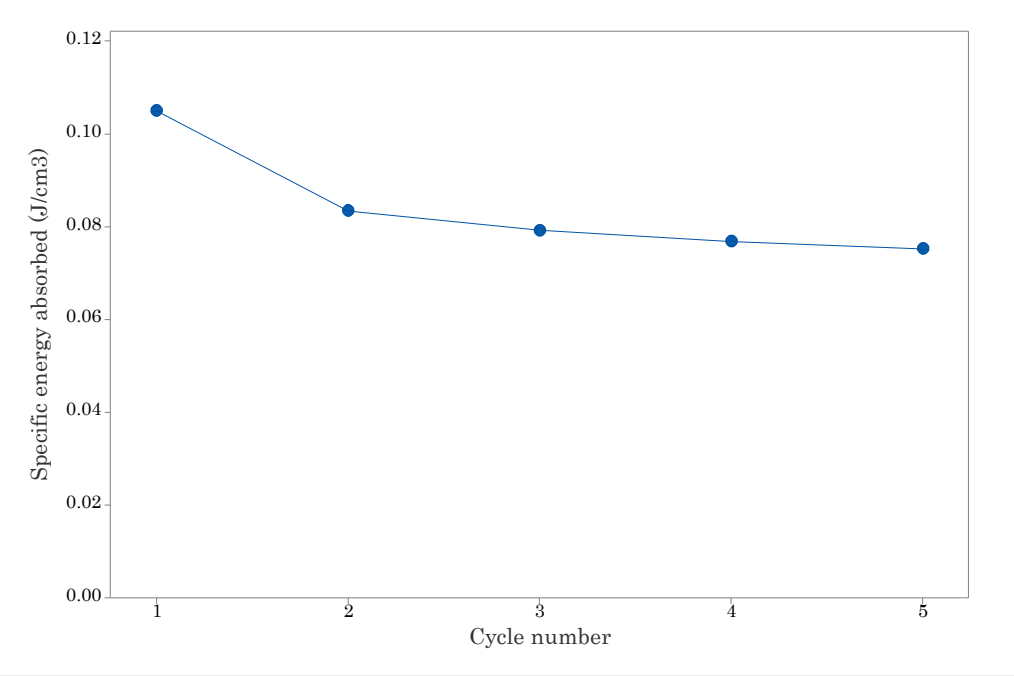

Figure 69. Energy absorbed on each compressive cycle on sample V0.8 with percentage reduction indicated.

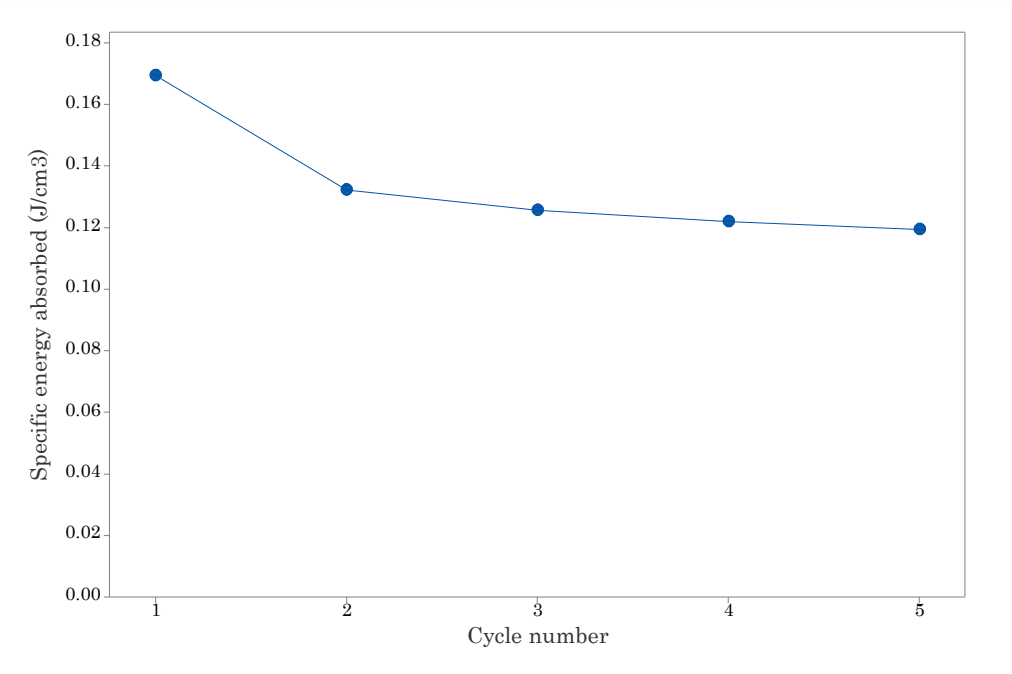

Figure 70. Energy absorbed on each compressive cycle on sample V1.0 with percentage reduction indicated.

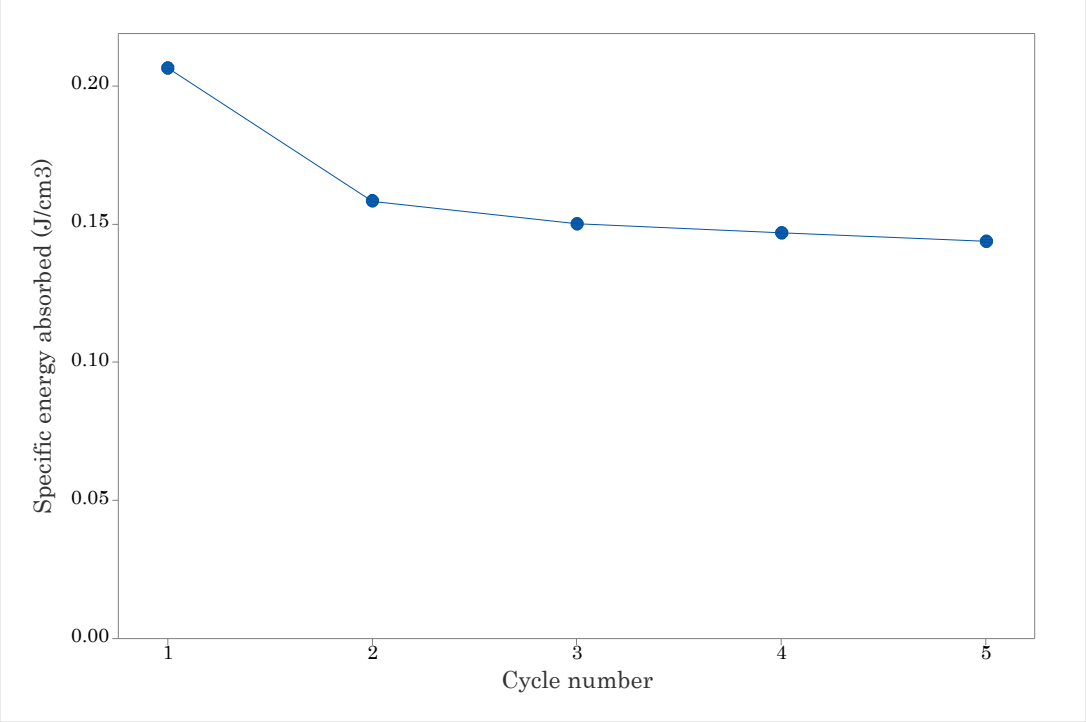

Figure 71. Energy absorbed on each compressive cycle on sample V1.2 with percentage reduction indicated.

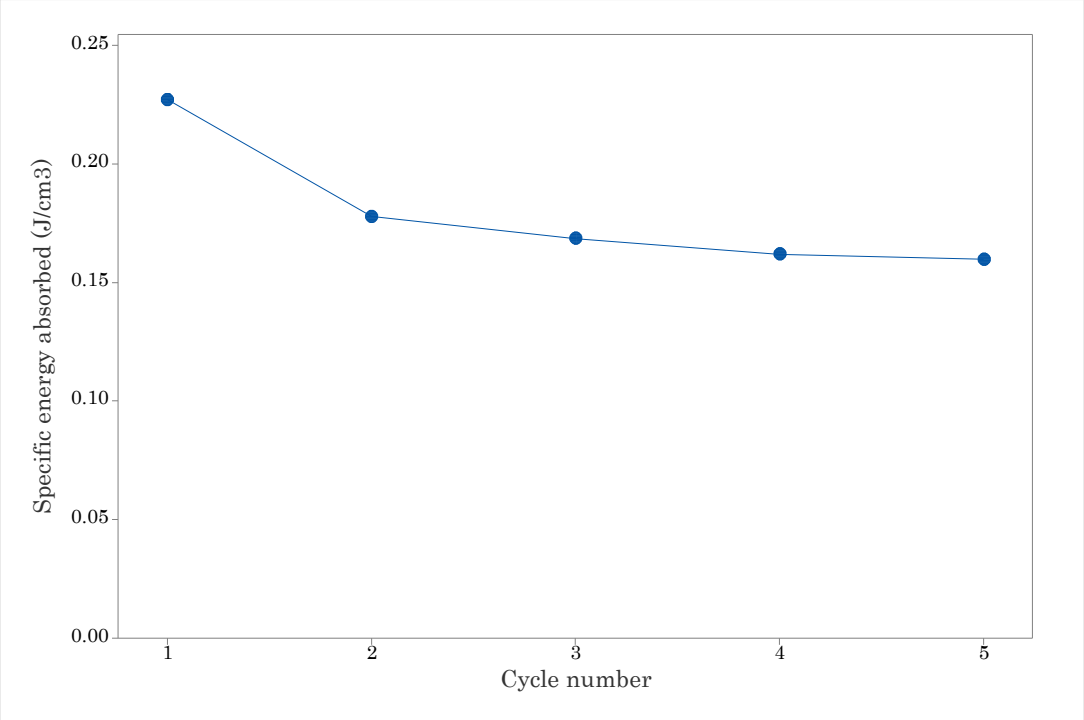

Figure 72. Energy absorbed on each compressive cycle on sample V1.4 with percentage reduction indicated.

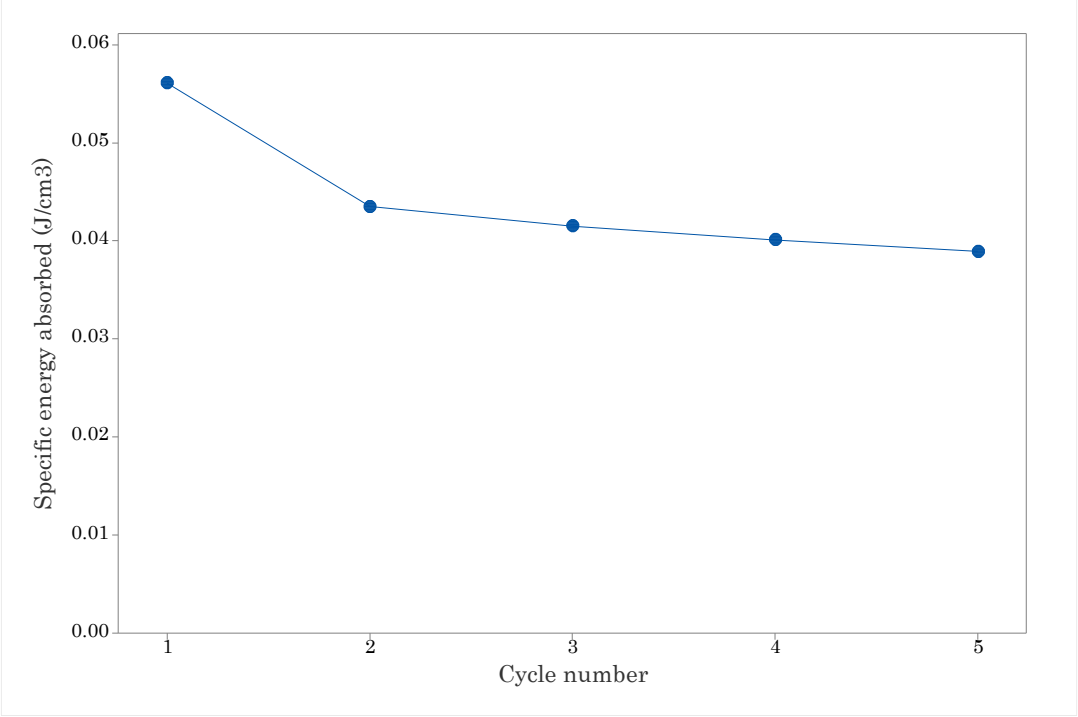

Figure 73. Energy absorbed on each compressive cycle on sample H0.6 with percentage reduction indicated.

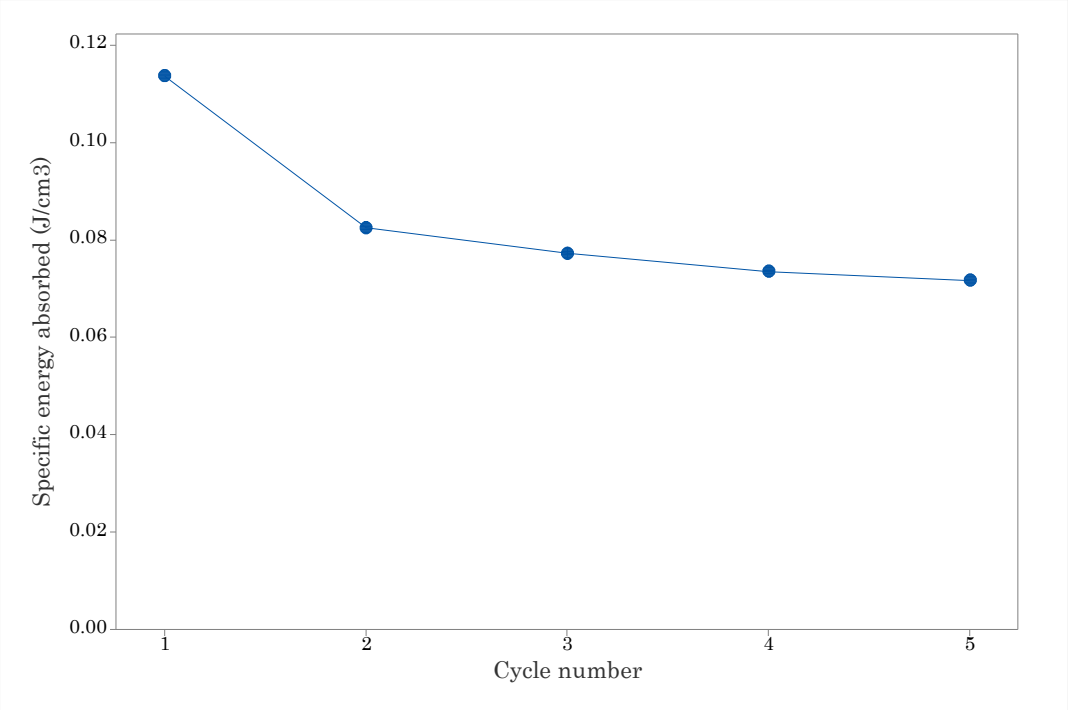

Figure 74. Energy absorbed on each compressive cycle on sample H0.8 with percentage reduction indicated.

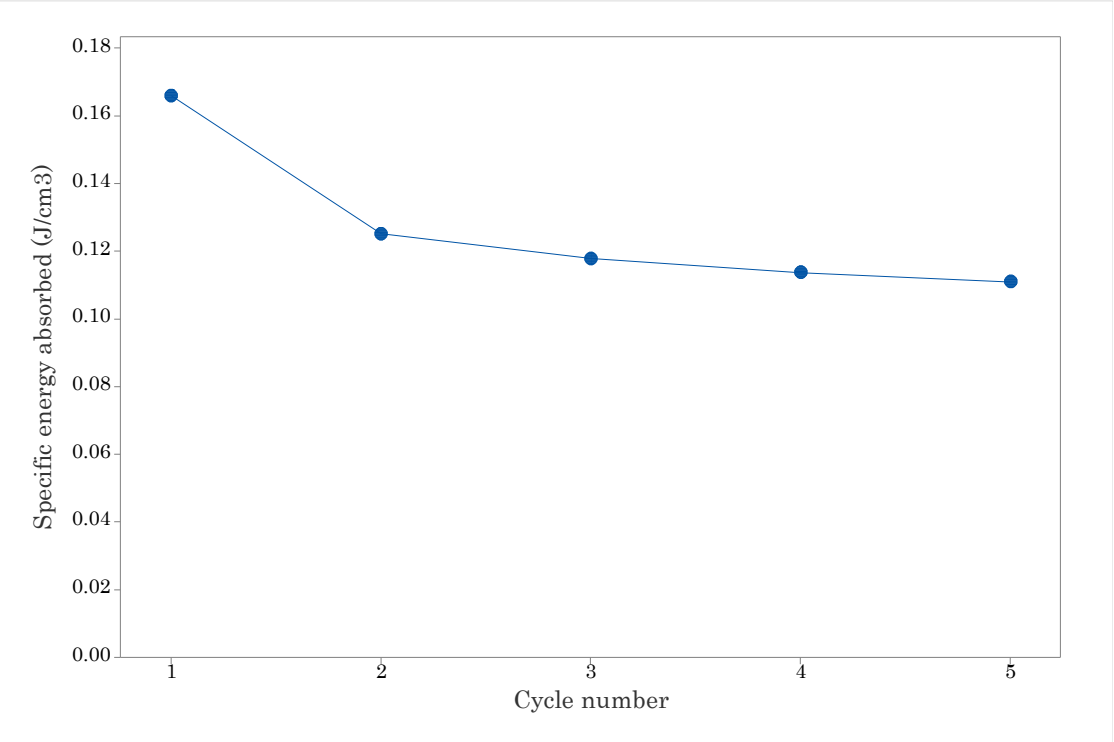

Figure 75. Energy absorbed on each compressive cycle on sample H1.0 with percentage reduction indicated.

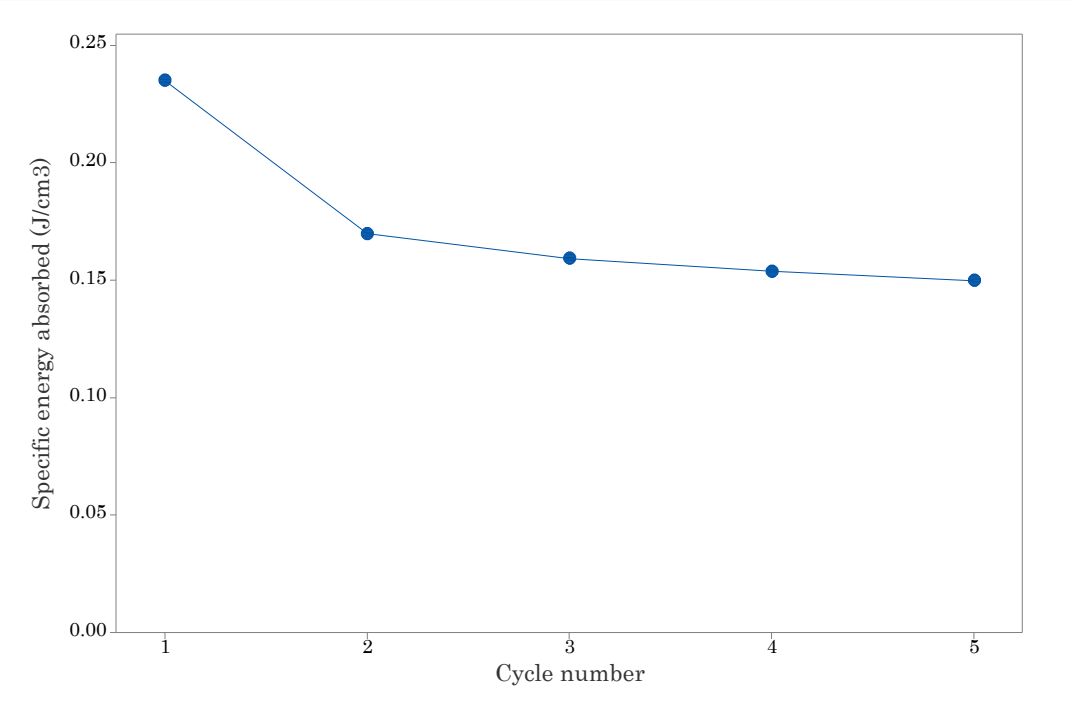

Figure 76. Energy absorbed on each compressive cycle on sample H1.2 with percentage reduction indicated.

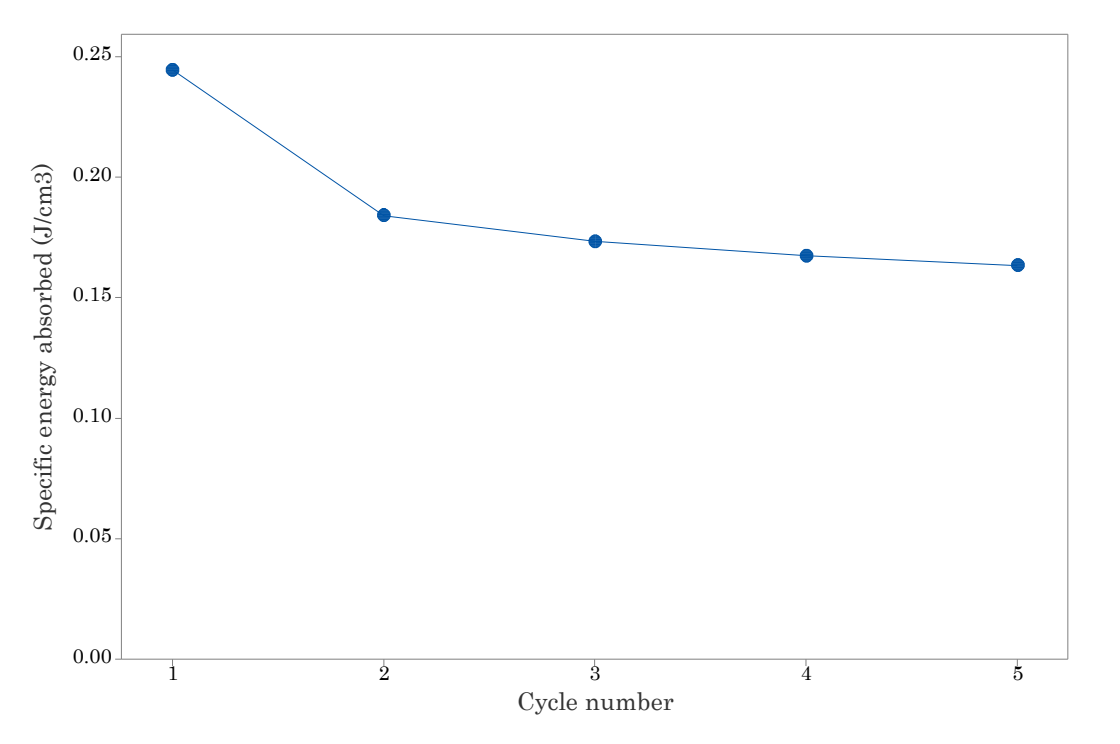

Figure 77. Energy absorbed on each compressive cycle on sample H1.4 with percentage reduction indicated.

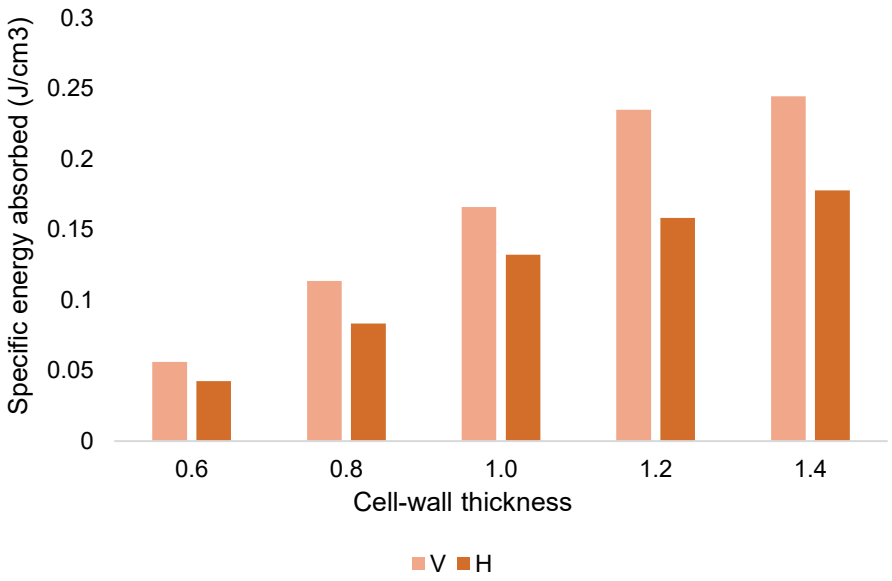

Figure 78. SEA by structures on their first loading cycle.

- Softening phenomenon

To analyze the softening behavior of TPU reentrant honeycombs structures after a set of compressive loadings up to full densification, the apparent Young's modulus for each loading cycle was calculated. The V1.0 and H1.0 samples were selected to do the analysis. A linear regression analysis was carried out on the elastic region of the samples (see Figs. 79-80) to calculate the slope of the curve. Results of the apparent Young's modulus are presented in Table 10 for each loading cycle.

Table 10. Apparent Young's modulus of TPU reentrant honeycombs when subjected to five loading cycles.

Sample	**Cycle number**				
	1	2	3	4	5
V1.0	2.608	0.987	0.969	0.953	0.932
H1.0	3.674	1.627	1.378	1.240	1.148

*Results are in MPa.

It is observed a softening phenomenon in the variation of apparent elastic modulus during the loading cycles. The highest change in the slopes is presented for both samples in the cycle number 2 with reductions of 62.16% and 55.72% for samples V1.0 and H1.0, respectively. Since during the first cycle all unit cells were compressed up until full densification, the elements created a deformed shape

memory making it easier to be deformed again, requiring less compressive forces, and generating lower stresses to displace the same number of millimeters as the previous cycles. This produces lower values of elastic modulus as presented in Fig. 81, with the biggest different during the first and second loading cycle, previously stated. After the fifth cycle it is observed a convergence on the results.

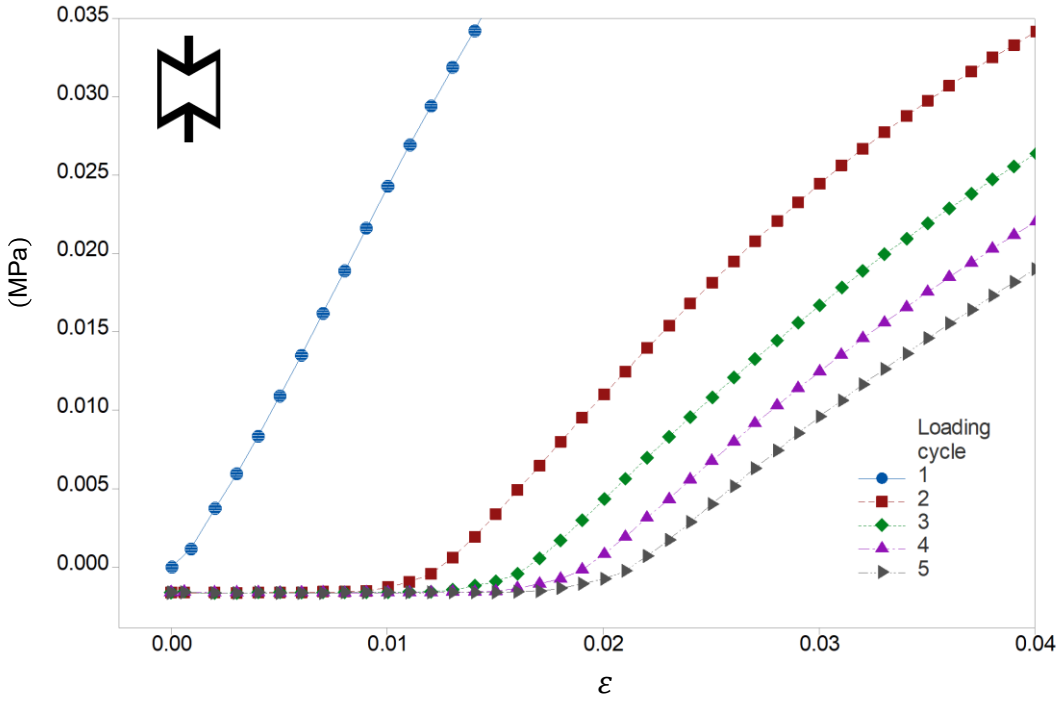

Figure 79. Linear elastic region of sample V1.0 when compressed along X direction during 5 loading cycles.

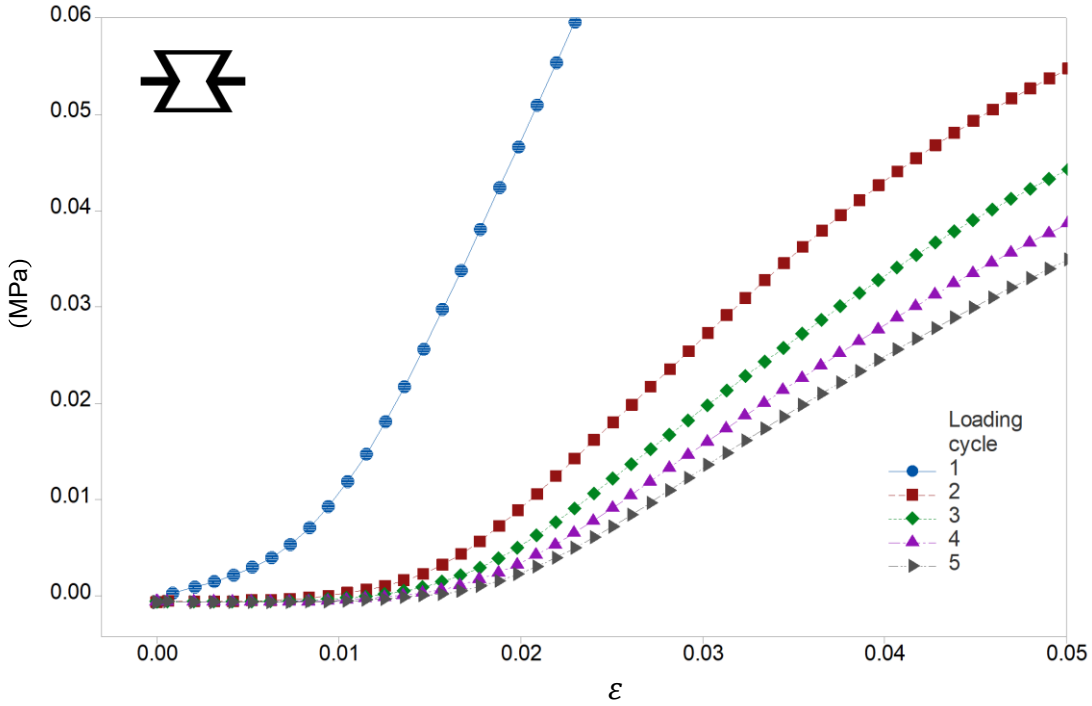

Figure 80. Linear elastic region of sample V1.0 when compressed along Y direction during 5 loading cycles.

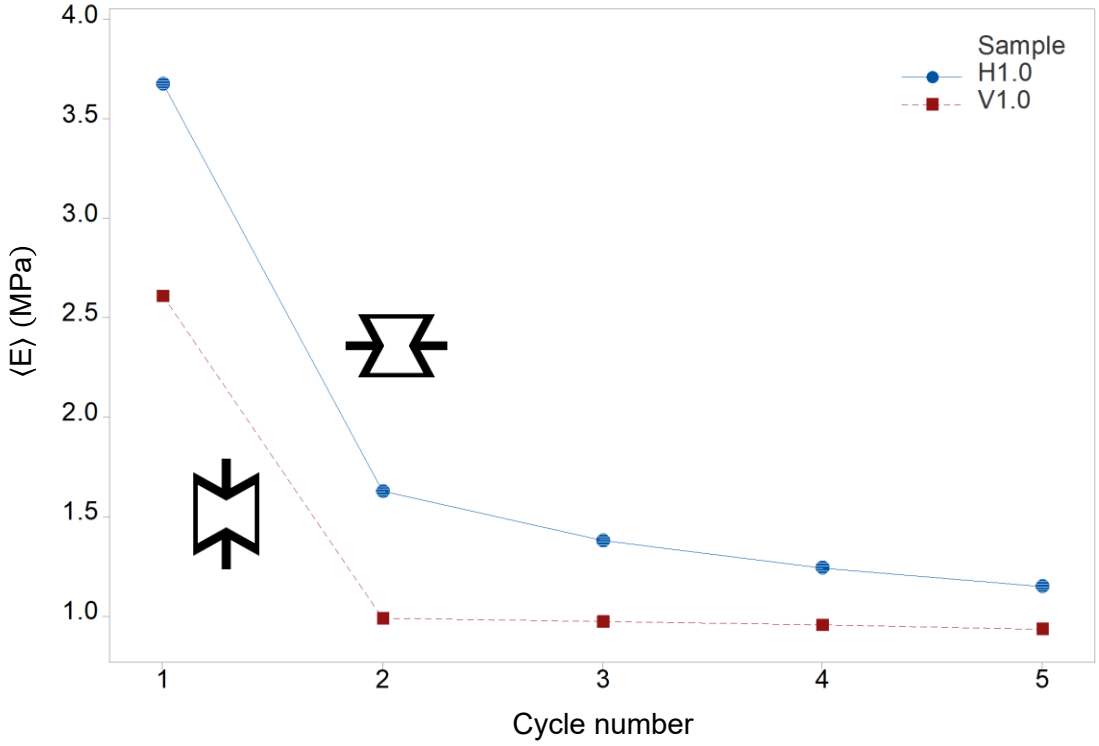

Figure 81. Variation of apparent elastic modulus in TPU reentrant honeycombs when subjected to five loading cycles.

- Effect of strain rate

TPU reentrant honeycomb structures V0.8 and V1.4 were compressed at different strain rates and the load vs. displacements results can be observed in Figs. 82-83. A variation in the velocity at which the structures were crushed demonstrated no significant difference in the curves. No tendency is observed to establish properly a relationship between the strain rate and the mechanical response of the structures. It is believed that even at the velocities proposed (24 mm/min, 50 mm/min, and 100 mm/min), a quasi-static phenomenon is still happening. For further work, it is necessary to crush the structures at much higher velocities of at least 1 m/s in order to evaluate the mechanical response of TPU cellular solids when subjected to impact events.

It is important to state that this study was carried out with only one compressing direction and one replicate, so it is required for future research to propose a more complete design of experiments with a minimum of 3 replicates and different compressing directions to generate results statistically significant.

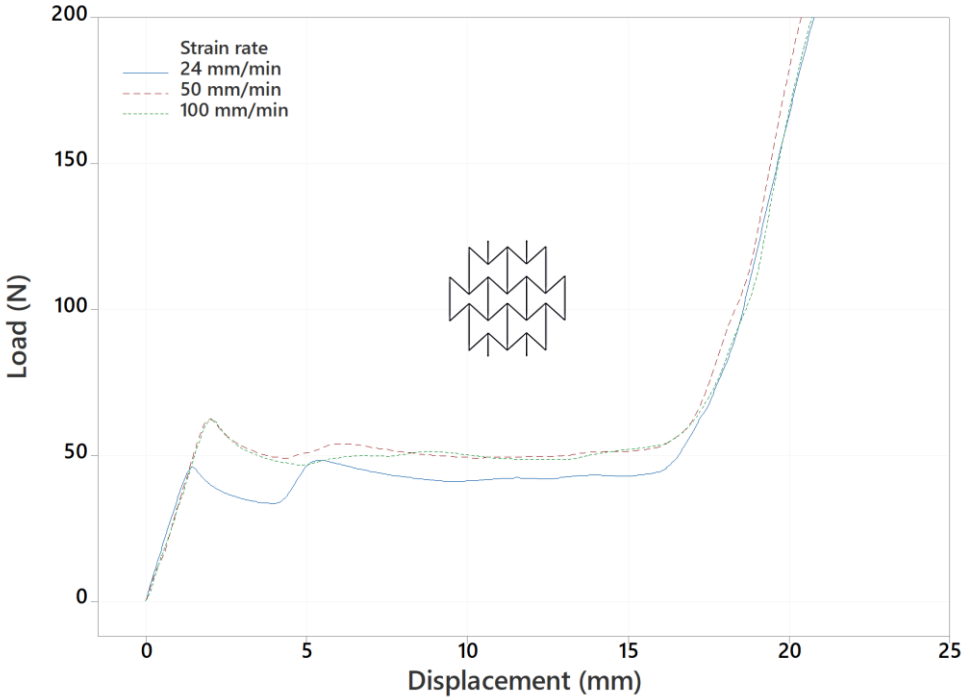

Figure 82. Load vs. displacement curve of sample V0.8 compressed at different strain rates.

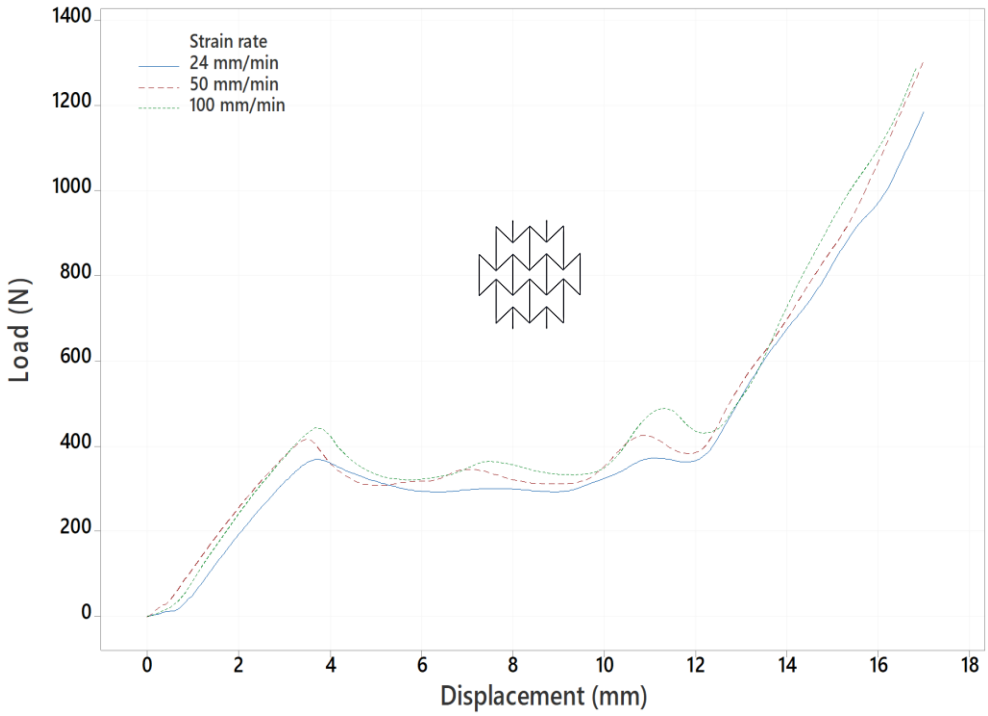

Figure 83. Load vs. displacement curve of sample V1.4 when compressed at different strain rates.

Chapter 5: Conclusions and recommendations

5.1 Conclusions

This research work was carried out to understand the mechanics of cellular solids when subjected to compressive loadings. The reentrant honeycomb topology was selected due to its demonstrated enhanced properties and potential applications in the field of packaging as energy absorbers. Two set of experiments were proposed to study the feasibility of fused deposition modeling technique as the manufacturing process for cellular solids, and to study the energy absorption capability of reentrant honeycombs structures when subjected to multiple compressive cycles. Some conclusions are presented below.

In Chapter 3 it was presented a set of experiments to study the effect of selecting the fdm technique to fabricate cellular solids. The samples were fabricated using polylactic acid filaments, which make them very rigid and non-resilient during the compression tests. The samples proposed and printed have the particularity that they were scaled up from one original model. This, to demonstrate that cellular solids with the same topology and relative density would exhibit the same apparent elastic modulus. Simulation results supported this hypothesis by showing the same results on the Young's modulus. In the other hand, 3D printed specimens behave different one from another and their elastic moduli were also very different. This must be attributed to the additive manufacturing technique which exhibited low accuracy during the shape formations and to the creation of empty spaces between line contours in the samples. This demonstrates that fdm technique does not have good accuracy, especially with the fabrication of thin wall elements and sharp ends. In order to use this technique, it is recommended to select it only for big cellular solids with cell-wall thicknesses higher than 1 mm.

In Chapter 4 it is analyzed the mechanical response of reentrant honeycombs structures under cyclic compressive loadings to study the effect of relative density on the apparent elastic modulus of the cellular solids and their energy absorption ability in two different loading orientations. Fused deposition modeling technique was selected as the manufacturing process due to its popular use among

researchers to fabricate prototypes. This technique is relatively cheap, easy to manipulate, and offers a wide variety of printing materials. Some of the disadvantages found during this project was its low accuracy to fabricate wall with thickness lower than 1 mm, and the creation of round ends where it was supposed to be sharped ones; this, can be attributed to the extruder trajectory during the change of direction. The use of thermoplastic polyurethane helped to fabricate very resilient samples that were able to withstand multiple compressions. Results demonstrated that by increasing the relative density of reentrant honeycombs, an increment of their apparent elastic modulus appeared. This was identified as a cubic relationship. H-samples offered higher apparent elastic modulus when compared to their counterparts. When structures have vertical elements, these are easier to suffer buckling at low forces because its small wall thickness. The diagrams for the loading and unloading cycles showed a softening behavior in TPU structures, presenting the biggest difference between the first and second loading cycle. The arrays are more compliant after the second cycle and at the five cycle it is reached a convergence for the amount of energy absorbed. It was observed that after each compression, the specimen did not return to its original height. This behavior was considered a viscoelastic effect rather than plastic deformation.

An analysis of the variation on the mechanical response of TPU reentrant honeycombs was also carried out to illustrate the effect of cyclic loadings on resilient cellular solids. Results demonstrated that even the selection of flexible polymers like thermoplastic polyurethane on the fabrication of very resilient cellular structures has a great potential, structures exhibited a diminish on the apparent elastic modulus as the number of cycles increased. Unit cells kept a deformed shape memory after each cycle loading which make them easier to deform the following cycle. Samples were observed to getting back almost to original height after the unloading, but with slight buckled cell walls.

5.2 Future work

It is important to continue this research work to explore deeply the effects of fdm process and design parameters on the energy absorption capabilities of reentrant honeycombs in order to be use as crash absorbers in the industry.

Some recommendations for further work are listed:

- Explore more variations on the relative density to establish a more accurate relationship with the mechanical properties of reentrant honeycombs,
- Increase the number of cycles to identify if the convergence found in this work starting from cycle number five is kept. It can be interesting to obtain the number of cycles will keep this convergence in its mechanical response before breaking, or even if it will ever break after hundreds or thousands of compressions.
- Test much higher compression velocities to analyze how these structures would behave as they are impacted at 1 m/s or more. Some experiments were carried out during this investigation to study the strain rate up until 100 mm/min, but no significant tendency was observed. It is necessary to identify the limit at which the process is no longer a quasi-static mechanical test.

References

[1] M. Sanami, N. Ravirala, K. Alderson, and A. Alderson, “Auxetic materials for sports applications,” *Procedia Eng.*, vol. 72, pp. 453–458, 2014, doi: 10.1016/j.proeng.2014.06.079.

[2] . A. Lvov, F. S. Senatov, A. M. Korsunsky, and A. I. Salimon, “Design and mechanical properties of 3D-printed auxetic honeycomb structure,” *Mater. Today Commun.*, vol. 24, no. February, p. 101173, 2020, doi: 10.1016/j.mtcomm.2020.101173.

[3] E. Barchiesi, M. Spagnuolo, and L. Placidi, “Mechanical metamaterials a state of the art,” *Math. Mech. Solids*, vol. 24, no. 1, pp. 212–234, 2019, doi: 10.1177/1081286517735695.

[4] X. Yu, J. Zhou, . L iang, Z. Jiang, and L. Wu, “Mechanical metamaterials associated with stiffness, rigidity and compressibility A brief review,” *Prog. Mater. Sci.*, vol. 94, pp. 114–173, 2018, doi: 10.1016/j.pmatsci.2017.12.003.

[5] *Gibson, L., & Ashby, M. (1997). Cellular Solids: Structure and Properties (2nd ed., Cambridge Solid State Science Series). Cambridge: Cambridge University Press. doi:10.1017/CBO9781139878326*. .

[6] “Foam Structures with a Negative Poisson ’ s Ratio Author (s) Roderic Lakes Source Science , New Series , Vol . 235 , No . 4792 (Feb . 27 , 1987), pp . 1038-1040 Published by American Association for the Advancement of Science Stable URL http //,” *Adv. Sci.*, vol. 235, no. 4792, pp. 1038–1040, 2011.

[7] R. Lakes, “Advances in negative poisson’s ratio materials,” *Adv. Mater.*, vol. 5, no. 4, pp. 293–296, 1993, doi: 10.1002/adma.19930050416.

[8] X. Li, Q. Wang, Z. Yang, and Z. Lu, “Novel auxetic structures with enhanced mechanical properties,” *Extrem. Mech. Lett.*, vol. 27, pp. 59–65, 2019, doi: 10.1016/j.eml.2019.01.002.

[9] D. Bhate, “Four questions in cellular material design,” *Materials (Basel).*, vol. 12, no. 7, 2019, doi: 10.3390/ma12071060.

[10] L. Yang, “A study about size effects of 3D periodic cellular structures,” *Solid Free. Fabr. 2016 Proc. 27th Annu. Int. Solid Free. Fabr. Symp. - An Addit. Manuf. Conf. SFF 2016*, pp. 2181–2193, 2016.

[11] T. Le, D. Bhate, J. M. Parsey, and K. . s u, “Determination of a shape and size independent material modulus for honeycomb structures in additive manufacturing,” *Solid Free. Fabr. 2017 Proc. 28th Annu. Int. Solid Free. Fabr. Symp. - An Addit. Manuf. Conf. SFF 2017*, pp. 2148–2169, 2020.

[12] S. Malek and L. Gibson, “Effective elastic properties of periodic hexagonal honeycombs,” *Mech. Mater.*, vol. 91, no. P1, pp. 226–240, 2015, doi: 10.1016/j.mechmat.2015.07.008.

[13] I. G. Masters and K. E. Evans, “Models for the elastic deformation of honeycombs,” *Compos. Struct.*, vol. 35, no. 4, pp. 403–422, 1996, doi: 10.1016/S0263-8223(96)00054-2.

[14] J. Lee, J. B. Choi, and K. Choi, “Application of homogenization FEM analysis to regular and re-entrant honeycomb structures,” *J. Mater. Sci.*, vol. 31, no. 15, pp. 4105–4110, 1996, doi: 10.1007/BF00352675.

[15] J. P. M. Whitty, F. Nazare, and A. Alderson, “Modelling the effects of density variations on the in-plane Poisson’s ratios and Young’s moduli of periodic conventional and re-entrant honeycombs - Part 1 Rib thickness variations,” *Cell. Polym.*, vol. 21, no. 2, pp. 69–98, 2002.

[16] D. U. Yang, S. Lee, and F. Y. u ang, “Geometric effects on micropolar elastic honeycomb structure with negative Poisson’s ratio using the finite element method,” *Finite Elem. Anal. Des.*, vol. 39, no. 3, pp. 187–205, 2003, doi: 10.1016/S0168-874X(02)00066-5.

[17] X. Zhang and D. Yang, “Mechanical properties of auxetic cellular material consisting of re-entrant hexagonal honeycombs,” *Materials (Basel).*, vol. 9, no. 11, 2016, doi: 10.3390/ma9110900.

[18] C. Yang, . D. ora, and Y. Chang, “Behavior of auxetic structures under compression and impact forces,” *Smart Mater. Struct.*, vol. 27, no. 2, 2018, doi: 10.1088/1361-665X/aaa3cf.

[19] H. Wan, H. htaki, S. Kotosaka, and G. u, “A study of negative Poisson’s ratios in auxetic honeycombs based on a large deflection model,” *Eur. J. Mech. A/Solids*, vol. 23, no. 1, pp. 95–106, 2004, doi: 10.1016/j.euromechsol.2003.10.006.

[20] M. H. Fu, O. T. Xu, L. L. u , and T. X. Yu, “Nonlinear shear modulus of re-entrant hexagonal honeycombs under large deformation,” *Int. J. Solids Struct.*, vol. 80, pp. 284–296, 2016, doi: 10.1016/j.ijsolstr.2015.11.015.

[21] S. yavahare and S. Kumar, “Numerical and experimental investigation of FDM fabricated re-entrant auxetic structures of ABS and PLA materials under compressive loading,” *Rapid Prototyp. J.*, vol. 27, no. 2, pp. 223–244, 2021, doi: 10.1108/RPJ-10-2019-0271.

[22] M. Chaudhari, B. F. Jogi, and R. S. Pawade, “Comparative Study of Part Characteristics Built Using Additive Manufacturing (FDM),” *Procedia Manuf.*, vol. 20, no. 2017, pp. 73–78, 2018, doi: 10.1016/j.promfg.2018.02.010.

[23] I. J. Solomon, P. Sevvel, and J. Gunasekaran, “A review on the various processing parameters in FDM,” *Mater. Today Proc.*, vol. 37, pp. 509–514, 2020, doi: 10.1016/j.matpr.2020.05.484.

[24] A. Rodríguez-Panes, J. Claver, and A. M. Camacho, “The influence of manufacturing parameters on the mechanical behaviour of PLA and ABS pieces manufactured by FDM: A comparative analysis,” *Materials (Basel).*, vol. 11, no. 8, 2018, doi: 10.3390/ma11081333.

[25] J. Chen, W. Chen, . ao , S. u an, and W. Tao, “Mechanical behaviors of 3D re-entrant honeycomb polyamide structure under compression,” *Mater. Today Commun.*, vol. 24, no. March, p. 101062, 2020, doi: 10.1016/j.mtcomm.2020.101062.

[26] C. oh imer, J. Christ, N. Aliheidari, C. Mo, and A. Ameli, “3D printed thermoplastic polyurethane with isotropic material properties,” *Behav. Mech. Multifunct. Mater. Compos. 2017*, vol. 10165, p. 1016511, 2017, doi: 10.1117/12.2259810.

[27] N. Elmrabet and P. Siegkas, “Dimensional considerations on the mechanical properties of 3D printed polymer parts,” *Polym. Test.*, vol. 90, no. June, 2020, doi: 10.1016/j.polymertesting.2020.106656.

[28] L. Yang, . arr ysson, . West, and D. Cormier, “Compressive properties of Ti-6Al-4V auxetic mesh structures made by electron beam melting,” *Acta Mater.*, vol. 60, no. 8, pp. 3370–3379, 2012, doi: 10.1016/j.actamat.2012.03.015.

[29] S. R. G. Bates, I. R. Farrow, and R. S. Trask, “3D printed polyurethane honeycombs for repeated tailored energy absorption,” *Mater. Des.*, vol. 112, pp. 172–183, 2016, doi: 10.1016/j.matdes.2016.08.062.

[30] K. P. Logakannan, . Ramachandran, J. Rengaswamy, and D. Ruan, “Dynamic Performance of a 3D Re-entrant Structure,” *Mech. Mater.*, vol. 148, no. June, p. 103503, 2020, doi: 10.1016/j.mechmat.2020.103503.

[31] D. Popescu, A. Zapciu, C. Amza, F. Baciu, and R. Marinescu, “FDM process parameters influence over the mechanical properties of polymer specimens A review,” *Polym. Test.*, vol. 69, no. April, pp. 157–166, 2018, doi: 10.1016/j.polymertesting.2018.05.020.

[32] S. Vyavahare and S. Kumar, “Re-entrant auxetic structures fabricated by fused deposition modeling: An experimental study of influence of process parameters under compressive

loading," *Polym. Eng. Sci.*, vol. 60, no. 12, pp. 3183–3196, 2020, doi: 10.1002/pen.25546.

[33] J. M. Chacón, M. A. Caminero, E. García-Plaza, and P. J. Núñez, "Additive manufacturing of PLA structures using fused deposition modelling: Effect of process parameters on mechanical properties and their optimal selection," *Mater. Des.*, vol. 124, pp. 143–157, 2017, doi: 10.1016/j.matdes.2017.03.065.

[34] X. Deng, Z. Zeng, B. Peng, S. Yan, and W. Ke, "Mechanical properties optimization of poly-ether-ether-ketone via fused deposition modeling," *Materials (Basel).*, vol. 11, no. 2, 2018, doi: 10.3390/ma11020216.

[35] R. G. Silva, M. J. Torres, J. Z. iñuela, and A. G. Zamora, "Manufacturing and characterization of 3D miniature polymer lattice structures using fused filament fabrication," *Polymers (Basel).*, vol. 13, no. 4, pp. 1–19, 2021, doi: 10.3390/polym13040635.

[36] Q. Zhou, "A study in Fabricating Microstructures (Part 1)." https //medium.com/3d-printing-stories/a-study-in-fabricating-microstructures-part-1-f267d298326e.

[37] L. Geng, W. Wu, L. Sun, and D. Fang, "Damage characterizations and simulation of selective laser melting fabricated 3D re-entrant lattices based on in-situ CT testing and geometric reconstruction," *Int. J. Mech. Sci.*, vol. 157–158, no. April, pp. 231–242, 2019, doi: 10.1016/j.ijmecsci.2019.04.054.

[38] B. Lozanovski *et al.*, "Computational modelling of strut defects in SLM manufactured lattice structures," *Mater. Des.*, vol. 171, p. 107671, 2019, doi: 10.1016/j.matdes.2019.107671.

[39] A. Beharic, R. Rodriguez Egui, and L. Yang, "Drop-weight impact characteristics of additively manufactured sandwich structures with different cellular designs," *Mater. Des.*, vol. 145, pp. 122–134, 2018, doi: 10.1016/j.matdes.2018.02.066.

[40] T. Shepherd, K. Winwood, P. enkatraman, A. Alderson, and T. Allen, " alidation of a Finite Element Modeling Process for Auxetic Structures under Impact," *Phys. Status Solidi Basic Res.*, vol. 257, no. 10, pp. 1–14, 2020, doi: 10.1002/pssb.201900197.

[41] R. Sengupta *et al.*, "The Morphology and Mechanical Properties of Sodium Alginate Based Electrospun Poly(ethylene oxide) Nanofiber," *Polym. Eng. Sci.*, vol. 47, pp. 21–25, 2007, doi: 10.1002/pen.

Curriculum Vitae

AMADOR CHAPA CÁRDENAS

Mechanical engineer with two years of work experience in new products/process introduction in the automotive industry. Researcher student in areas related to additive manufacturing and mechanics of materials.

Education

2019-2021 **ITESM Campus Monterrey** – Master of Science in Manufacturing Systems.
2014-2018 **TNM Campus Nuevo Laredo** – Mechanical Engineering

Aptitudes and abilities

-Responsible
-Work ethic
-Analytical thinking
-Teamwork
-Proactive
-Leadership
-Problem solving
-Time management

Technical skills

- Microsoft Office
  - Word
  - Excel
  - Power Point
- CAD Software
  - SolidWorks
  - Fusion 360
  - ANSYS
- Math Software
  - Matlab
  - Minitab

Languages

Spanish Native speaker
English Level B2 (TOEFL ITP score: 593)
French Beginner (3-year course)

Work Experience

2019 TNM Campus Nuevo Laredo – Professor (Courses: Heating Transfer / Hydraulics Systems)
2017-2019 Caterpillar Nuevo Laredo Finsa 3 – New Process Introduction (as student)
2017 Modine, Transferencia de Calor, Aluminum Division – New Process Introduction (as student)

This document was typed in using Microsoft Word by Amador Chapa Cárdenas.